Unlocking the Potential of Organopalladium Complexes for High-Grade Serous Ovarian Cancer Therapy

Thomas Scattolin,[*,†,a] Enrico Cavarzerani,[†,b] Dario Alessi,[a] Matteo Mauceri,[a] Eleonora Botter,[b] Giovanni Tonon,[b] Isabella Caligiuri,[c] Ombretta Repetto,[d] Urska Kamensek,[e] Simona Kranjc Brezar,[e] Maria Dalla Pozza,[f] Stefano Palazzolo,[c] Maja Cemazar,[e] Vincenzo Canzonieri,[c,g] Nicola Demitri,[h] Steven P. Nolan,[i] Gilles Gasser,[f] Fabiano Visentin*[b] and Flavio Rizzolio*[b,c]

[a] Dr. T. Scattolin, Dr. D. Alessi, Dr. M. Mauceri
Dipartimento di Scienze Chimiche
Università degli studi di Padova
via Marzolo 1, 35131, Padova, Italy
E-mail: thomas.scattolin@unipd.it Website: https://www.organometallics.it Twitter: @ThomasScattoli1 and @OrganoMetalsPD

[b] Dr. E. Cavarzerani, Prof. Dr. F. Rizzolio, E. Botter, G. Tonon, Prof. Dr. F. Visentin.
Department of Molecular Sciences and Nanosystems
Università Ca' Foscari
Campus Scientifico Via Torino 155, 30174, Venezia-Mestre, Italy
E-mail: flavio.rizzolio@unive.it and fvise@unive.it

[c] Dr. S. Palazzolo, Dr. I. Caligiuri, Prof. Dr. F. Rizzolio, Prof. Dr. V. Canzonieri
Pathology Unit, Centro di Riferimento Oncologico di Aviano (C.R.O.) IRCCS
via Franco Gallini 2, 33081, Aviano, Italy

[d] Dr. O. Repetto
Immunopathology and Cancer Biomarkers, Centro di Riferimento Oncologico di Aviano (CRO), IRCCS
via Franco Gallini 2, 33081, Aviano, Italy

[e] Dr. U. Kamensek, Dr. S. K. Brezar, Dr. M. Cemazar
Department of Experimental Oncology, Institute of Oncology Ljubljana, Ljubljana, 1000, Slovenia.

[f] Dr. M. Dalla Pozza, Prof. Dr. G. Gasser
ChimieParisTech, PSL University, CNRS
Institute of Chemistry for Life and Health Sciences, Laboratory for Inorganic Chemical Biology, 75005, Paris, France

[g] Prof. Dr. V. Canzonieri
Department of Medical, Surgical and Health Sciences
Università degli Studi di Trieste
Strada di Fiume 447, Trieste, Italy

[h] Dr. N. Demitri
Area Science Park
Elettra-Sincrotrone Trieste, S.S. 14 Km 163.5
Basovizza, 34149, Trieste, Italy

[i] Prof. Dr. S. P. Nolan
Department of Chemistry and Centre for Sustainable Chemistry
Ghent University
Krijgslaan 281, S-3, 9000 Ghent, Belgium

[†] These authors contributed equally to this work

Supporting information for this article is given via a link at the end of the document

Abstract: *High-Grade Serous Ovarian Cancer (HGSOC) is the most common and lethal subtype of ovarian cancer, known for its high aggressiveness and extensive genomic alterations. Typically diagnosed at an advanced stage, HGSOC presents formidable challenges in drug therapy. The limited efficacy of standard treatments, development of chemoresistance, scarcity of targeted therapies, and significant tumor heterogeneity render this disease incurable with current treatment options, highlighting the urgent need for novel therapeutic approaches to improve patient outcomes.*

In this study we report a straightforward and stereoselective synthetic route to novel Pd(II)-vinyl and -butadienyl complexes bearing a wide range of monodentate and bidentate ligands. Most of the synthesized complexes exhibited good to excellent in vitro anticancer activity against ovarian cancer cells. Particularly promising is the water-soluble complex bearing two PTA (PTA = 1,3,5-triaza-7-phosphaadamantane) ligands and the Pd(II)-butadienyl fragment. This compound combines excellent cytotoxicity towards cancer cells with substantial inactivity towards non-cancerous ones. This derivative was selected for further studies on ex vivo tumor organoids and in vivo mouse models, which demonstrate its remarkable efficacy with surprisingly low collateral toxicity even at high dosages. Moreover, this class of compounds appears to operate through a ferroptotic mechanism, thus representing the first such example for an organopalladium compound.

Introduction

Ovarian cancer (OC), especially its most common and aggressive hystotype, high-grade serous ovarian cancer (HGSOC), exhibits molecular diversity and complex clinical profiles.[1] Genomic features include prevalent TP53 mutations, homologous recombination repair defects, and widespread copy-number variations. About 25% of HGSOC cases have alterations in breast cancer (BRCA) genes and disruptions in tumor suppressor and cell-cycle-regulating genes.[2]

This heterogeneity contributes to the non-curative nature of the disease and the challenges in formulating an effective therapeutic plan. Significant advances in therapy have been made in the past years, particularly with molecular targeted drugs such as the anti-VEGF antibody bevacizumab (VEGF = Vascular Endothelial Growth Factor) and PARP inhibitors (PARP = Poly ADP Ribose Polymerase) like olaparib, rucaparib, and niraparib.[3] However, given the rarity of mismatch repair-deficient Epithelial Ovarian Cancer (EOC) and the limited efficacy demonstrated by immunotherapies, with a low response rate in OC, the development of new targeted drugs and biomarkers remains

critical.[4] In fact, the primary treatment for HGSOC patients is still surgery and platinum-based chemotherapy, but there is a high relapse rate of 70-80% and growing treatment resistance.[4,5] Given HGSOC's genetic variability, a multitarget approach could be more effective. The therapeutic landscape for OC is evolving with the emergence of antibody-drug conjugates (ADCs) such as raludotatug deruxtecan, an ADC consisting of a humanized IgG1 antibody against cadherin 6 (CDH6), is currently in a Phase 1 trial for OC therapy[6] and mirvetuximab soravtansine, which targets FRα (FRα = Folate Receptor α) showing efficacy and safety in the MIRASOL trial.[7] Trastuzumab deruxtecan has also demonstrated significant results in HER2-positive solid tumors (HER2 = human epidermal growth factor receptor 2).[8] These ADCs deliver potent cytotoxic agents directly to cancer cells, optimizing efficacy and minimizing side effects,[9] suggesting that potent multitarget agents could be an effective strategy in OC therapy. The efficacy of treatments is often hindered by mutations in cancer cells that activate compensatory pathways, contributing to the high mortality rate from drug resistance, which is implicated in up to 90% of cancer-related deaths.[10,11] Chemo-resistant cancer cells often result from enhanced DNA repair mechanisms or dysfunctional apoptosis pathways.[12] Therefore, strategies that bypass the resistance to cell death, like ferroptosis, can be highly effective in treating HGSOC, which lacks specific targets and shows significant genetic variability and high recurrence rates.

The recognition of regulated cell death (RCD) in the 1960s opened the door to the concept of modulating cell death processes.[13] For many years, the induction of caspase-dependent apoptosis represented the cornerstone of anti-cancer therapies.[14] As research has advanced, it is now well-established that cancer cells may become resistant to apoptosis, prompting a shift in research to other types of RCD mechanisms.[15] Current strategies in cancer treatments are evolving to address these resistances by harnessing non-apoptotic pathways to eliminate cancer cells more effectively.

Among the few non-apoptotic mechanisms, particularly interesting is ferroptosis. Cells undergoing this process display unique features such as increased mitochondrial membrane density and reduced mitochondrial volume.[16,17] Importantly, some drug candidates operating via this mechanism have proven effective against several apoptosis-resistant cancer cells.[18] Hence, the advent of ferroptosis paves the way for a novel research direction in the pursuit of potent cancer therapies.
However, most potential anticancer agents that act according to this mechanism are purely organic molecules.[16,17] Far fewer contributions are present in the literature regarding organometallic compounds inducing ferroptosis,[16a] with only one example (an iridium complex) concerning OC and limited to *in vitro* studies on A2780 cells (cisplatin-sensitive).[19]

It is well-established that organometallic anticancer drugs possess some distinct advantages compared to purely organic counterparts, primarily due to their unique chemical properties that enable precise targeting of cancer cells while minimizing damage to healthy tissues.[20] Indeed, their metal-containing cores offer diverse coordination geometries, facilitating interactions with specific cellular targets and overcoming resistance mechanisms. Moreover, organometallic compounds often exhibit enhanced stability and tunable reactivity, allowing for tailored optimization of therapeutic efficacy and reduced side effects.[20]

Some recent classes of organometallic compounds that have provided encouraging *in vitro* results towards OC cells contain palladium as the metal center.[21] It has to be noted that palladium complexes are considerably less explored as potential antitumor agents compared to platinum, ruthenium, and gold complexes, which have passed or are still involved in clinical trials for cancer therapy.[22] The main reason for this lies in the high reactivity of palladium complexes in biological media, which significantly increases the speciation and toxicity of this metal.[23] However, it is possible to substantially mitigate this issue by employing ligands strongly anchored to the metal center, which suppress the hydrolysis of the complex, allowing it to reach the biotarget.[24] In this context, the best option is usually the utilization of at least one metal-carbon bond (organometallic fragment), which provides the complex with high stability in solution, even under physiological conditions.[25,26]

Since the pioneering studies conducted by Köpf and Köpf-Maier in the early 1980s on the promising antitumor activity of metallocene complexes,[27] many research groups have focused on the synthesis and the study of therapeutic effects of compounds bearing a wide range of organometallic fragments. The nature of the organometallic portion highly influences the hydrophilicity/hydrophobicity of the complexes, with a profound impact on the main cellular target and cellular uptake.[28] Furthermore, given that most metallodrugs are prodrugs, the organometallic fragment as well as the metal center are crucial for modulating the reactivity of the complex towards nucleophiles or reducing agents present in the biological environment.[29] These processes may involve the other ligands present in the coordination sphere of the metal (*e.g.* ligand substitution) as well as the organometallic fragment (e.g. attack on coordinated ligand, insertion or ligand substitution).

Among the numerous scenarios involving organometallic compounds with potential biological activity, summarized in a recent review by Sadler and co-workers (Scheme 1),[30] the metal-vinyl and metal-butadienyl complexes are almost unexplored.

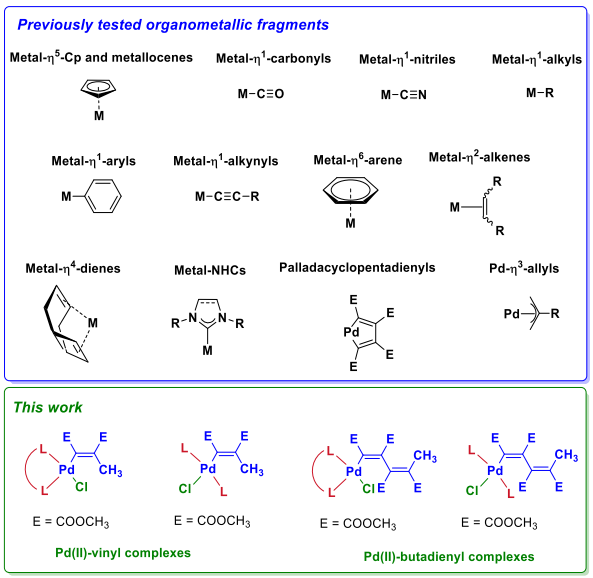

Scheme 1. Overview of organometallic fragments with promising biological activity.

In this context, we now report the synthesis of novel Pd(II)-vinyl and Pd(II)-butadienyl complexes and an in-depth study of their *in vitro*, *ex vivo* and *in vivo* antitumor activity on HGSOC models as

well as some hypothesis about their mechanism of action, which seems to involve an unprecedent ferroptotic pathway, thus marking a significant step forward in targeted OC therapy. As mentioned above, the ferroptosis mechanism has been observed only in a very limited number of organometallic compounds with potential anticancer activity[16a] and, to the best of our knowledge, there are no examples of organopalladium compounds that act through this mode of action. These latter usually target DNA, interacting with it through either covalent or non-covalent bonds,[31] or induce the death of tumor cells through an apoptotic process involving an early mitochondrial damage, often resulting from the inhibition of key proteins such as thioredoxin reductase (TrxR).[32]

Results and Discussion

Synthesis of Pd(II)-vinyl and -butadienyl complexes bearing N-N, P-P and C-C bidentate ancillary ligands

Since Pd(II)-vinyl and Pd(II)-butadienyl complexes play a crucial role as intermediates in numerous cross-coupling, oligomerization, and polymerization processes of alkynes,[33] some previous studies have highlighted that such organometallic species can be isolated through oxidative addition of Pd(0) complexes,[34] addition of halogens/organohalides on palladacyclopentadienyl complexes,[35] or by insertion of an alkyne into a Pd-C bond.[36] We believe that this latter synthetic strategy, which appears to involve the formation of a Pd(II)-η^2-alkyne intermediate,[37-39] is most suitable for the purposes of this work. This route involves a stereoselective insertion of an electron-deficient alkyne such as dimethyl-2-butynoate (DMAD) onto a Pd-methyl bond. Interestingly, in a previous work published by our group, we found that a particular N-S bidentate ligand, namely 2-methyl-6-(phenylthiomethyl)pyridine, allows to surprisingly control the number of alkyne molecules involved in the insertion (Scheme 2).[36]

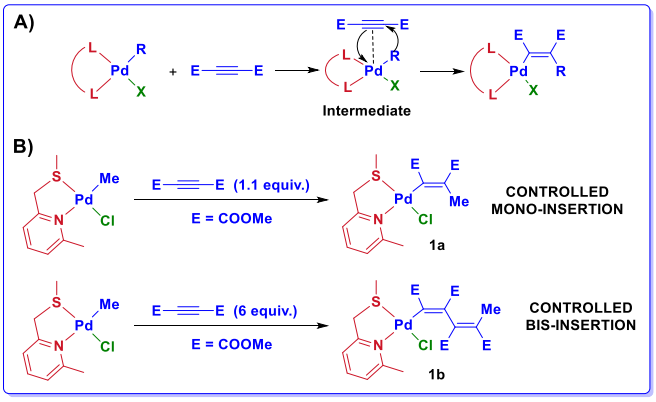

Scheme 2. A) General mechanism of formation of Pd(II)-vinyl complexes via insertion; B) 2-methyl-6-(phenylthiomethyl)pyridine enable the controlled mono- and bis-insertion.

Conversely, the use of P-P and N-N bidentate ligands leads to mixtures of mono- and poly-insertion products or hinders the reaction from proceeding beyond the mono-insertion product, respectively.[40-44]

The 2-methyl-6-(phenylthiomethyl)pyridine ligand, in addition to facilitating and making the alkyne insertion process controllable, has also another indisputable advantage. In fact, due to the distorting effect of the methyl substituent on the chelate ring, this pyridylthioether ligand can be effortlessly replaced by other ligands.[45] With this approach, we have an easy access to numerous palladium vinyl and butadienyl complexes which cannot be obtained by direct insertion.

With this valuable information in hand, we have successfully reacted the Pd(II)-vinyl and -butadienyl precursors **1a-b** with one equivalent of three different bidentate ligands (1,10-phenanthroline, neocuproine and dppp = 1,3-bis(diphenylphosphino)propane), and the corresponding complexes **2a-b**, **3a-b** and **4a-b** were obtained in high yields and purity (Scheme 3). With a similar procedure, the dppe (dppe = 1,2-bis (diphenylphosphino)ethane) derivatives **5a-b** were previously synthesized.[36] All reactions proceed at room temperature within 30 minutes, with the only exception of complex **3b** which requires about 6 days to complete the replacement of the pyridylthioether ligand with neocuproine. This is most likely due to the simultaneous presence of the methyl groups in the ancillary ligand and to the higher steric demand of the butadienyl moiety compared to the vinyl one.

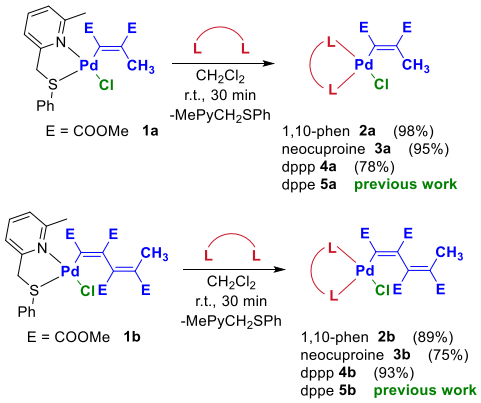

Scheme 3. Synthetic procedure leading to Pd-vinyl and -butadienyl complexes bearing N-N (**2a-b** and **3a-b**) and P-P bidentate ligands (**4a-b** and **5a-b**).

The products were exhaustively characterized by NMR, IR, elemental analysis and, in some cases, by single crystal X-ray diffraction (see Crystal structure determination section). In the ^{1}H NMR and ^{13}C NMR spectra of complexes **2a-b** and **3a-b**, the signals of coordinated 1,10-phenanthroline or neocuproine usually appear at higher chemical shifts with respect to those of the free ligand. On the other hand, the coordination of the vinyl or butadienyl moieties is evidenced by the presence in the ^{1}H NMR spectra of the terminal methyl protons signal (2.1-2.6 ppm) and those ascribable to the ester protons OCH_3 (3.2-3.9 ppm). Moreover, in the ^{13}C NMR spectra the organopalladium fragment shows the following diagnostic signals: carbonyl carbons (161-174 ppm), vinyl carbons (127-168 ppm), ester carbons OCH_3 (51-52 ppm) and the terminal methyl carbon (19-22 ppm).

In the case of the diphosphine complexes **4a-b** and **5a-b**, the ^{31}P NMR spectra confirm the coordination of dppp and dppe. More in detail, it is possible to observe the presence of two doublets (-6 and 11-15 ppm with $J_{P\text{-}P}$ = 41-46 Hz for **4a-b**; 53-56 and 40-45 ppm with $J_{P\text{-}P}$ = 19-24 Hz for **5a-b**), significantly downshifted compared to uncoordinated dppp and dppe ligands.

Similarly to the complexes bearing N-N bidentate ligands, all vinyl and butadienyl signals as well as the alkyl/aryl signals of the diphosphine ligand are present in the ^{1}H and ^{13}C NMR spectra. Particularly diagnostic is the signal ascribable to the vinyl carbon directly bound to palladium which resonates as a doublet at ca. 170 ppm ($J_{C\text{-}P} \approx 120$ Hz). Finally, in the IR spectra the stretching bands of the carbonyl groups at 1700 cm^{-1} are particularly worthy of mention.

The last class of bidentate ligands that we have considered in this work is that of diNHCs (NHCs = *N*-heterocyclic carbenes). Such ligands are strong σ-donors and generally efficiently stabilize late transition metal complexes.[46] However, it must be remembered that, in some cases, their high *trans*-labilizing effect tends to labilize the fragment *trans* to the carbene carbon. It is therefore always necessary to modulate the steric and electronic characteristics of both the diNHC ligand and the other coordinated fragments to ensure the obtainment of the species of interest in a pure form and with sufficient stability. With these premises we carried out the reaction between the precursors **1a-b** and the silver complex **6**, which is equipped with a methylene bridge and benzyl wingtip substituents (Scheme 4).

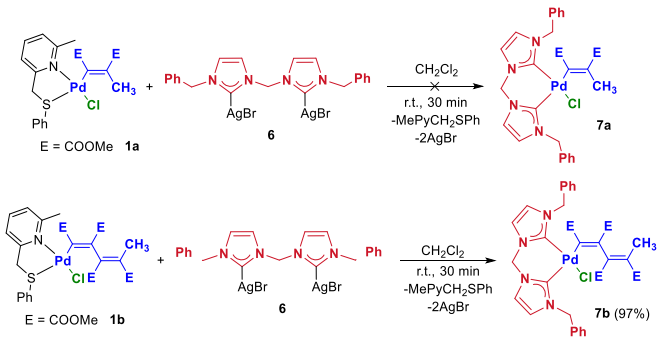

Scheme 4. Synthetic procedure leading to Pd-vinyl and -butadienyl complexes bearing chelating diNHC ligands (**7a-b** and **3a-b**).

Although the transmetallation reaction took place in both cases, it was possible to isolate in a pure form and in good yield only the butadienyl derivative **7b**. The reduced steric hindrance of the vinyl unit compared to the butadienyl one compromises the stability of **7a**, generating a mixture of by-products that are difficult to identify and increase in percentage over time. The ^{1}H NMR spectrum of **7b** presents, in addition to the typical signals of the butadienyl fragment, all those attributable to the dicarbene ligand. In particular, the methylene protons NCH_2Ph and NCH_2N resonate as AB systems between 4.7 and 6.3 ppm, due to the blocked rotation about the NCH_2-Ph bonds and the blocked conformational movement of the chelate ring, respectively. In the ^{13}C NMR spectrum, the signals of the 3 methylene carbons (54-64 ppm) and those of the two carbene carbons (166 and 175 ppm) deserve to be highlighted.

Synthesis of Pd(II)-vinyl and -butadienyl complexes bearing monodentate ancillary ligands

The lability of 2-methyl-6- (phenylthiomethyl)pyridine also enables the introduction of two monodentate ligands into the coordination sphere of palladium. Therefore, by adding 2 equivalents of PPh_3, PTA (PTA = 1,3,5-triaza-7-phosphaadamantane) or $AsPh_3$ to the palladium precursors **1a-b** it is possible to selectively obtain the complexes **8a-b**, **9a-b** and **10a-b** in high yields (Scheme 5).

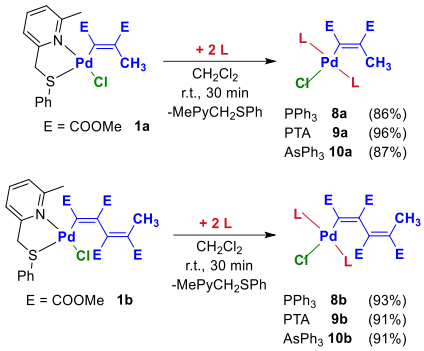

Scheme 5. Synthetic procedure leading to Pd-vinyl and -butadienyl complexes bearing two monodentate ancillary ligands (**8a-b**, **9a-b** and **10a-b**).

The formation of the *trans* isomers (thermodynamic products) is confirmed by the presence in the ^{31}P NMR spectra of **8a-b** and **9a-b** of one singlet significantly downshifted with respect to the uncoordinated phosphine ($\Delta\delta \approx 30$-40 ppm). Consistently, in the ^{1}H and ^{13}C NMR spectra it is possible to identify a single set of aryl signals for complexes **8a-b**/**10a-b** and, as regards the PTA derivatives **9a-b**, a single signal attributable to the protons and methylene carbons (NCH_2P and NCH_2N). In particular, the NCH_2P and NCH_2N protons resonate as tight multiplets at 4.3 and 4.5 ppm, respectively, whereas the corresponding carbons are located at ca. 50 and 70 ppm. Finally, the vinyl carbon signal directly bound to palladium appears as a triplet at 157-170 ppm ($J_{C\text{-}P} \approx 10$ Hz), owing to the coupling with the two magnetically equivalent phosphorus nuclei in the complexes **9a-b**.

The choice of PTA is mainly due to the high solubility in water of this particular phosphine and its transition metal complexes.[47] This feature, together with the stability of PTA to oxidation, is the reason for its success in the development of new generations of metal-based anticancer agents.[48] Furthermore, since PTA is a less encumbered phosphine than the classical triphenylphosphine (cone angles = 102° and 145°, respectively), its derivatives **9a-b** might be significantly different from a steric point of view compared to their triphenylphosphine congeners **8a-b**. On the contrary, the electronic characteristics of these two phosphines are known to be similar.

Interestingly, any attempt to introduce two monodentate NHC ligands resulted in mixtures of unidentified products and significant decomposition to metallic palladium, suggesting poor stability of the desired complexes. Two examples of such reactions are reported in Scheme 6.

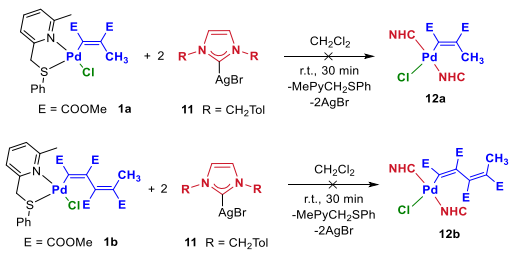

Scheme 6. Reaction between **1a-b** and 2 equiv. of silver-NHC complex **11**.

For completeness, we conducted a classical study of organometallic reactivity involving Pd(II)-vinyl complexes and [(PhC≡C)Sn(n-Bu)$_3$]. This study dealing with the vinyl fragment

extrusion, which is reported in detail in the Supporting Information, allowed the isolation of an unprecedented palladium complex containing both Pd(II)-vinyl and Pd(II)-phenylacetylide fragments. Complex **13**, owing to its unique structure and high stability in solution, was subsequently considered for biological tests.

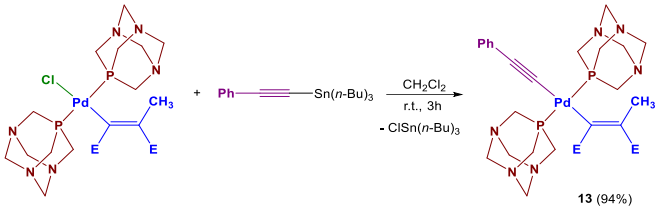

Scheme 7. Synthetic procedure leading to complex **13**.

Stability of Pd(II)-vinyl and -butadienyl complexes

Before carrying out the biological tests, we have monitored the stability of the synthesized complexes in a 1:1 D_2O/DMSO-d^6 solution by NMR spectroscopy. After 48 hours no significant changes of the spectra are detectable, indicating that the complexes retain their structural integrity. Taking advantage of the solubility in water of PTA derivatives, we have additionally monitored the stability of complex **9b** in D_2O by ^1H and ^{31}P NMR as well as in an aqueous buffer solution containing a mixture of ammonium bicarbonate (150 mM) by ESI-MS. The complex was stable even under these conditions, without releasing the chloride ligand and/or the other fragments bound to palladium.

Crystal Structure Determination

2a, **2b**, **3b**, **5a** and **13** crystalline forms bear one crystallographically independent palladium complex each (Figure 1). All the molecules are neutral and the corresponding palladium centers show square planar coordination spheres, with geometries in agreement with previously published data (Tables S2-7). Significant longer bond lengths can be clearly highlighted replacing the phenanthroline based ligands with a bidentate phosphine. Monodentate PTA moieties in **13** allow P ligands to adopt a *trans* configuration and relaxed Pd angles with neighbour ligands (i.e. closer to "ideal value" of 90°). 1,10-phenantroline based complexes (**2a**, **2b**, **3b**) show perfectly superimposable Pd coordination spheres in **2a** and **2b** and a notable ligand planarity distortion in **3b**, due to steric hindrance introduced by methyl groups. This effect allows also a deep conformational rearrangement of butadiene ligand which can form an intramolecular stacking interaction with the dimethyl-phenanthroline (the average angle between the phenanthroline and the peripheric olefine mean planes is ~22° in **3b**, while it's ~72° in **2b**). Equivalent methyl maleate dimethyl ester conformation is present in complexes **2a**, **13** and **5a** (R.M.S.D. ~1.1 Å, mostly due to $-COOCH_3$ rotations) with an average angle between the phenanthroline and the olefin mean planes of ~85°. Crystal packing show hydrophobic contacts among neighbour molecules, involving intermolecular π···π stacking among phenanthroline moieties and CH···π interactions, involving peripheral methoxy groups. Solvent molecules (chloroform) have been found in the crystal packing of **2a**, **13** and **5a** and they are bound to ligand heteroatoms through polar contacts (with shortest $d_{CH\cdots O}$ = 3.204(2) Å in **2a**, $d_{CH\cdots N}$ = 3.189(3) Å in **13**, $d_{CH\cdots O}$ = 3.180(3) Å in **5a**).

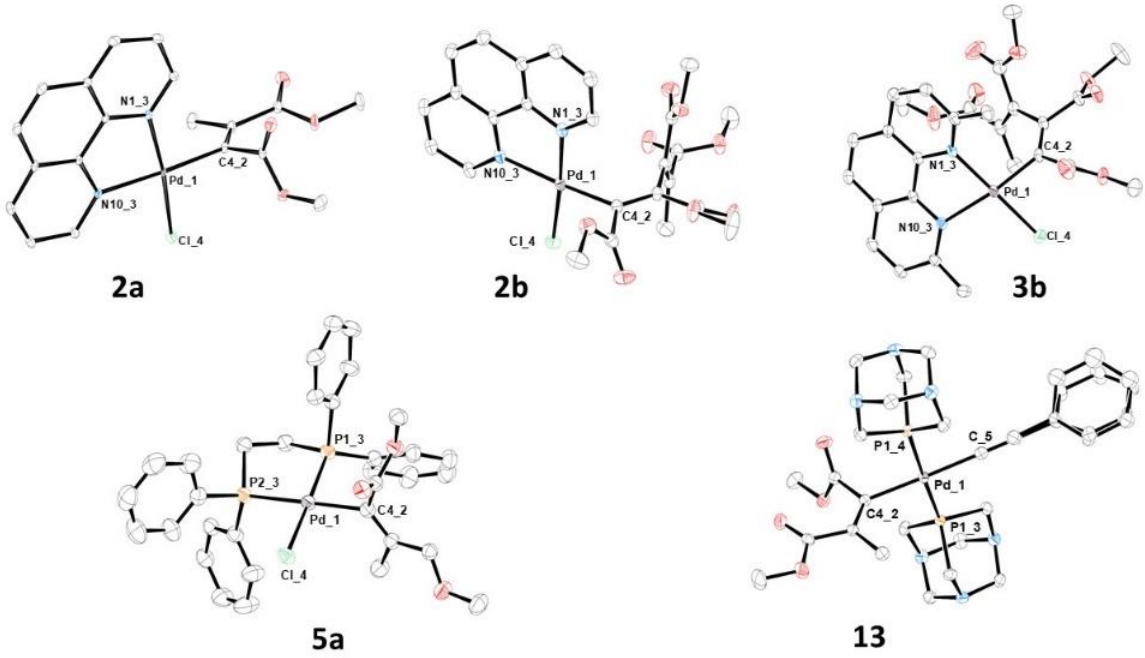

Figure 1. X-ray molecular structures of complexes **2a**, **2b**, **3b**, **5a** and **13** are presented, showing thermal displacement ellipsoids at the 50% probability level with hydrogen atoms and solvent molecules omitted for clarity.

Anticancer activity on human cancer and non-cancerous cell lines and patient derived tumor organoids grown from patient tissues or ascites fluids

With the aim of investigating the potential anticancer activity of the Pd(II)-vinyl and -butadienyl complexes, a panel of four different human tumor cell lines (OC A2780, with its cisplatin resistant clone A2780*cis*, triple-negative breast cancer MDA-MB231 and colon cancer DLD1) and MRC-5 non-cancerous cells (human lung fibroblasts) were treated for 96 hours with our compounds and cisplatin (positive control). In Figure 2A are reported the resulting half inhibitory concentrations (IC_{50}) values.

Based on the IC_{50} values obtained, it is possible to make some important considerations. As far as concerned the two OC cell lines (A2780 and A2780*cis*), all the compounds examined, except for those containing triphenylarsine (**10a** and **10b**), have comparable or lower IC_{50} values than cisplatin, especially in the cisplatin-resistant cell line (A2780*cis*). Most of the compounds exhibit comparable activity between these two OC lines, suggesting a different mechanism of action from that of cisplatin. For the latter, there are in fact almost two orders of magnitude between the IC_{50} values obtained in the two cell lines (0.4 μM vs 27 μM).

As for the triple-negative breast cancer cells MDA-MB231, all compounds, except those containing triphenylarsine (**10a** and **10b**), show a marked anticancer activity compared to cisplatin. In the colon cancer line (DLD-1), only compounds **3a-b**, **8a** and **9a-b** are more active than cisplatin. In the same line, compounds **2a-b**, **4a-b**, **5a-b** and **8b** show good cytotoxicity, while complexes **7b**, **10a-b** and **13** are practically inactive.

Comparing the cytotoxicity of compounds containing the same ancillary ligands (monodentate or bidentate), there is not a clear difference in activity between the vinyl derivatives and their butadienyl congeners.

Interestingly, the analyses on MRC-5 non-cancerous cells show that most compounds that exhibited antitumor activity, except for those bearing N-N bidentate ligands (**2a-b** and **3a-b**), are at the same time poorly cytotoxic towards non-cancerous cells. In this context, compounds **8a**, **9a** and **9b** are particularly promising, since they show excellent antitumor activity on all cancer cell lines examined and reduced cytotoxicity towards human lung fibroblasts. It should be noted that the selectivity of the compounds containing the PTA ligand has already been observed in the past with Pd(II)-allyl,[32a,48d] palladacyclopentadienyl[21b] and Pd(0)-olefin[45e] complexes.

Based on these encouraging biological data, we selected compound **9b** for further studies on more complex biological systems such as tumoroids extracted from OC patients (*ex vivo* tests) as well as on animal models (*in vivo* tests).

As shown in Figure 2C, compound **9b** was evaluated across five patient-derived tumor organoids (PDTOs) originating from both primary tumors and ascites fluid in patients diagnosed with HGSOC (PDTO-2, 3, 4, 5) and one low-grade serous OC (LGSOC) (PDTO-1), and one mouse-derived liver organoid (MDO-liver). Surprisingly, compound **9b** proved to be effective in three out of the five PDTOs, including two that are resistant to carboplatin (PDTO-1 and PDTO-2). Notably, the sensitivity of the PDTOs to carboplatin (the reference compound for clinical standard therapy) is representative of the actual clinical response of the patient from whom these PDTOs were derived. This suggests that compound **9b** might represent a novel therapeutic option for a subset of patients that show resistance to carboplatin, the standard first-line chemotherapy for ovarian cancer. Additionally, the toxicity profile of **9b** was evaluated in MDO-liver, demonstrating no toxicity in comparison to carboplatin.

A

Anticancer activity on human cancer and non cancerous cell lines

Complex	A2780	A2780cis	MDA-MB231	DLD1	MRC-5
CisPt	0.4±0.1	27±5	37±9	0.63±0.08	8±1
2a	3.6±0.2	4.2±0.7	6.2±0.2	2.8±0.8	4.5±0.1
2b	2.7±0.5	2.3±0.6	3.7±0.5	2.4±0.3	3.3±0.2
3a	0.3±0.2	0.03±0.01	0.38±0.03	0.31±0.03	0.27±0.05
3b	0.05±0.01	0.07±0.01	0.14±0.04	0.09±0.01	0.04±0.01
4a	1.0±0.3	2.0±0.5	1.6±0.1	4.0±0.6	>100
4b	3.4±0.1	5.5±0.8	0.5±0.4	3.7±0.5	>100
5a	4.1±0.8	0.6±0.2	3.5±0.1	3.59±0.08	>100
5b	2.8±0.4	5±2	1.0±0.5	4.1±0.8	>100
7b	1.0±0.2	16±3	2.0±0.6	>100	>100
8a	0.12±0.01	0.08±0.04	0.4±0.3	0.7±0.2	36±6
8b	0.13±0.06	0.4±0.1	>100	2.7±0.7	>100
9a	0.17±0.04	2.2±0.3	0.3±0.1	0.17±0.03	>100
9b	0.08±0.04	0.6±0.4	0.10±0.01	0.06±0.02	>100
10a	>100	>100	>100	>100	22±6
10b	>100	>100	31±6	>100	13±2
13	0.04±0.01	1.8±0.2	7±1	>100	>100

B

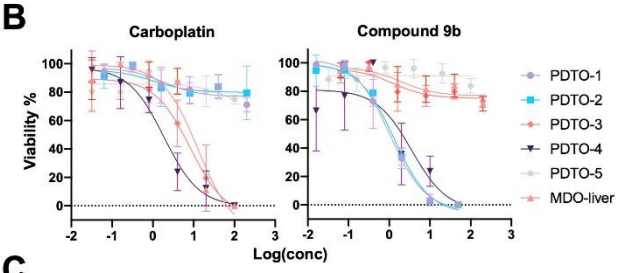

C

Anticancer activity of complex 9b on human and mouse derived organoids

Samples	OC Type	Origin	Carboplatin	9b
PDTO-1	LGSOC	Ascites	> 200	1.0 ± 0.5
PDTO-2	HGSOC	Ascites	> 200	1.3 ± 0.5
PDTO-3	HGSOC	Ascites	15 ± 2	> 200
PDTO-4	HGSOC	Primary tissue	3.8 ± 0.9	4 ± 2
PDTO-5	HGSOC	Primary tissue	> 200	> 200
MDO-liver	Normal	Mouse liver	15.5 ± 6.7	> 200

Figure 2: (A) IC_{50} values after 96 h of incubation. Stock solutions in DMSO for all complexes; stock solutions in H_2O for cisplatin. A2780 and A2780*cis* (cisplatin-sensitive and cisplatin-resistant OC cell lines), MDA-MB231 (triple-negative breast cancer cell line), DLD1 (colon cancer cell line) and MRC-5 (normal lung fibroblasts); (B) Dose-response curves and (C) IC_{50} values of patient-derived and mouse-derived organoids after 96 h of incubation.

Mechanism of cell death

After observing promising cytotoxic effects in OC PDTOs, we decided to investigate how **9b** acts in these cells by carrying out specific assays to unravel the mechanisms by which this compound might lead to cell death. Before proceeding with the elucidation of the mechanism of action, it is crucial to underline that cell death is not exclusively associated with malignancy; rather, it is a vital process regulated by complex molecular mechanisms that are essential for maintaining bodily homeostasis

and facilitating normal development. This understanding sets the stage for exploring the specific pathways through which therapeutic agents may induce cell death in cancer cells, allowing us to distinguish between pathological and physiological cell death processes.[49] It is important to note that a variety of cell death mechanisms such as apoptosis, necroptosis, pyroptosis, and autophagy have been identified and each of them have its unique mechanism.[50] Therefore, experiments aimed at deciphering the cellular death mechanism were conducted. As demonstrated by subsequent treatments with compound **9b** in A2780 and OVCAR5 (IC_{50} value is reported in Figure S1A) cells at different time points up to 96 hours, there was no observed increase in the expression of apoptosis-related proteins such as cytochrome C (Figures S1B, E) and caspases 3/7 (Figure S1C-D). Intriguingly, there was a statistically significant increase in reactive oxygen species (ROS) in both A2780 and OVCAR5 cells after treatment with compound **9b** (Figures 3A-B). Summarizing, as reported in Figure 3C, the lack of caspase 3/7 and Cytochrome C activation excludes apoptotic cell death, while absence of nuclear atypia and cellular swelling/blebbing (data not shown), excludes necrosis cell death suggesting the potential involvement of ferroptosis.[51] The potential implication of ferroptosis in these observations is underscored by its distinction in morphological and biochemical profiles from established programmed cell death pathways, such as apoptosis, necroptosis, pyroptosis, and autophagy.[52] Characterized by a disruption in cellular redox homeostasis, ferroptosis manifests through elevated intracellular reactive oxygen species (ROS) and a reduction in NADPH levels, without the typical features of plasma membrane blebbing, DNA fragmentation, or Caspase-3 activation. Additionally, the lack of activation in the pro-apoptotic proteins Bax and Bak suggests that apoptosis inhibitors do not thwart this mode of cell death.[53]

To further explore the molecular mechanisms underlying the cell death, we proceeded to profile the proteome of OVCAR5 cells following treatment with compound **9b**. From around 2000 proteins studied, label-free LC-MS/MS analysis identified a group of proteins significantly differing in abundance between 1 µM **9b**-treated OVCAR5 versus NT cells ($P_{adjusted}$ <0.05, Figure S2). As shown in Figure 3D this analysis highlighted a statistically significant reduction in the expression of Phospholipid hydroperoxide glutathione peroxidase (GPX4), Ferritin light chain (FTL) and Glutaredoxin-1 (GLRX). It is well-established that the inhibition of GPX4 constitutes a key step in the induction of ferroptosis.[54] This understanding has led us to propose the hypothesis that the cytotoxic effects of compound **9b** observed in OC cell systems could be ascribed to ferroptosis, as illustrated in Figure S3. Ferroptosis induction is closely linked to GPX4 inhibition, which mitigates lipid peroxidation by reducing peroxides using glutathione, thereby safeguarding cells from oxidative stress. Impaired GPX4 function results in ROS build-up and subsequent cell death.[55] Additionally, the ferroptotic mechanism can be facilitated by blocking the synthesis of glutathione (GSH), such as through the inhibition of GLRX, or by the increase in Fe^{3+}, a substrate of the Fenton reaction, caused by an inhibition of FTL (FTL = Formate Tetrahydrofolate Ligase).[56]

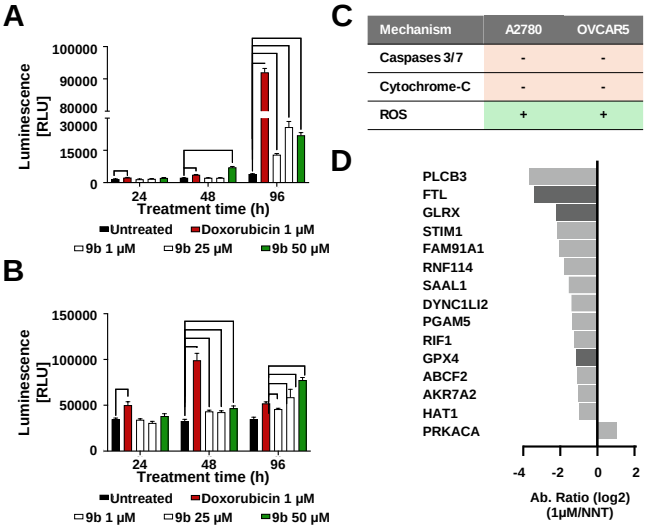

Figure 3. ROS production in OVCAR5 (A) and A2780 (B) cells treated with compound **9b** (1, 25, 50 µM) and Doxorubicin (1 µM as positive control) at 24, 48, and 96-hour intervals; (C) Summary of the assays performed to identify the mechanism of **9b** in A2780 and OVCAR-5: the lack of apoptotic mechanism due to non-activation of caspase 3/7 and Cytochrome-C, and the generation of ROS leads to the hypothesis of a ferroptosis mechanism; (D) Proteomic profile: graphical representation of the abundance (Ab.) of proteins in 1 µM treated OVCAR5 versus NT groups ($P_{adjusted}$ <0.05).

In vivo experiments on an ovarian cancer mouse model

Finally, to test the efficacy of compound **9b** in an *in vivo* model, mice were treated intravenously up to 100 mg/kg. Surprisingly, the body weight of mice does not change (Figure 4A). Following, we compared the effect of compound **9b** to cisplatin in a subcutaneous model of OC. Compound **9b** significantly inhibits the growth of OVCAR5 tumor mass like cisplatin (Figures 4B-C). Even the overall survival of the mice increases significantly compared to untreated mice (Figure 4D). As confirmation, the analyses of body weight of mice do not reveal signs of toxicity (Figure 4A).

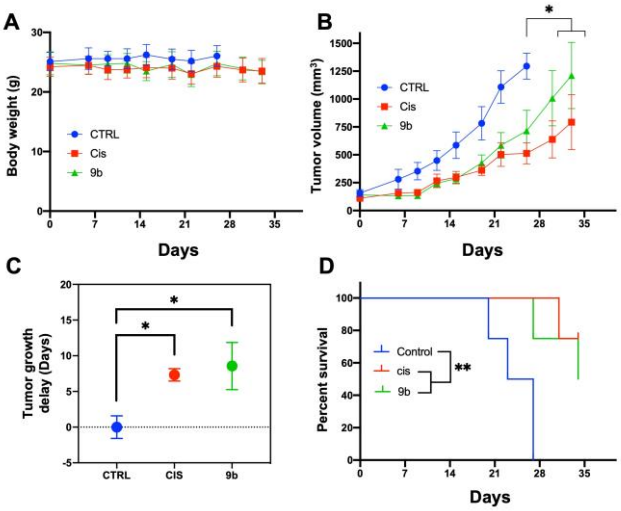

Figure 4: Therapeutic effectiveness (intravenously) in OVCAR5 tumors after treatment with cisplatin or complex **9b** (n=6); (A) Animal body weight after treatment with cisplatin or complex 9b, data represent the mean and standard deviation; (B) Tumor growth curves, data represent the mean and standard error

of the mean. *p*-values were calculated using two-way ANOVA * $p \leq 0.05$; (C) Tumor growth delay of tumors compared to untreated tumors (CTRL), data represent the mean and standard error; (D) Kaplan-Meier survival curve illustrating the percentage of survival over 35 days for a control group, a group treated with cisplatin (Cis), and a group treated with compound **9b**. Both treatment groups exhibit improved survival rates over the control, *p*-values calculated by log-rank test * $p \leq 0.05$.

Conclusion

We have described the synthesis of novel Pd(II)-vinyl and -butadienyl complexes using a simple and stereoselective synthetic route that involved the controlled mono- or bis-insertion of an electron-poor alkyne, followed by the exchange of the pyridyl-thioether ligand with a wide range of mono- and bidentate ligands. All compounds were characterized by NMR, IR, elemental analyses, and, in some cases, by X-ray diffraction.

Most of the synthesized complexes exhibited good to excellent *in vitro* anticancer activity against ovarian, breast, and colon cancer cell lines. Specifically, the performance of the vinyl complexes was comparable to that of their butadienyl congeners, with IC_{50} values in the micro- and sub-micromolar range, often significantly lower than those of cisplatin. Particularly interesting are compounds **8a**, **9a**, and **9b**, which showed excellent activity against all examined tumor lines and reduced cytotoxicity towards MRC-5 non-cancerous cells. Among these derivatives, compound **9b** was selected for further studies on *ex vivo* and *in vivo* models.

Experiments on PDTO derived HGSOC revealed a generally higher cytotoxicity of **9b** compared to carboplatin (standard therapy), even in these more complex biological models. Interestingly, the selectivity of **9b** towards cancer tissues was also confirmed in *ex vivo* models, as it was found to be substantially inactive towards non-cancerous MDO.

This organopalladium compound has proven to be exceedingly effective not only *in vitro* and *ex vivo* (PDTOs) models but has also delivered excellent results in an animal model. It was found to be non-toxic at high dosages and effective in reducing tumor growth in an animal model of HGSOC.

Even more interestingly, a detailed analysis of the mechanism of action of compound **9b** suggests that this organopalladium derivative operates through a ferroptotic mechanism. To the best of our knowledge, this represents the first case of an organopalladium compound inducing tumor cell death through such a biological pathway. In the few cases studied, organopalladium compounds typically operate through apoptotic pathways involving DNA or mitochondrial proteins as the main biotargets.

The completely novel mechanism of action for this class of organopalladium derivatives suggests that it holds considerable promise for future studies in the field of HGSOC, offering a new frontier in the targeted treatment of this challenging cancer subtype.

Experimental Section

Materials and methods

All syntheses of Pd(II)-vinyl and butadienyl complexes were carried out under an atmosphere of argon. Solvents were dried according to standard procedures. Palladium precursors **1a-b**,[36] silver NHC complexes **6**[45d] and **11**,[45b] and palladium complexes **5a-b**[36] were synthesized according to previously published procedures.

All other monodentate/bidentate ligands and $[(PhC{\equiv}C)Sn(n\text{-}Bu)_3$ were purchased from Sigma Aldrich and used without any further purification. ^1H, $^{13}C\{^1H\}$ and $^{31}P\{^1H\}$ NMR spectra were recorded on a Bruker Advance 400 spectrometer at room temperature (298K). The IR spectra were recorded on a Perkin-Elmer Spectrum One spectrophotometer and elemental analysis was carried out using an Elemental CHN "CUBO Micro Vario" analyzer. ESI-MS analyses were performed using a LCQ-Duo (Thermo-Finnigan) operating in positive ion mode (capillary voltage 10 V, spray voltage 4.5 kV, capillary temperature 200 °C, mass scan range from 150 to 2000 amu). X-ray intensity data were collected at 100 K at the XRD2 beamline of the Elettra Synchrotron, Trieste (Italy).

Synthesis of [Pd(1,10-phen)Cl(C_2(COOMe)$_2$$CH_3$)] (2a)

0.0820 g (0.1594 mmol) of the palladium precursor [Pd(Me-PyCH_2SPh)Cl(C_2(COOMe)$_2$$CH_3$)] (**1a**) was dissolved in 15 mL of anhydrous dichloromethane in a 100 mL two-necked flask under inert atmosphere (Ar). Subsequently, 0.0316 g (0.1754 mmol) of 1,10-phenanthroline previously dissolved in ca. 5 mL of CH_2Cl_2 was added. The mixture was stirred at room temperature for 30 min and the solvent was then reduced under vacuum. The final product (pink microcrystalline powder) was precipitated by addition of diethylether and filtered off on a gooch filter.
0.0753 g of **2a** was obtained (yield 98%).

^1H-NMR (300 MHz, $CDCl_3$, T = 298 K, ppm) δ: 2.56 (s, 3H, =CCH_3), 3.76 (s, 3H, OCH_3), 3.86 (s, 3H, OCH_3), 7.85-7.93 (m, 2H, phen-H^3, phen-H^8), 8.00-8.02 (AB system, J = 8.9 Hz, 2H, phen-H^5, phen-H^6), 8.53-8.58 (m, 2H, phen-H^4, phen-H^7), 9.31 (dd, J = 5.2, 1.4 Hz, phen-H^9), 9.48 (dd, J = 5.0, 1.5 Hz, phen-H^2).
$^{13}C\{^1H\}$-NMR (T = 298K, $CDCl_3$, ppm) δ: 21.5 (CH_3, =CCH_3), 51.7 (CH_3, OCH_3), 51.9 (CH_3, OCH_3), 125.3, 125.7 (CH, phen-CH^3, phen-CH^8), 127.0, 127.2 (CH, phen-CH^5, phen-CH^6), 127.3 (C, =CCH_3), 129.6, 130.1 (C, phen-C^{13}, phen-C^{14}), 138.1, 138.2 (CH, phen-CH^4, phen-CH^7), 145.3, 147.1 (C, phen-C^{11}, phen-CH^{12}), 149.6 (CH, phen-CH^9), 153.3 (CH, phen-CH^2), 159.2 (C, Pd-C=), 163.6 (C, CO), 173.7 (C, CO).
IR (KBr pellet): $\nu_{C=O}$ = 1693 cm^{-1}
Elemental analysis calcd (%) for $C_{19}H_{17}ClN_2O_4Pd$: C, 47.62, H, 3.58, N, 5.85; found: C, 47.94, H, 3.40, N, 5.73.

Synthesis of [Pd(1,10-phen)Cl(C_4(COOMe)$_4$$CH_3$)] (2b)

Complex **2b** was prepared using a similar procedure, starting from 0.0820 g (0.1249 mmol) of the precursor [Pd(Me-PyCH_2SPh)Cl(C_4(COOMe)$_4$$CH_3$)] (**1b**) and 0.0584 g (0.1374 mmol) of 1,10-phenanthroline.
0.0692 g (yield 89%) of **2b** was obtained (pink microcrystalline powder). *n*-Hexane/diethylether (1:1) was used instead of diethylether for the precipitation of the title complex.

^1H-NMR (300 MHz, $CDCl_3$, T = 298 K, ppm) δ: 2.17 (s, 3H, =CCH_3), 3.23 (s, 3H, OCH_3), 3.67 (s, 3H, OCH_3), 3.77 (s, 3H, OCH_3), 3.92 (s, 3H, OCH_3), 7.81-7.87 (m, 2H, phen-H^3, phen-H^8), 7.96-7.99 (AB system, J = 8.9 Hz, 2H, phen-H^5, phen-H^6), 8.50-8.55 (m, 2H, phen-H^4, phen-H^7), 9.32 (dd, J = 4.6, 1.4 Hz, phen-H^9), 9.41 (dd, J = 4.6, 1.4 Hz, phen-H^2).

$^{13}C\{^1H\}$-NMR (T = 298K, $CDCl_3$, ppm) δ: 19.2 (CH_3, $=CCH_3$), 51.5 (CH_3, OCH_3), 52.1 (CH_3, OCH_3), 52.2 (CH_3, OCH_3), 52.2 (CH_3, OCH_3), 125.0, 125.1 (CH, phen-CH^3, phen-CH^8), 126.9, 127.2 (CH, phen-CH^5, phen-CH^6), 127.3 (C, $=CCH_3$), 129.6, 129.7 (C, phen-C^{13}, phen-C^{14}), 132.4 (C, C=C), 138.0, 138.2 (CH, phen-CH^4, phen-CH^7), 141.8 (C, C=C), 145.3, 146.9 (C, phen-C^{11}, phen-CH^{12}), 149.6 (CH, phen-CH^9), 154.1 (CH, phen-CH^2), 161.3 (C, CO), 167.3 (C, CO), 167.6 (C, Pd-C=), 170.1 (C, CO), 173.5 (C, CO).
IR (KBr pellet): $\nu_{C=O}$ = 1716, 1728 cm^{-1}
Elemental analysis calcd (%) for $C_{25}H_{23}ClN_2O_8Pd$: C, 48.33, H, 3.73, N, 4.51; found: C, 47.98, H, 3.81, N, 4.60.

Synthesis of [Pd(neocuproine)Cl(C_2(COOMe)$_2$$CH_3$)] (3a)

Complex **3a** was prepared using a similar procedure, starting from 0.0820 g (0.1594 mmol) of the precursor [Pd(Me-PyCH_2SPh)Cl(C_2(COOMe)$_2$$CH_3$)] (**1a**) and 0.0365 g (0.1754 mmol) of neocuproine.
0.0764 g (yield 95%) of **3a** was obtained (yellow microcrystalline powder).

^{1}H-NMR (300 MHz, $CDCl_3$, T = 298 K, ppm) δ: 2.64 (s, 3H, $=CCH_3$), 3.00 (s, 3H, neoc-CH_3), 3.26 (s, 3H, neoc-CH_3), 3.59 (s, 3H, OCH_3), 3.68 (s, 3H, OCH_3), 7.56-7.63 (m, 2H, neoc-H^3, neoc-H^8), 7.81-7.83 (AB system, J = 8.8 Hz, 2H, neoc-H^5, neoc-H^6), 8.25-8.33 (m, 2H, neoc-H^4, neoc-H^7).
$^{13}C\{^1H\}$-NMR (T = 298K, $CDCl_3$, ppm) δ: 21.8 (CH_3, $=CCH_3$), 26.8 (CH_3, neoc-CH_3), 28.5 (CH_3, neoc-CH_3), 51.6 (CH_3, OCH_3), 51.7 (CH_3, OCH_3), 125.5, 125.9 (CH, neoc-CH^3, neoc-CH^8), 126.3, 126.5 (CH, neoc-CH^5, neoc-CH^6), 127.4, 127.5 (C, phen-C^{13}, phen-CH^{14}), 128.7 (C, $=CCH_3$), 137.5, 138.0 (CH, neoc-CH^4, neoc-CH^7), 145.9, 147.3 (C, neoc-C^{11}, neoc-C^{12}), 150.9 (C, Pd-C=), 162.9 (C, CO), 164.6 (C, neoc-CH^9), 165.9 (C, neoc-CH^2), 172.1 (C,CO).
IR (KBr pellet): $\nu_{C=O}$ = 1697, 1711 cm^{-1}
Elemental analysis calcd (%) for $C_{21}H_{21}ClN_2O_4Pd$: C, 49.72, H, 4.17, N, 5.52; found: C, 50.04, H, 4.07, N, 5.42.

Synthesis of [Pd(neocuproine)Cl(C_4(COOMe)$_4$$CH_3$)] (3b)

Complex **3b** was prepared using a similar procedure, starting from 0.0820 g (0.1249 mmol) of the precursor [Pd(Me-PyCH_2SPh)Cl(C_4(COOMe)$_4$$CH_3$)] (**1b**) and 0.0286 g (0.1374 mmol) of neocuproine.
0.0606 g (yield 75%) of **3b** was obtained (yellow microcrystalline powder). *n*-Hexane/diethylether (1:1) was used instead of diethylether for the precipitation of the title complex.

^{1}H-NMR (300 MHz, $CDCl_3$, T = 298 K, ppm) δ: 2.08 (s, 3H, $=CCH_3$), 3.18 (s, 6H, neoc-CH_3), 3.32 (s, 3H, O-CH_3), 3.48 (s, 3H, OCH_3), 3.64 (s, 3H, OCH_3), 3.86 (s, 3H, OCH_3), 7.49-7.52 (m, 2H, neoc-H^3, neoc-H^8), 7.85 (bs, 2H, neoc-H^5, neoc-H^6), 8.27 (d, J = 8.4Hz, 2H, neoc-H^4, neoc-H^7).
$^{13}C\{^1H\}$-NMR (T = 298K, $CDCl_3$, ppm) δ: 20.8 (CH_3, $=CCH_3$), 27.0 (CH_3, neoc-CH_3), 28.6 (CH_3, neoc-CH_3), 51.6 (CH_3, OCH_3), 51.7 (CH_3, OCH_3), 51.8 (CH_3, OCH_3), 51.9 (CH_3, OCH_3), 125.4, 125.7 (CH, neoc-CH^3, neoc-CH^8), 125.7, 126.0 (CH, neoc-CH^5, neoc-CH^6), 129.2 (C, $=CCH_3$), 129.6 (C, C=C), 129.9, (C, phen-C^{13}, phen-CH^{14}), 136.2 (C, C=C), 137.5 (CH, neoc-CH^4, neoc-CH^7), 144.6 (C, neoc-C^{11}, neoc-C^{12}), 155.4 (C, Pd-C=), 162.6 (C, CO), 165.0 (C, neoc-CH^9), 165.0 (C, neoc-CH^2), 162.4 (C, CO), 169.9 (C, CO), 172.2 (C, CO).
IR (KBr pellet): $\nu_{C=O}$ = 1710 cm^{-1}
Elemental analysis calcd (%) for $C_{27}H_{27}ClN_2O_8Pd$: C, 49.94, H, 4.19, N, 4.31; found: C, 50.38, H, 4.05, N, 4.20.

Synthesis of [Pd(dppp)Cl(C_2(COOMe)$_2$$CH_3$)] (4a)

Complex **4a** was prepared using a similar procedure, starting from 0.0820 g (0.1594 mmol) of the precursor [Pd(Me-PyCH_2SPh)Cl(C_2(COOMe)$_2$$CH_3$)] (**1a**) and 0.0745 g (0.1754 mmol) of 1,3-bis(diphenylphosphino)propane (dppp).
0.0888 g (yield 78%) of **4a** was obtained (pink microcrystalline powder).

^{1}H-NMR (300 MHz, $CDCl_3$, T = 298 K, ppm) δ: 1.85 (m, 3H, $=CCH_3$), 1.93-2.66 (m, 6H, CH_2), 3.42 (s, 3H, OCH_3), 3.52 (s, 3H, OCH_3), 7.19-7.93 (m, 30H, Ph).
$^{13}C\{^1H\}$-NMR (T = 298K, $CDCl_3$, ppm) selected peaks, δ: 18.8 (CH_3, $=CCH_3$), 22.1 (CH_2, CH_2 central), 26.1 (dd, CH_2, $J_{C\text{-}P}$ = 22.6, 4.9 Hz, PCH_2), 27.9 (dd, CH_2, $J_{C\text{-}P}$ = 30.1, 9.0 Hz, PCH_2), 51.0 (CH_3, OCH_3), 51.0 (CH_3, OCH_3), 127.5 (C, $=CCH_3$), 170.6 (d, C, $J_{C\text{-}P}$ = 123.9 Hz, Pd-C=), 163.2 (d, C, $J_{C\text{-}P}$ = 15.7, CO), 172.7 (C, CO).
$^{31}P\{^1H\}$-NMR (T = 298K, $CDCl_3$, ppm) δ: -5.6 (d, $J_{P\text{-}P}$ = 49.1 Hz), 15.3 (d, $J_{P\text{-}P}$ = 49.1 Hz)
IR (KBr pellet): $\nu_{C=O}$ = 1702 cm^{-1}
Elemental analysis calcd (%) for $C_{34}H_{35}ClO_4P_2Pd$: C, 57.40, H, 4.96; found: C, 57.17, H, 5.11.

Synthesis of [Pd(dppp)Cl(C_4(COOMe)$_4$$CH_3$)] (4b)

Complex **4b** was prepared using a similar procedure, starting from 0.0820 g (0.1249 mmol) of the precursor [Pd(Me-PyCH_2SPh)Cl(C_4(COOMe)$_4$$CH_3$)] (**1b**) and 0.0584 g (0.1374 mmol) of 1,3-bis(diphenylphosphino)propane (dppp).
0.0991 g (yield 93%) of **4b** was obtained (orange microcrystalline powder). *n*-Hexane/diethylether (1:1) was used instead of diethylether for the precipitation of the title complex.

^{1}H-NMR (300 MHz, $CDCl_3$, T = 298 K, ppm) δ: 1.18 (m, 3H, $=CCH_3$), 2.17-3.00 (m, 6H, CH_2), 3.51 (s, 3H, OCH_3), 3.65 (s, 3H, OCH_3), 3.78 (s, 3H, OCH_3), 3.83 (s, 3H, OCH_3), 7.02-7.86 (m, 30H, Ph).
$^{13}C\{^1H\}$-NMR (T = 298K, $CDCl_3$, ppm) selected peaks, δ: 16.4 (CH_3, $=CCH_3$), 22.1 (CH_2, CH_2 central), 26.1 (dd, CH_2, $J_{C\text{-}P}$ = 22.6, 6.4 Hz, PCH_2), 25.9 (dd, CH_2, $J_{C\text{-}P}$ = 29.8, 7.2 Hz, PCH_2), 51.4 (CH_3, OCH_3), 51.6 (CH_3, OCH_3), 52.2 (CH_3, OCH_3), 53.1 (CH_3, OCH_3), 164.7 (d, C, $J_{C\text{-}P}$ = 14.8, CO), 168.4 (C, CO), 170.2 (C, CO),172.8 (C, CO), (the four signals C=C are not detectable).
$^{31}P\{^1H\}$-NMR (T = 298K, $CDCl_3$, ppm) δ: -5.0 (d, $J_{P\text{-}P}$ = 45.5 Hz), 11.3 (d, $J_{P\text{-}P}$ = 45.5 Hz).
IR (KBr pellet): $\nu_{C=O}$ = 1713 cm^{-1}
Elemental analysis calcd (%) for $C_{40}H_{41}ClO_8P_2Pd$: C, 56.29, H, 4.84; found: C, 56.50, H, 4.73.

Synthesis of [Pd(BnImCH$_2$ImBn)Cl(C_4(COOMe)$_4$$CH_3$)] (7b)

Complex **7b** was prepared using a similar procedure, starting from 0.0820 g (0.1249 mmol) of the precursor [Pd(Me-PyCH_2SPh)Cl(C_4(COOMe)$_4$$CH_3$)] (**1b**) and 0.0767 g (0.1249

mmol) of silver complex **6** (AgBr was removed after 30 min by filtration on millipore membrane filter).
0.0937 g (yield 97%) of **7b** was obtained (brownish microcrystalline powder).

^{1}H-NMR (300 MHz, $CDCl_3$, T = 298 K, ppm) δ: 2.34 (s, 3H, $=CCH_3$), 3.37 (s, 3H, OCH_3), 3.56 (s, 3H, OCH_3), 3.74 (s, 3H, OCH_3), 3.79 (s, 3H, OCH_3), 4.79-6.29 (AB system, J = 14.8 Hz, 2H, CH_2Ph), 5.09-6.27 (AB system, J = 15.0 Hz, 2H, CH_2Ph), 5.42-6.75 (AB system, J = 13.2 Hz, 2H, NCH_2N), 6.51 (d, J = 2.1 Hz, 1H, $CH=CH^{Im}$), 6.65 (d, J = 1.9 Hz, 1H, $CH=CH^{Im}$), 6.90 (d, J = 1.9 Hz, 1H, $CH=CH^{Im}$), 6.91 (d, J = 2.1 Hz, 1H, $CH=CH^{Im}$), 7.21-7.35 (10H, Ar-H).
^{13}C{^{1}H}-NMR (T = 298K, $CDCl_3$, ppm) δ: 20.9 (CH_3, $=CCH_3$), 51.3 (CH_3, OCH_3), 51.6 (CH_3, OCH_3), 52.2 (CH_3, OCH_3), 54.3 (CH_2, CH_2Ph), 54.9 (CH_2, CH_2Ph), 63.6 (CH_2, NCH_2N), 119.5 (CH, $CH=CH^{Im}$), 119.8 (CH, $CH=CH^{Im}$), 120.7 (CH, $CH=CH^{Im}$), 121.0 (CH, $CH=CH^{Im}$), 127.0-146.1 (Ar-C, C=C), 163.9 (C, CO), 165.3 (C, CO), 166.0 (C, carbene), 169.6 (C, Pd-C=), 172.6 (C, CO), 175.0 (C, carbene), 175.8 (C, CO).
IR (KBr pellet): $\nu_{C=O}$ = 1713 cm^{-1}
Elemental analysis calcd (%) for $C_{34}H_{35}ClN_4O_8Pd$: C, 53.07, H, 4.58, N, 7.28; found: C, 53.40, H, 4.46, N, 7.19.

Synthesis of *trans*-[Pd(PPh$_3$)$_2$Cl(C$_2$(COOMe)$_2$CH$_3$)] (8a)

Complex **8a** was prepared using a similar procedure, starting from 0.0820 g (0.159 mmol) of the precursor [Pd(Me-PyCH$_2$SPh)Cl(C$_2$(COOMe)$_2$CH$_3$)] (**1a**) and 0.0920 g (0.351 mmol) of triphenylphosphine (PPh_3).
0.1120 g (yield 86%) of **8a** was obtained (pale-yellow microcrystalline powder).

^{1}H-NMR (300 MHz, $CDCl_3$, T = 298 K, ppm) δ: 7.72 (m, 12H, Ar-H), 7.40 (m, 18H), 3.42 (s, 3H, $COOCH_3$), 3.13 (s, 3H, $COOCH_3$), 1.22 (t, $J_{H\text{-}P}$ = 1.2 Hz, 3H, $=C\text{-}CH_3$).
^{13}C{^{1}H}-NMR (T= 298K, $CDCl_3$, ppm) δ: 22.1 (CH_3, $=CCH_3$), 50.3 (CH_3, OCH_3), 50.7 (CH_3, OCH_3), 127.7-135.0 (Ar-C, $=CCH_3$, C=C), 164.0 (C, CO), 167.2 (C, Pd-C=), 170.6 (C, CO).
^{31}P{^{1}H} NMR ($CDCl_3$, T = 298 K, ppm) δ: 26.0.
IR (KBr pellet): $\nu_{C=O}$ = 1709 cm^{-1}
Elemental analysis calcd (%) for $C_{43}H_{39}ClO_4P_2Pd$: C, 62.71, H, 4.77; found: C, 62.86, H, 4.63.

Synthesis of *trans*-[Pd(PPh$_3$)$_2$Cl(C$_4$(COOMe)$_4$CH$_3$)] (8b)

Complex **8b** was prepared using a similar procedure, starting from 0.1000 g (0.1520 mmol) of the precursor [Pd(Me-PyCH$_2$SPh)Cl(C$_4$(COOMe)$_4$CH$_3$)] (**1b**) and 0.0880 g (0.336mmol) of triphenylphosphine (PPh_3).
0.1370 g (yield 93%) of **9b** was obtained (pale orange microcrystalline powder).

^{1}H-NMR (300 MHz, $CDCl_3$, T = 298 K, ppm) δ: 7.68 (m, 12H, Ar-H), 7.37 (m, 18H), 3.74 (s, 3H, $COOCH_3$), 3.56 (s, 3H, $COOCH_3$) 3.33 (s, 3H, $COOCH_3$), 2.94 (s, 3H, $COOCH_3$), 0.82 (t, 3H, $=C CH_3$).
^{13}C{^{1}H}-NMR (T= 298K, $CDCl_3$, ppm) δ: 15.4 (CH_3, $=CCH_3$), 51.0 (CH_3, OCH_3), 51.7 (CH_3, OCH_3), 52.2 (CH_3, OCH_3), 52.3 (CH_3, OCH_3), 127.8-136.5 (Ar-C, C=C), 165.4 (C, Pd-C=), 167.4 (C, CO), 168.0 (C, CO), 168.8 (C, CO), 171.1 (C, CO).
^{31}P{^{1}H} NMR ($CDCl_3$, T = 298, ppm) δ: 20.5.
IR (KBr pellet): $\nu_{C=O}$ = 1709 cm^{-1}
Elemental analysis calcd (%) for $C_{49}H_{45}ClO_8P_2Pd$: C, 60.94, H, 4.70; found: C, 60.69, H, 4.81.

Synthesis of *trans*-[Pd(PTA)$_2$Cl(C$_2$(COOMe)$_2$CH$_3$)] (9a)

Complex **9a** was prepared using a similar procedure, starting from 0.0820 g (0.1594 mmol) of the precursor [Pd(Me-PyCH$_2$SPh)Cl(C$_2$(COOMe)$_2$CH$_3$)] (**1a**) and 0.0526 g (0.3348 mmol) of 1,3,5-triaza-7-phosphaadamantane (PTA).
0.0938 g (yield 96%) of **9a** was obtained (white microcrystalline powder).

^{1}H-NMR (300 MHz, CD_2Cl_2, T = 298 K, ppm) δ: 2.49 (t, J_{HP} = 1.4 Hz, 3H, $=CCH_3$), 3.68 (s, 3H, OCH_3), 3.79 (s, 3H, OCH_3), 4.25 (s, 12H, NCH_2P), 4.51 (s, 12H, NCH_2N).
^{13}C{^{1}H}-NMR (T= 298K, CD_2Cl_2, ppm) δ: 22.7 (CH_3, $=CCH_3$), 50.3 (*pseudo*-t, CH_2, NCH_2P), 51.4 (CH_3, OCH_3), 51.5 (CH_3, OCH_3), 73.1 (CH_2, NCH_2N), 125.8 (C, $=CCH_3$), 157.4 (t, C, $J_{C\text{-}P}$ = 10.2 Hz, Pd-C=), 163.2 (C, CO), 172.2 (C, CO).
^{31}P{^{1}H}-NMR (T=298K, CD_2Cl_2, ppm) δ: -59.3.
IR (KBr pellet): $\nu_{C=O}$ = 1709 cm^{-1}
Elemental analysis calcd (%) for $C_{19}H_{33}ClN_6O_4P_2Pd$: C, 37.21, H, 5.42, N, 13.70; found: C, 37.40, H, 5.33, N, 13.58.

Synthesis of *trans*-[Pd(PTA)$_2$Cl(C$_4$(COOMe)$_4$CH$_3$)] (9b)

Complex **9b** was prepared using a similar procedure, starting from 0.0820 g (0.1249 mmol) of the precursor [Pd(Me-PyCH$_2$SPh)Cl(C$_4$(COOMe)$_4$CH$_3$)] (**1b**) and 0.0412 g (0.2623 mmol) of 1,3,5-triaza-7-phosphaadamantane (PTA).
0.0860 g (yield 91%) of **9b** was obtained (pale orange microcrystalline powder).

^{1}H-NMR (300 MHz, $CDCl_3$, T = 298 K, ppm) δ: 1.95 (s, 3H, $=CCH_3$), 3.74 (s, 3H, OCH_3), 3.82 (s, 3H, OCH_3), 3.83 (s, 3H, OCH_3), 3.89 (s, 3H, OCH_3),4.29 (m, 12H, NCH_2P), 4.51 (m, 12H, NCH_2N).
^{13}C{^{1}H}-NMR (T= 298K, $CDCl_3$, ppm) δ: 17.6 (CH_3, $=CCH_3$), 50.3 (*pseudo*-t, CH_2, NCH_2P), 50.0 (CH_3, OCH_3), 52.3 (CH_3, OCH_3), 52.6 (CH_3, OCH_3), 52.9 (CH_3, OCH_3), 73.2 (CH_2, NCH_2N), 127.8 (C, $=CCH_3$), 135.4 (C, C=C), 136.4 (C, C=C), 162.4 (C, CO), 168.1 (C, CO), 168.9 (C, CO), 170.3 (t, C, $J_{C\text{-}P}$ = 9.8 Hz, Pd-C=), 172.4 (C, CO).
^{31}P{^{1}H}-NMR (T=298K, $CDCl_3$, ppm) δ: -55.8.
IR (KBr pellet): $\nu_{C=O}$ = 1718 cm^{-1}
Elemental analysis calcd (%) for $C_{25}H_{39}ClN_6O_8P_2Pd$: C, 39.75, H, 5.20, N, 11.12; found: C, 40.01, H, 5.09, N, 11.04.

Synthesis of *trans*-[Pd(AsPh$_3$)$_2$Cl(C$_2$(COOMe)$_2$CH$_3$)] (10a)

Complex **10a** was prepared using a similar procedure, starting from 0.0820 g (0.1594 mmol) of the precursor [Pd(Me-PyCH$_2$SPh)Cl(C$_2$(COOMe)$_2$CH$_3$)] (**1a**) and 0.1025 g (0.3348 mmol) of triphenylarsine ($AsPh_3$).
0.1272 g (yield 87%) of **10a** was obtained (white microcrystalline powder). *n*-Hexane/diethylether (1:1) was used instead of diethylether for the precipitation of the title complex.

^{1}H-NMR (300 MHz, $CDCl_3$, T = 298 K, ppm) δ: 1.39 (s, 3H, $=CCH_3$), 3.09 (s, 3H, OCH_3), 3.38 (s, 3H, OCH_3), 7.35-7.46 (m, 18H, Ph), 7.68-7.71 (m, 12H, Ph).

$^{13}C\{^1H\}$-NMR (T= 298K, $CDCl_3$, ppm) δ: 22.0 (CH_3, $=CCH_3$), 50.5 (CH_3, OCH_3), 50.9 (CH_3, OCH_3), 128.5 (CH, CH-Ph), 128.6 (C, $=CCH_3$), 129.9 (CH, CH-Ph), 132.7 (C, C-Ph), 134.2 (CH, CH-Ph), 160.8 (C, Pd-C=), 162.9 (C, CO), 170.7 (C, CO).
IR (KBr pellet): $\nu_{C=O}$ = 1701 cm^{-1}
Elemental analysis calcd (%) for $C_{43}H_{39}As_2ClO_4Pd$: C, 56.66, H, 4.31; found: C, 56.90, H, 4.19.

Synthesis of *trans*-[Pd(AsPh$_3$)$_2$Cl(C$_4$(COOMe)$_4$CH$_3$)] (10b)

Complex **10b** was prepared using a similar procedure, starting from 0.0820 g (0.1249 mmol) of the precursor [Pd(Me-PyCH$_2$SPh)Cl(C$_4$(COOMe)$_4$CH$_3$)] (**1b**) and 0.0803 g (0.2623 mmol) of triphenylarsine ($AsPh_3$).
0.1202 g (yield 91%) of **10b** was obtained (pale orange microcrystalline powder). *n*-Hexane/diethylether (1:1) was used instead of diethylether for the precipitation of the title complex.

^1H-NMR (300 MHz, $CDCl_3$, T = 298 K, ppm) δ: 0.84 (s, 3H, $=CCH_3$), 2.92 (s, 3H, OCH_3), 3.40 (s, 3H, OCH_3), 3.60 (s, 3H, OCH_3), 3.74 (s, 3H, OCH_3), 7.33-7.44 (m, 20H, Ph), 7.69-7.71 (m, 10H, Ph).
$^{13}C\{^1H\}$-NMR (T= 298K, $CDCl_3$, ppm) δ: 15.2 (CH_3, $=CCH_3$), 50.9 (CH_3, OCH_3), 51.8 (CH_3, OCH_3), 52.2 (CH_3, OCH_3), 52.5 (CH_3, OCH_3), 128.4 (CH, CH-Ph), 128.6 (C, $=CCH_3$), 129.8 (CH, CH-Ph), 133.0 (C, C-Ph), 134.4 (CH, CH-Ph), 135.1 (C, C=C), 136.6 (C, C=C), 163.8 (C, CO), 165.3 (C, Pd-C=), 168.0 (C, CO), 168.7 (C, CO), 171.2 (C, CO).
IR (KBr pellet): $\nu_{C=O}$ = 1697, 1723 cm^{-1}
Elemental analysis calcd (%) for $C_{49}H_{45}As_2ClO_8Pd$: C, 55.86, H, 4.31; found: C, 59.01, H, 4.22.

Synthesis of *trans*-[Pd(PTA)$_2$(C≡C-Ph)(C$_2$(COOMe)$_2$CH$_3$)] (13)

0.0795 g (0.1297 mmol) of **9a** was dissolved in 7 mL of anhydrous dichloromethane in a 50 mL two-necked flask under inert atmosphere (Ar). Subsequently, 0.0670 g (60 µL, 0.1712 mmol) of [(PhC≡C)Sn(*n*-Bu)$_3$] was added. The mixture was stirred at room temperature for 3 hours and the solvent was then removed under vacuum. The final product (white microcrystalline powder) was triturated with *n*-hexane/diethylether (1:1) and filtered off on a gooch filter.
0.0828 g of **13** was obtained (yield 94%).

^1H-NMR (300 MHz, CD_2Cl_2, T = 298 K, ppm) δ: 2.03 (t, $J_{H\text{-}P}$ = 1.3 Hz, 3H, $=CCH_3$), 3.67 (s, 3H, OCH_3), 3.74 (s, 3H, OCH_3), 4.33 (s, 12H, NCH_2P), 4.54 (s, 12H, NCH_2N), 7.21-7.40 (m, 5H, Ph).
$^{13}C\{^1H\}$-NMR (T = 298K, $CDCl_3$, ppm) δ: 22.7 (CH_3, $=CCH_3$), 51.1 (CH_3, OCH_3), 51.6 (CH_3, OCH_3), 52.0 (*pseudo*-t, CH_2, NCH_2P), 73.3 (CH_2, NCH_2N), 101.4 (t, C, $J_{C\text{-}P}$ =23.1Hz, ≡C-Pd), 115.0 (C, ≡C-Ph), 126.2 (CH, CH-Ph), 126.6 (C, $=CCH_3$), 126.7 (C, C-Ph), 128.2 (CH, CH-Ph), 131.1 (CH, CH-Ph), 163.9 (C, CO), 168.0 (t, C, $J_{C\text{-}P}$ = 11.1 Hz, Pd-C=), 175.3 (C, CO).
$^{31}P\{^1H\}$-NMR (T=298K, CD_2Cl_2, ppm) δ: -58.5.
IR (KBr pellet): $\nu_{C=O}$ = 1701, $\nu_{C\equiv C}$ = 2100 cm^{-1}
Elemental analysis calcd (%) for $C_{27}H_{38}ClN_6O_4P_2Pd$: C, 47.76, H, 5.64, N, 12.38; found: C, 47.50, H, 5.73, N, 12.51.

Cell viability assay

Cells were grown in agreement with the supplier and incubated at 37°C (5% of CO_2). 1.5 x 10^3 cells were plated in 96 wells and treated with six different concentrations of palladium compounds (0.001, 0.01, 0.1, 1, 10, and 100 µM). After 96 hours, cell viability was evaluated with CellTiter glow assay (Promega, Madison, WI, USA) with a Tecan M1000 instrument. IC_{50} values were obtained from triplicates, and error bars are standard deviations.

PDTOs culture and viability assay

Specimens were completely de-identified prior to use, and consent for research utilization was secured through the biobank at the National Cancer Institute (CRO) in Aviano.
Clusters of cells from ascites was isolated by spinning at 1,000 rpm for 10 minutes and then washed twice with two rounds of HBSS (Gibco, Massachusetts, United States). To remove erythrocytes, the samples were treated with a chilled erythrocyte lysis solution (Roche Diagnostics, Basel, Switzerland) while stirring on ice for 10 minutes. After another centrifugation at 1,000 rpm for 10 minutes, the resulting cell pellet was suspended in Geltrex™ Reduced Growth Factor Basement Membrane Matrix (Gibco, Massachusetts, United States). For solid tumors, the protocol included a 30-minutes incubation in a cocktail of antibiotics and antifungal agents in Dulbecco's Modified Eagle Medium/Nutrient Mixture F-12 Ham, followed by mincing into 0.5–1 mm^3 fragments and enzymatic dissociation using a 4 mg/mL collagenase IV (Gibco, Massachusetts, United States) solution at 37°C for a maximum of 45 minutes. The resulting clusters of cells were again spun down, reconstituted in Geltrex™ Reduced Growth Factor Basement Membrane Matrix, and plated in a 24-well format. Following Geltrex™ solidification, the organoids were maintained in a specialized medium as specified by Kopper et al., refreshed triweekly, and incubated at 37°C with a 5% CO_2 atmosphere.[57] Clusters of organoids were mixed in an appropriate volume of Geltrex™ Reduced Growth Factor Basement Membrane matrix and 2 µL of this mixture was seeded in 96-wells plates in four replicates. The organoids were treated with six different concentrations of carboplatin and compound **9b**. After 96 h, cell viability was measured using CellTiter-Glo 3D (Promega, Madison, WI, United States). The luminescence was acquired with BioTek Synergy H1 instrument.

ROS production

A2780 and OVCAR5 cells were plated in a 96-well plate at a concentration of $1.5 \cdot 10^3$ cells per well. Cells were treated at the predetermined time points (24, 48, and 96 hours) with compound **9b** at concentrations of 1, 25, and 50 µM. Doxorubicin at 1 µM was used as a positive control. After 96 hours from the seeding, ROS production was evaluated using the ROS-Glo™ H_2O_2 Assay (catalog no. G8821, Promega) with BioTek Synergy H1 instrument.

Caspases activity

A2780 and OVCAR5 cells were plated in a 96-well plate at a concentration of $1.5 \cdot 10^3$ cells per well. Cells were treated at the predetermined time points (24, 48, and 96 hours) with compound **9b** at concentrations of 1, 25, and 50 µM. Doxorubicin at 1 µM was used as a positive control. After 96 hours from the seeding, ROS production was evaluated using the Caspase-Glo® 3/7

Assay (catalog no. G8090, Promega) with BioTek Synergy H1 instrument.

Cytochrome C release assay

To assess the release of cytochrome C from the mitochondrial membrane, OVCAR-5 cells were seeded on 8-well chamber slides (20000 cells per well). Cells were placed in incubator overnight (37 °C, 5% CO_2) and then treated with compound **9b** at the concentration 0.1 µM, 1 µM and 10 µM for 3, 6, 24, 48, 72 and 96 hours. A negative and a positive controls (for positive control, cisplatin at the concentration 10 µM was used) were considered for each timepoint. At the end of the treatment, the medium was removed from each well and cells were fixed in 4% paraformaldehyde (DPBS solution; incubation for 20 min at room temperature), permeabilized with a 3% solution of Triton-X-100 in DPBS (incubation for 15 min at room temperature) and then blocked in 8% BSA (DPBS solution; incubation for 1 h at room temperature). Cells were subsequently incubated overnight with a 1% BSA solution in DPBS with the primary antibody (Cytochrome C (6H2.B4) Mouse mAb, cat. #12963, Cell Signaling, Danvers, MA, USA) (1:100 dilution). Each well was washed three times with DPBS and then the secondary antibody (Goat anti-Mouse IgG (H+L) Highly Cross-Adsorbed Secondary Antibody, Alexa Fluor™ Plus 488, cat. # A32723, Invitrogen, Waltham, MA, USA) was added (1:1000 dilution in 1% BSA solution in DPBS). After 1 h of incubation, cells were washed three times with DPBS and subsequently stained with DAPI 0.1 µg/mL (DBPS solution; incubation for 1 min at room temperature) to visualize nuclei. Cells were washed three times with DPBS and finally the slides were mounted with a mounting solution (FluorSave™ Reagent, cat. # 345789, Millipore, Burlington, MA, USA). Each slide was examined using the confocal microscope NIKON Eclipse TI2 (equipped with X-Light V2 L-FOV spinning disk and lumencore lamp) and the fluorescent images were analysed with NIS software.

Proteomic Analysis

Proteins were extracted from a minimum of $5 \cdot 10^6$ ovarian cancer cells belonging to the following groups: (i) NT and (ii) 1 µM with a lysis buffer (Thermo Fisher Scientific, Massachusetts, USA) containing Universal Nuclease (Thermo Fisher Scientific), 1 x protease inhibitor cocktail (Thermo Fisher Scientific) and 0.1% (w/v) RapiGest SF (Waters, Massachusetts, USA). Protein concentration was measured with the Pierce BCA Protein Assay Kit (Thermo Fisher Scientific). Protein extracts were immediately subjected to further down-stream analyses.
Briefly, proteins (100 µg) were reduced, alkylated and digested and peptides cleaned-up with the EasyPep Mini MS Sample Prep Kit (Thermo Fisher Scientific) according to the manufacturer's protocol. The extracted peptides were lyophilized and then resuspended in 50 µL of 0.1% formic acid before analysis by LC-MS/MS. Peptide concentration was measured with the Pierce BCA Protein Assay Kit (Thermo Fisher Scientific). Three biological replicates were analyzed per group.
The digested peptide mixtures were analyzed with LC-MS/MS, using a Q-Exactive Plus Hybrid Orbitrap mass spectrometer equipped with a UHPLC Vanquish (Thermo Fisher Scientific). Individual samples (loading amount 15 µg) were analyzed in duplicate. Each peptide sample was fractionated in a XBridge Peptide BEH C18 column (3.5 µm 2.1 x 150, Waters, Sesto San Giovanni, Milan, Italy) at a total flow rate of 200 µL/min using 0.1% formic acid/acetonitrile gradient over a period of 61.5 min and sprayed onto the mass spectrometer using a heated electrospray source probe in positive mode (Thermo Fisher Scientific). Acetonitrile, formic acid and water, all LC-MS grade, were purchased from Sigma Aldrich Srl (Milan, Italy). The mass spectrometer was run in a data-dependent mode with positive polarity. The full scan was performed between 375 and 1500 m/z followed by MS/MS scans on the top 10 intense ion. Raw MS files were analysed and searched against the human database (UniProt release 2022_02) using Proteome Discoverer software (version 2.5.0.400) and its Sequest search engine. Relative protein amount across our samples was determined for most of the identified proteins through label-free quantification (LFQ). Only proteins identified with a high false discovery rate (FDR) (1%), Score Sequest>1 and unique peptides>1 were considered. All potential contaminants coming from culture media were filtered. The abundance ratio (or fold change, FC) of statistically significant proteins was calculated as the ratio of the average LFQ values between the two matched groups. Proteins differing in abundance between the two groups were defined as those with a FC≥2 (FC Log2≥1) (proteins increasing in abundance) or a FC≤2 (FC Log2≤-1) (proteins decreasing in abundance), grouped abundances CV (%) < 30 and FC $P_{adjusted}$ <0.05.

In vivo experiments

Animal experiments were approved by the National Ethical Committee and the Administration of the Republic of Slovenia for Food Safety, Veterinary and Plant Protection. Mice from Envigo were housed in filtertop cages (2–5 per cage) with bedding and enrichment materials (paper towel) and under controlled conditions of temperature (22 ± 2 ˚C), humidity (55 ± 10%), and light (12 h/12 h light–dark cycle) with unlimited access to food and water.

Tumor induction

OVCAR5 cells were cultured, harvested after trypsinization, and suspended in a saline solution enriched with 30% Matrigel HC (Corning) to a density of $3 \cdot 10^7$ cells/mL. Subsequently, 100 µL of this suspension was subcutaneously injected into the flank of mice. The mice were maintained under specific pathogen-free conditions in a carousel mouse IVC rack system (Animal Care Systems Inc., USA), with environmental controls set to 55 ± 10% humidity and temperatures between 20–24 °C, under a 12-hour light/dark cycle. They had continuous access to sterile food and water.

Efficacy study

Upon reaching a volume of 100 mm^3, tumor-bearing mice were assorted into different groups: a control group (CTRL), a cisplatin treatment group (CIS), and a group receiving compound **9b** (9b). The treatments were administered intravenously in 100 µL volumes, with cisplatin dosed at 1 mg/kg and **9b** at 100 mg/kg, on days 0, 6, 9, 12, 16, 20, 23, 27, 31, and 34. Tumor sizes were measured three times weekly using Vernier calipers, and volumes

calculated using the formula V = ½(Length × Width^2). To evaluate tumor growth delay, we identified the time it took for each tumor to double in size from its volume at the start of treatment. We then determined the tumor growth delay for each tumor by deducting its individual tumor doubling time from the average doubling time of the control group's tumors. The average tumor growth delay was calculated for each treatment group. Animal well-being was monitored during the experiment by weighing the animal and visual inspection.

XRD analysis

2a, **2b**, **3b**, **5a** and **13** crystals data were collected at the XRD1 and XRD2 beamlines of the Elettra Synchrotron, Trieste (Italy),[58] using a monochromatic wavelength of 0.620 Å, at 100K. The data sets were integrated, scaled and corrected for Lorentz, absorption and polarization effects using XDS package.[59] Data from two random orientations have been merged to obtain complete datasets for the triclinic **2a**, **2b**, **3b** and **13** crystal forms, using CCP4-Aimless code.[60] The structures were solved by direct methods using SHELXT program[61] and refined using full−matrix least−squares implemented in SHELXL−2018/3.[62]
Thermal motions for all non−hydrogen atoms have been treated anisotropically and hydrogens have been included on calculated positions, riding on their carrier atoms. Geometric and thermal restrains (SAME, FLAT, SIMU) have been applied to disordered fragments in **13**. The Coot program was used for structure building.[63] The crystal data are given in Table S1. Pictures were prepared using Ortep3[64] and Pymol[65] softwares.
Crystallographic data have been deposited at the Cambridge Crystallographic Data Centre and allocated the deposition number CCDC 2343666, 2343667, 2343668, 2343670 and 2343669 for **2a**, **2b**, **3b**, **5a** and **13**, respectively. These data can be obtained free of charge via https://www.ccdc.cam.ac.uk/structures.

Acknowledgements

We are grateful to the BOF (starting and senior grants) and the FWO to SPN for financial support. FR was financially supported by Fondazione AIRC per la Ricerca sul Cancro (Grant AIRC IG23566) and VC from Ministero della Salute – Ricerca Corrente.

Keywords: Organopalladium complexes • Anticancer activity • *In vivo* and *ex vivo* studies • Organoids • Ferroptosis • High-grade serous ovarian cancer

[1] G. C. Jayson, E. C. Kohn, H. C. Kitchener, J. A. Ledermann, *Lancet* **2014**, *384*, 1376–1388.
[2] D. T. Le, J. N. Durham, K. N. Smith, H. Wang, B. R. Bartlett, L. K. Aulakh, S. Lu, H. Kemberling, C. Wilt, B. Luber, F. Wong, N. S. Azad, A. A. Rucki, D. Laheru, R. C. Donehower, A. Zaheer, G. A. Fisher, T. S. Crocenzi, J. J. Lee, T. F. Greten, A. G. Duffy, K. K. Ciombor, A. Eyring, B. Lam, A. K. Joe, S. P. Kang, M. Holdhoff, L. Danilova, L. Cope, C. F. Meyer, S. Zhou, R. M. Goldberg, D. K. Armstrong, K. M. Bever, A. N. Fader, J. M. Taube, F. Housseau, D. Spetzler, N. Xiao, D. M. Pardoll, N. Papadopoulos, K. W. Kinzler, J. R. Eshleman, B. Vogelstein, R. A. Anders, L. A. Díaz, *Science* **2017**, *357*, 409–413.
[3] U. A. Matulonis, R. Shapira-Frommer, A. D. Santin, A. Lisyanskaya, S. Pignata, I. Vergote, F. Raspagliesi, G. S. Sonke, M. J. Birrer, D. Provencher, J. Sehouli, N. Colombo, A. González-Martín, A. Oaknin, P. B. Ottevanger, V. Rudaitis, K. Katchar, H. Wu, S. M. Keefe, J. Ruman, J. A. Ledermann, *Ann. Oncol.* **2019**, *30*, 1080–1087.
[4] a) S. Pignata, S. C. Cecere, A. Du Bois, P. Harter, F. Heitz, *Ann. Oncol.* **2017**, *28*, 51–56; b)
[5] L. A. Torre, B. Trabert, C. DeSantis, K. D. Miller, G. Samimi, C. D. Runowicz, M. M. Gaudet, A. Jemal, R. L. Siegel, *Ca* **2018**, *68*, 284–296.
[6] D. Mauricio, S. Bellone, L. Mutlu, B. McNamara, D. Manavella, C. Demirkiran, M. S. Verzosa, N. Buza, P. Hui, T. M. P. Hartwich, J. Harold, Y. Yang-Hartwich, M. Zipponi, G. Altwerger, E. Ratner, G. S. Huang, M. Clark, V. Andikyan, M. Azodi, P. E. Schwartz, A. D. Santin, *Gynecol. Oncol.* **2023**, *170*, 38–45.
[7] H. Suzuki, S. Nagase, C. Saito, A. Takatsuka, M. Nagata, K. Honda, Y. Kaneda, Y. Nishiya, T. Honda, T. Ishizaka, K. Nakamura, T. Nakada, Y. Abe, T. Agatsuma, *Mol. Cancer Ther.* **2024**, DOI 10.1158/1535-7163.mct-23-0287.
[8] Y.-A. Heo, *Drugs* **2023**, *83*, 265–273.
[9] B. Feroz, C. Marth, A. G. Zeimet, *Mag. Eur. Med. Oncol.* **2024**, DOI 10.1007/s12254-024-00959-9.
[10] a) Z. Liu, Y. Zhang, W. Lu, Y. Han, J. Yang, W. Jiang, X. You, Y. Luo, S. Wen, Y. Hu, P. Huang, *Redox Biol.* **2020**, *36*, 101652; b) X. Song, X. Wang, Z. Liu, Z. Yu, *Front. Oncol.* **2020**, *10*, DOI 10.3389/fonc.2020.597434; c) N. Vasan, J. Baselga, D. M. Hyman, *Nature* **2019**, *575*, 299–309; d) X. Wang, H. Zhang, X. Chen, *Cancer Drug Resist.* **2019**, DOI 10.20517/cdr.2019.10.
[11] a) W. Dong, M. A. Keibler, G. Stephanopoulos, *Metab. Eng.* **2017**, *43*, 113–124; b) J. V. Voorde, T. Ackermann, N. Pfetzer, D. Sumpton, G. Mackay, G. Kalna, C. Nixon, K. Blyth, E. Gottlieb, S. Tardito, *Sci. Adv.* **2019**, *5*, DOI 10.1126/sciadv.aau7314; c) J. D. Weyandt, C. B. Thompson, A. J. Giaccia, W. K. Rathmell, *Am. Soc. Clin. Oncol. Educ. Book* **2017**, 825–832.
[12] a) J. Roh, E. H. Kim, H. J. Jang, J. Y. Park, D. Shin, *Cancer Lett.* **2016**, *381*, 96–103; b) M. J. Hangauer, V. S. Viswanathan, M. Ryan, D. Bole, J. K. Eaton, A. Matov, J. Galeas, H. D. Dhruv, M. E. Berens, S. L. Schreiber, F. McCormick, M. T. McManus, *Nature* **2017**, *551*, 247–250; c) L. F. Ye, K. Chaudhary, F. Zandkarimi, A. Harken, C. J. Kinslow, P. S. Upadhyayula, A. Dovas, D. Higgins, H. Tan, Y. Zhang, M. Buonanno, T. J. C. Wang, T. K. Hei, J. N. Bruce, P. Canoll, S. K. Cheng, B. R. Stockwell, *ACS Chem. Biol.* **2020**, *15*, 469–484.
[13] T. Hirschhorn, B. R. Stockwell, *Free Radic. Biol. Med.* **2019**, *133*, 130–143.
[14] K. Schulze-Osthoff, D. Ferrari, M. Łos, S. Wesselborg, M. E. Peter, *Eur.J. Biochem.* **1998**, *254*, 439–459.
[15] D. Hanahan, R. A. Weinberg, *Cell* **2011**, *144*, 646–674.
[16] a) S. Li, H. Yuan, Y. Chen, Z. Guo, *Fundam. Res.* **2023**, *3*, 525–528; b) K. Peng, Y. Zheng, W. Xia, Z. Mao, *Chem. Soc. Rev.* **2023**, *52*, 2790–2832.
[17] H. Zhao, Y. Xu, H. Shang, *Int. J. Med. Sci.* **2022**, *19*, 1847–1855.
[18] G. Lei, Z. Li, B. Gan, *Nat. Rev. Cancer* **2022**, *22*, 381–396.
[19] X. Wang, F. Chen, J. Zhang, J. Sun, X. Zhao, Y. Zhu, W. Wei, J. Zhao, Z. Guo, *Sci. China Chem.* **2019**, *63*, 65–72.
[20] E. J. Anthony, E. M. Bolitho, H. E. Bridgewater, O. W. L. Carter, J. M. Donnelly, C. Imberti, E. C. Lant, F. Lermyte, R. J. Needham, M. Palau, P. J. Sadler, H. Shi, F.-X. Wang, W. Zhang, Z. Zhang, *Chem. Sci.* **2020**, *11*, 12888–12917.
[21] a) T. Scattolin, E. Bortolamiol, S. Palazzolo, I. Caligiuri, T. Perin, V. Canzonieri, N. Demitri, F. Rizzolio, L. Cavallo, B. Dereli, M. V. Mane, S. P. Nolan, F. Visentin, *Chem. Commun.*, **2020**, *56*, 12238–12241; b) T. Scattolin, S. Giust, P. Bergamini, I. Caligiuri, L. Canovese, N. Demitri, R. Gambari, I. Lampronti, F. Rizzolio, F. Visentin, *Appl. Organomet. Chem.* **2019**, *33*, e4902; c) T. Scattolin, I. Caligiuri, L. Canovese, N. Demitri, R. Gambari, I. Lampronti, F. Rizzolio, C. Santo, F. Visentin, *Dalton Trans.* **2018**, *47*, 13616–13630.
[22] a) S. Y. Lee, C. Y. Kim, T. Nam, *Drug Des. Dev. Ther.* **2020**, *14*, 5375–5392; b) G. Moreno-Alcántar, P. Picchetti, A. Casini, *Angew. Chem.* **2023**, *62*, e202218000; b) M. Mora, M. C. Gimeno, R. Visbal, *Chem. Soc. Rev.*, **2019**, 48, 447–462; d) T. A. C. A. Bayrakdar, T. Scattolin, X. Ma, S. P. Nolan, *Chem. Soc. Rev.* **2020**, 49, 7044–7100; e) B. Bertrand, A. Casini, *Dalton Trans.* **2014**, *3*, 4209–4219; f) S. Nobili, E. Mini, I. Landini, C. Gabbiani, A. Casini, L. Messori, *Med. Res. Rev.* **2010**, *30*, 550–80; g)

S. Y. Lee, C. Y. Kim, T.-G. Nam, *Drug Des. Dev. Ther.* **2020**, 14, 5375–5392; h) S. Q. Zhang, L.-H. Gao, H. Zhao, K.-Z. Wang, *Curr. Med. Chem.* **2020**, *27*, 3735–3752.
[23] A. S. Abu-Surrah, M. Kettunen, *Curr. Med. Chem.* **2006**, *13*, 1337–1357.
[24] J. Albert, J. Granell, J. A. Durán, A. Lozano, A. Luque, A. Mate, J. Quirante, M. K. Khosa, C. Calvis, R. Messeguer, L. Baldomà, J. BadíA, *J. Organomet. Chem.* **2017**, *839*, 116–125.
[25] T. Scattolin, V. A. Voloshkin, F. Visentin, S. P. Nolan, *Cell Rep. Phys. Sci.* **2021**, *2*, 100446.
[26] R. Paprocka, M. Wiese-Szadkowska, S. Janciauskiene, T. Kosmalski, M. Kulik, A. Helmin-Basa, *Coord. Chem. Rev.* **2022**, *452*, 214307.
[27] P. Köpf-Maier, W. Wagner, H. Köpf, *Cancer Chemother. Pharmacol.* **1981**, *5*, 237–241.
[28] a) I. Romero-Canelón, P. J. Sadler, *Inorg. Chem.* **2013**, *52*, 12276–12291; b) Z. Liu, P. J. Sadler, *Acc. Chem. Res.* **2014**, *47*, 1174–1185.
[29] E. Boros, P. J. Dyson, G. Gasser, *Chem* **2020**, *6*, 41–60.
[30] P. Zhang, P. J. Sadler, *J. Organomet. Chem.*, **2017**, 839, 5–14.
[31] a) T. Scattolin**,** I. Caligiuri, N. Mouawad, M. El Boustani, N. Demitri, F. Rizzolio, F. Visentin, *Eur. J. Med. Chem.* **2019**, *179*, 325–334; b) A. R. Kapdi, I. J. Fairlamb, *Chem. Soc. Rev.* **2014**, *43*, 4751; c) G. Kalaiarasi, S. Dharani, V. M. Lynch, R. Prabhakaran, *Dalton Transactions* **2019**, *48*, 12496–12511.
[32] a) T. Scattolin, E. Bortolamiol, F. Visentin, S. Palazzolo, I. Caligiuri, T. Perin, V. Canzonieri, N. Demitri, F. Rizzolio, A. Togni, *Chem. Eur. J.* **2020**, *26*, 11868–11876; b) T. Scattolin, I. Pessotto, E. Cavarzerani, V. Canzonieri, L. Orian, N. Demitri, C. Schmidt, A. Casini, E. Bortolamiol, F. Visentin, F. Rizzolio, S. P. Nolan, *Eur. J. Inorg. Chem.* **2022**, e202200103; c) A. Madabeni, T. Scattolin, E. Bortolamiol, F. Visentin, L. Orian, *Organometallics* **2024**, DOI 10.1021/acs.organomet.3c00514; d) T.-H. Fong, C.-N. Lok, C. Y.-S. Chung, Y.-M. E. Fong, P.-K. Chow, P.-K. Wan, C.-M. Che, *Angew. Chem. Int. Ed.* **2016**, *55*, 11935.
[33] a) J. H. Groen, C. J. Elsevier, K. Vrieze, W. J. J. Smeets, A. L. Spek *Organometallics* **1996**, *15*, 3445–3455; b) B. Cazes, *Pure Appl. Chem*. **1990**, *62*, 1867–1878; c) M. Ahmar, B. Cazes, *J. Gore Tetrahedron Lett*. **1984**, *25*, 4505–4508; d) M. Ahmar, B. Cazes, J. J. Barieux, *J. Gore Tetrahedron* **1987**, *43*, 513–526.
[34] A. Jutand, S. Négri, *Organometallics* **2003**, *22*, 4229–4237.
[35] a) R. Van Belzen, C. J. Elsevier, A. Didieu, N. Veldman, A. L. Speck, *Organometallics* **2003,** *22,* 722–736; b) L. Canovese, F. Visentin, T. Scattolin, C. Santo, V. Bertolasi, *J. Organomet. Chem.* **2016**, *808*, 48–56; c) L. Canovese, F. Visentin, T. Scattolin, C. Santo, V. Bertolasi, *Polyhedron* **2016**, *113*, 25–34; d) T. Scattolin, F. Visentin, C. Santo, V. Bertolasi, L. Canovese, *Dalton Trans.* **2016**, *45*, 11560–11567; e) L. Canovese, F. Visentin, T. Scattolin, C. Santo, V. Bertolasi, *Dalton Trans.* **2015**, *44*, 15049–15058; f) L. Canovese, C. Santo, T. Scattolin, F. Visentin, V. Bertolasi, J. *Organomet. Chem.* **2015**, *794*, 288–300; g) F. Visentin, C. Santo, T. Scattolin, N. Demitri, L. Canovese, *Dalton Trans.* **2017**, *46*, 10399–10407.
[36] L. Canovese, F. Visentin, G. Chessa, P. Uguagliati, C. Santo, A. Dolmella, *Organometallics* **2005**, *24*, 3297–3308.
[37] K. Moseley, P. M. Maitlis, *J. Chem. Soc. Dalton Trans.* **1974**, 169–175.
[38] a) J. Vicente, J. A. Abad, E. Martinez-Viviente, M. C. Ramirez de Arellano, P. G. Jones, *Organometallics* **2000**, *19*, 5597–5607; b) A. M. La Pointe, M. Brookhart, *Organometallics* **1998**, *17*, 1530–1537; c) J. Vicente, J. A. Abad, K. F. Shaw, J. Gil-Rubio, M. C. Ramirez de Arellano, P. G. Jones, *Organometallics* **1997**, *16*, 4557–4566.
[39] P. M. Maitlis, *J. Organomet. Chem.* **1980**, *200*, 161–176.
[40] J. R. Clark, S. T. Diver, *Org. Lett.* **2011**, *13*, 2896–2899.
[41] H. C. Clark, C.R. C. Milne, C. S. Wong, *J. Organomet. Chem*. **1977**, *136*, 265–279.
[42] A. Yamamoto, in Organotransition Metal Chemistry, *Wiley*, New York, **1986**.
[43] C. Carfagna, G. Gatti, L. Mosca, P. Paoli, A. Guerri, *Organometallics* **2003**, *22*, 3967–3970.
[44] E. G. Samsel, J. R. Norton, *J. Am. Chem. Soc.* **1984**, *106*, 5505–5512.
[45] a) T. Scattolin, C. Santo, N. Demitri, L. Canovese, F. Visentin, *Dalton Trans.* **2020**, *173*, 114144; b) T. Scattolin, E. Bortolamiol, I. Caligiuri, F. Rizzolio, N. Demitri, F. Visentin, *Polyhedron* **2020**, *186*, 114607; c) L. Canovese, F. Visentin, T. Scattolin, C. Santo, V. Bertolasi, *Polyhedron* **2018**, *144*, 131–143; d) T. Scattolin, L. Canovese, F. Visentin, C. Santo, N. Demitri, *Polyhedron* **2018**, *154*, 382–389; e) T. Scattolin, N. Pangerc, I. Lampronti, C. Tupini, R. Gambari, L. Marvelli, F. Rizzolio, N. Demitri, L. Canovese, F. Visentin, *J. Organomet. Chem.* **2019**, *899*, 120857; f) T. Scattolin, L. Canovese, N. Demitri, C. Santo, F. Visentin, *Polyhedron* **2019**, *173*, 114144;
[46] a) T. Scattolin, A. A. Logvinov, N. V. Tzouras, C. S. J. Cazin, S. P. Nolan, *Organometallics* **2023**, *42*, 2692–2730; b) M. N. Hopkinson, C. Richter, M. Schedler, F. Glorius, *Nature* **2014**, *510*, 485–496.
[47] J. Bravo, S. Bolaño, L. Gonsalvi, M. Peruzzini, *Coord. Chem. Rev.*, **2010**, *254*, 555–607.
[48] a) C. Sonkar, S. Sarkar, S. Mukhopadhyay, *RSC Med. Chem.* **2022**, *13*, 22–38; b) J. Quero, F. Ruighi, J. Osada, M. C. Gimeno, E. Cerrada, M. J. Rodriguez-Yoldi, *Biomedicine* **2021**, *9*, 1848; c) A. K Renfrew, J. Karges, R. Scopelliti, F. D Bobbink, P. Nowak-Sliwinska, G. Gasser, P. J. Dyson, *ChemBioChem* **2019**, *20*, 2876–2882; d) T. Scattolin, E. Bortolamiol, F. Rizzolio, N. Demitri, F. Visentin, *Appl. Organomet. Chem.* **2020**, *34*, e5876.
[49] a) Y. Wu, D. Wang, W. Fang, F. Xiong, S. Zhang, Z. Gong, L. Shi, X. Li, B. Xiang, J. Ma, H. Deng, Y. He, Q. Liao, W. Zhang, X. Li, Y. Li, C. Guo, Z. Zeng, G. Li, W. Xiong, *FASEB J.***2020**, *34*, 16205–16223; b) D. Wang, Z. Zeng, S. Zhang, F. Xiong, B. He, Y. Wu, W. Liu, L. Tang, W. Fang, B. Xiang, Z. Li, Y. Zhou, M. Zhou, X. Li, Y. Li, G. Li, W. Xiong, C. Guo, *FASEB J.* **2020**, *34*, 8012–8027.
[50] a) Y. Wang, Y. Mo, P. Miao, S. Zhang, Z. Gong, Q. Yan, Y. Tang, Y. He, Q. Liao, X. Li, X. Wu, B. Xiang, M. Zhou, Y. Li, G. Li, X. Li, Z. Zeng, C. Guo, *Autophagy* **2021**, *18*, 240–253; b) S. Bedoui, M. J. Herold, A. Strasser, *Nat. Rev. Mol. Cell Biol*. **2020**, *21*, 678–695.
[51] a) B. A. Carneiro, W. S. El-Deiry, *Nat. Rev. Clin. Oncol.* **2020**, *17*, 395–417; b) Y. K. Dhuriya, D. Sharma, *J. Neuroinflammation* **2018**, *15*, DOI 10.1186/s12974-018-1235-0; c) Q. Nie, Y. Hu, X. Yu, X. Li, X. Fang, *Cancer Cell Int.* **2022**, *22*, DOI 10.1186/s12935-021-02366-0; d) J. Hou, R. Zhao, W. Xia, C. W. Chang, Y. You, J. M. Hsu, L. Nie, Y. Chen, Y. C. Wang, C. Liu, W. Wang, Y. Wu, B. Ke, J. L. Hsu, K.-B. Huang, Z. Ye, Y. Yang, X. Xia, Y. Li, C. W. Li, B. Shao, J. A. Tainer, M. Hung, *Nat. Cell Biol.* **2020**, *22*, 1264–1275; e) J. Shi, Y. Zhao, K. Wang, X. Shi, Y. Wang, H. Huang, Y. Zhuang, T. Cai, F. Wang, F. Shao, *Nature* **2015**, *526*, 660–665; f) J. M. M. Levy, C. G. Towers, A. Thorburn, *Nat. Rev. Cancer* **2017**, *17*, 528–542.
[52] X. Yu, Y. Long, *Sci. Rep.* **2016**, *6*, DOI 10.1038/srep30033.
[53] a) J. P. F. Angeli, D. V. Krysko, M. Conrad, *Nat. Rev. Cancer* **2019**, *19*, 405–414; b) N. Jyotsana, K. T. L. Ta, K. E. DelGiorno, *Front. Oncol.* **2022**, *12*, DOI 10.3389/fonc.2022.858462; c) S. Doll, B. Proneth, Y. Y. Tyurina, E. Panzilius, S. Kobayashi, I. Ingold, M. Irmler, J. Beckers, M. Aichler, A. Walch, H. Prokisch, D. Trümbach, G. Mao, F. Qu, H. Bayır, J. Füllekrug, C. Scheel, W. Wurst, J. Schick, V. E. Kagan, J. P. F. Angeli, M. Conrad, *Nat. Chem. Biol.* **2016**, *13*, 91–98; d) S. Neitemeier, A. Jelinek, V. Laino, L. Hoffmann, I. Eisenbach, R. Eying, G. K. Ganjam, A. M. Dolga, S. Oppermann, C. Culmsee, *Redox Biol.* **2017**, *12*, 558–570; e) M. Zille, S. S. Karuppagounder, Y. Chen, P. J. Gough, J. Bertin, J. N. Finger, T. A. Milner, E. A. Jonas, R. R. Ratan, *Stroke* **2017**, *48*, 1033–1043.
[54] a) N. Jyotsana, K. T. L. Ta, K. E. DelGiorno, *Front. Oncol.* **2022**, *12*, DOI 10.3389/fonc.2022.858462; b) D. Wang, L. Tang, Y. Zhang, G. Ge, X. Jiang, Y. Mo, P. Wu, X. Deng, L. Li, S. Zuo, Q. Yan, S. Zhang, F. Wang, L. Shi, X. Li, B. Xiang, M. Zhou, Q. Liao, C. Guo, Z. Zeng, W. Xiong, Z. Gong, *Cell Death Dis.* **2022**, *13*, DOI 10.1038/s41419-022-04927-1; c) J. Lee, J. H. You, D.-H. Shin, J. Roh, *Theranostics* **2020**, *10*, 7775–7786; d) K. Kalishwaralal, C. K. Keerthana, M. Mohan, J. Arivalagan, J. R. S. S. Christyraj, M. A. Firer, M. H. A. Choudry, R. J. Anto, Y. J. Lee, *J. Cell. Biochem.* **2021**, *123*, 532–542; e) Q. Nie, Y. Hu, X. Yu, X. Li, X. Fang, *Cancer Cell Int.* **2022**, *22*, DOI 10.1186/s12935-021-02366-0; f) E. C. Cheung, K. H. Vousden, *Nat. Rev. Cancer* **2022**, *22*, 280–297; g) Y. Liu, W. Gu, *Cell Death Differ*. **2022**, *29*, 895–910; h) S. Dolma, S. L. Lessnick, W. C. Hahn, B. R. Stockwell, *Cancer Cell* **2003**, *3*, 285–296.
[55] J. Y. Cao, S. J. Dixon, *Cellular and Molecular Life Sciences* **2016**, *73*, 2195–2209.
[56] a) X. Yang, Y. Ding, L. Sun, M. Shi, P. Zhang, Z. Huang, J. Wang, A. He, J. Wang, J. Wei, M. Liu, J. Liu, G. Wang, X. Yang, R. Li, *Redox Biol.* **2022**, *58*, 102555; b) Y. Wang, S. Qiu, H. Wang, J. Cui, X. Tian, Y. Miao, C.

Zhang, L. Cao, L. Ma, X. Xu, Y. Qiao, X. Zhang, *Front. Cell and Dev. Biol.* **2021**, *9*, DOI 10.3389/fcell.2021.719187.

[57] O. Kopper, C. J. De Witte, K. Lõhmussaar, J. E. Valle-Inclán, N. Hami, L. Kester, A. V. Balgobind, J. Korving, N. Proost, H. Begthel, L. M. Van Wijk, S. A. Revilla, R. Theeuwsen, M. Van De Ven, M. J. Van Roosmalen, B. Ponsioen, V. W. Ho, B. G. Neel, T. Bosse, K. N. Gaarenstroom, H. Vrieling, M. P. G. Vreeswijk, P. J. Van Diest, P. O. Witteveen, T. N. Jonges, J. L. Bos, A. Van Oudenaarden, R. P. Zweemer, H. J. G. Snippert, W. P. Kloosterman, H. Clevers, *Nat. Med.* **2019**, *25*, 838–849.

[58] A. Lausi, M. Polentarutti, S. Onesti, J. R. Plaisier, E. Busetto, G. Bais, L. Barba, A. Cassetta, G. Campi, D. Lamba, A. Pifferi, S. C. Mande, D. D. Sarma, S. M. Sharma, G. Paolucci, *Eur. Phys. J. Plus* **2015**, *130*, 43.

[59] W. Kabsch, *Acta Crystallogr. D Biol. Crystallogr.* **2010**, *66*, 125–132.

[60] P. R. Evans, G. N. Murshudov, *Acta Crystallogr. D Biol. Crystallogr.* **2013**, *69*, 1204–1214.

[61] G.M. Sheldrick, *Acta Crystallogr. A*, **2015**, *71*, 3.

[62] G.M. Sheldrick, *Acta Crystallogr. C*, **2015**, *71*, 3.

[63] P. Emsley, B. Lohkamp, W. G. Scott, K. Cowtan, *Acta Crystallogr. D Biol. Crystallogr.* **2010**, *66*, 486–501.

[64] L. J. Farrugia, *J. Appl. Crystallogr.* **2012**, *45*, 849–854.

[65] L. Schrodinger, The PyMOL Molecular Graphics System. Schrodinger, **2015,** LLC. http://www.pymol.org.

Supporting Information

Unlocking the Potential of Organopalladium Complexes for High-Grade Serous Ovarian Cancer Therapy

Thomas Scattolin,*,†,[a] Enrico Cavarzerani,†,[b] Dario Alessi,[a] Matteo Mauceri,[b] Eleonora Botter,[b] Giovanni Tonon,[b] Isabella Caligiuri,[c] Ombretta Repetto,[d] Urska Kamensek,[e] Simona Kranjc Brezar,[e] Maria Dalla Pozza,[f] Stefano Palazzolo,[c] Maja Cemazar,[e] Vincenzo Canzonieri,[c,g] Nicola Demitri,[h] Steven P. Nolan,[i] Gilles Gasser,[f] Fabiano Visentin*[b] and Flavio Rizzolio*[b,c]

Abstract: *High-Grade Serous Ovarian Cancer (HGSOC) is the most common and lethal subtype of ovarian cancer, known for its high aggressiveness and extensive genomic alterations. Typically diagnosed at an advanced stage, HGSOC presents formidable challenges in drug therapy. The limited efficacy of standard treatments, development of chemoresistance, scarcity of targeted therapies, and significant tumor heterogeneity render this disease incurable with current treatment options, highlighting the urgent need for novel therapeutic approaches to improve patient outcomes. In this study we report a straightforward and stereoselective synthetic route to novel Pd(II)-vinyl and -butadienyl complexes bearing a wide range of monodentate and bidentate ligands. Most of the synthesized complexes exhibited good to excellent in vitro anticancer activity against ovarian cancer cells. Particularly promising is the water-soluble complex bearing two PTA (PTA = 1,3,5-triaza-7-phosphaadamantane) ligands and the Pd(II)-butadienyl fragment. This compound combines excellent cytotoxicity towards cancer cells with substantial inactivity towards non-cancerous ones. This derivative was selected for further studies on ex vivo tumor organoids and in vivo mouse models, which demonstrate its remarkable efficacy with surprisingly low collateral toxicity even at high dosages. Moreover, this class of compounds appears to operate through a ferroptotic mechanism, thus representing the first such example for an organopalladium compound.*

DOI: XXXX

Table of Contents

Reactivity of Pd(II)-vinyls towards [(PhC≡C)Sn(n-Bu)$_3$]

The extrusion of the vinyl fragment was carried out by reacting the synthesized vinyl complexes with [(PhC≡C)Sn(*n*-Bu)$_3$]. It should be remembered that stannanes are widely used to remove organic residues from a metal center. This process is divided into two steps: transmetallation and subsequent reductive elimination (Scheme S1).

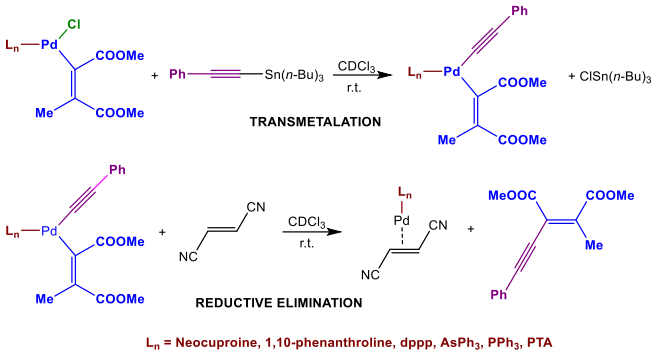

Scheme S1. Transmetalation and reductive elimination steps involved in the reaction between Pd(II)-vinyl complexes and stannanes.

We have chosen to study only the vinyl derivatives since, from preliminary tests we have verified that their butadienyl congeners react much more slowly. Furthermore, [(PhC≡C)Sn(*n*-Bu)$_3$] was chosen as it is known to efficiently promote the release of the phenylethynyl fragment in the transmetallation process.

The addition of fumaronitrile in the reactivity study allows the stabilization of the resulting Pd(0) complex, avoiding the formation of metallic palladium which could trigger parasitic reactions and/or perturb the system during the NMR analysis. The coordination of fumaronitrile has been demonstrated to be faster than the two reactions that precede it. In fact, the rate of the entire process is independent of the concentration of added olefin.

All reactions were monitored by ^{1}H NMR spectroscopy, using a $1.82 \cdot 10^{-2}$ M CD_2Cl_2 solution of the complex, 1.1 equivalents of [(PhC≡C)Sn(*n*-Bu)$_3$] and an excess of fumaronitrile (3.7 equiv.).

The results obtained, expressed as half-life (min) of the initial complex, are reported in Table S1.

Table S1. Half-life ($t_{1/2}$) of Pd(II)-vinyl complexes in the reaction with [(PhC≡C)Sn(*n*-Bu)$_3$].

Complex	Ligand	$t_{1/2}$
2a	1,10-Phenanthroline	18 min
3a	Neocuproine	6 min
4a	1,3-bis(diphenylphosphino)propane	> 24 h
8a	triphenylphosphine	120 min
9a	1,3,5-triaza-7-phosphaadamantane	9 min
10a	triphenylarsine	54 min

From the $t_{1/2}$ values obtained it is evident that the two most reactive complexes are those containing 1,10-phenanthroline and neocuproine (**2a** and **3a**). This high reactivity is probably due to the reduced steric demand of the N-N ancillary ligand, allowing easy access of stannane above and below the main coordination plane. On the contrary, the use of a chelating diphosphine such as dppp results in considerably disadvantage the process. The low reactivity of complex **4a** is due both to the higher steric hindrance of dppp compared to the phenanthroline-based ligands and to the stronger bond that this diphosphine forms with palladium. Considering this latter aspect, it is difficult to easily free coordination sites, a condition that may be required at some stage of the process.

The complexes coordinating two PPh_3 or $AsPh_3$ ligands have an intermediate reactivity between derivatives **2a**/**3a** and **4a**. The lower reactivity compared to complexes containing bidentate N-N ligands is probably due to the need to promote the isomerization of the *trans* transmetallation intermediate in its *cis* congeners, enabling the reductive elimination process.

Curiously, in the case of complex **9a** which coordinates two PTA ligands, the reaction with [(PhC≡C)Sn(*n*-Bu)$_3$] ends with the transmetallation step, without evolving over time with the extrusion of the organic fragment. This means that the intermediate species is particularly stable and does not undergo *trans*/*cis* isomerization, which is crucial for allowing the final reductive elimination step. Based on this evidence, the synthesis of intermediate **13** was carried out in dichloromethane, with a reaction time of 3 hours at room temperature.

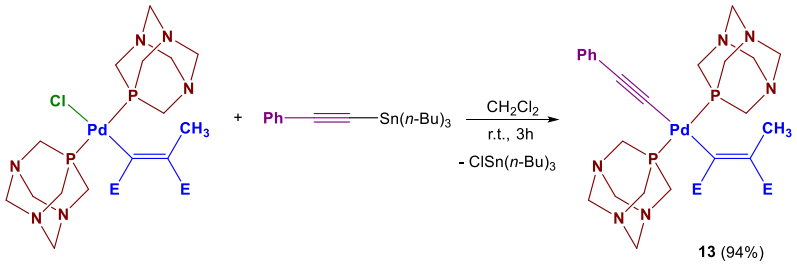

Scheme S2. Synthetic procedure leading to complex **13**.

The ^{31}P NMR spectrum of **13** shows a singlet at -58.5 ppm, confirming the *trans* configuration of the transmetallation product. This conclusion can also be inferred from the ^{1}H and ^{13}C NMR spectra, where only one set of methylene protons/carbons (NCH_2N and NCH_2P), slightly shifted with respect to the starting material, can be detected. Furthermore, all the signals attributable to alkynyl protons and carbons are observable. In particular, the alkynyl carbon directly bound to palladium resonates as a triplet ($J_{C\text{-}P}$ = 23.1 Hz) at 101.4 ppm, whereas that bound to the phenyl substituent appears as a singlet at 115 ppm. In the IR spectrum, the C≡C stretching band at 2100 cm^{-1} is particularly worthy of mention. Finally, the atom connectivity was unambiguously established by single crystal X-ray diffraction (see Crystal structure determination section).

Biological data

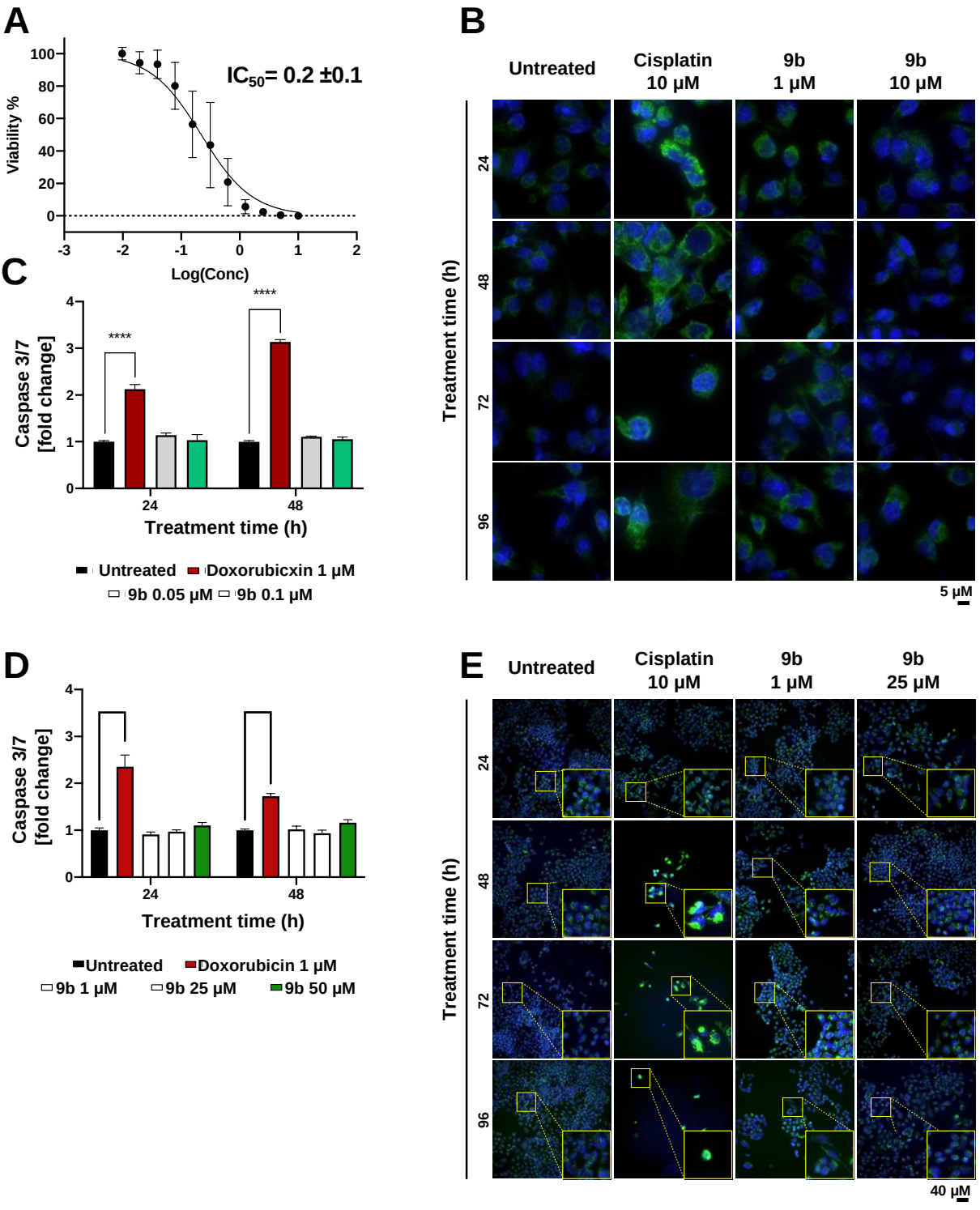

Figure S1: IC_{50} *(**A**) Dose–response curve of OVCAR5 treated with Compound 9b. Dots represent the mean of nine replicates. Error bars represent the SD. IC_{50} value is reported in the graph; (**B**) Immunofluorescence analysis of cytochrome C release on OVCAR5 after 24, 48, 72 and 96 h of treatment with Compound **9b** and cisplatin as positive control; (**C**)* Caspases 3/7 activation in OVCAR5 and (**D**) A2780 cells treated with compound **9b** (1, 25, 50 µM) and Doxorubicin (1 µM as positive control) at 24 and 48-hour intervals; (**E**) *Immunofluorescence analysis of cytochrome C release on A2780 after 24, 48, 72 and 96 h of treatment with Compound **9b** and cisplatin as positive control.*

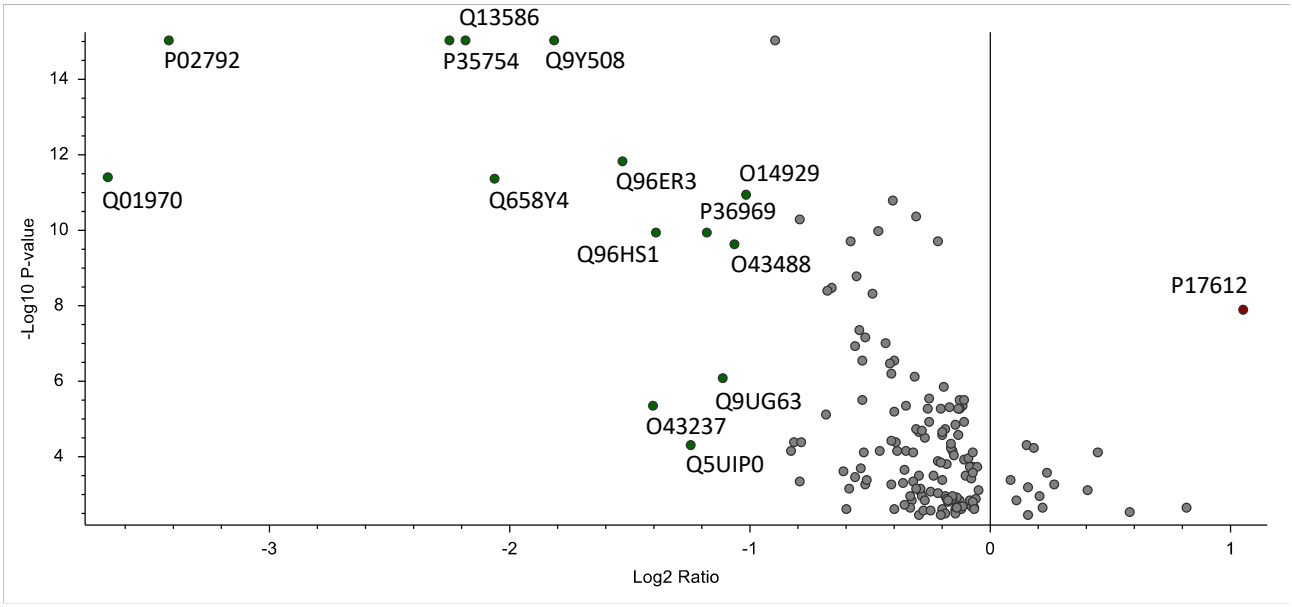

Figure S2: Volcano plot showing proteomic data by cell treatment (1 µM versus NT). Log2 transformed abundance ratios for each protein are plotted on the x-axis. Negative log10 transformed p-values are plotted on the y-axis. Proteins significantly more abundant and less abundant are represented as red and green circles, respectively, 1 µM treated groups than in NT groups. The red and green panels evidence areas containing proteins significantly different for $P_{adj.}$<0.05 and Log_2FC >1 or <-1, respectively. Protein gene names are indicated.

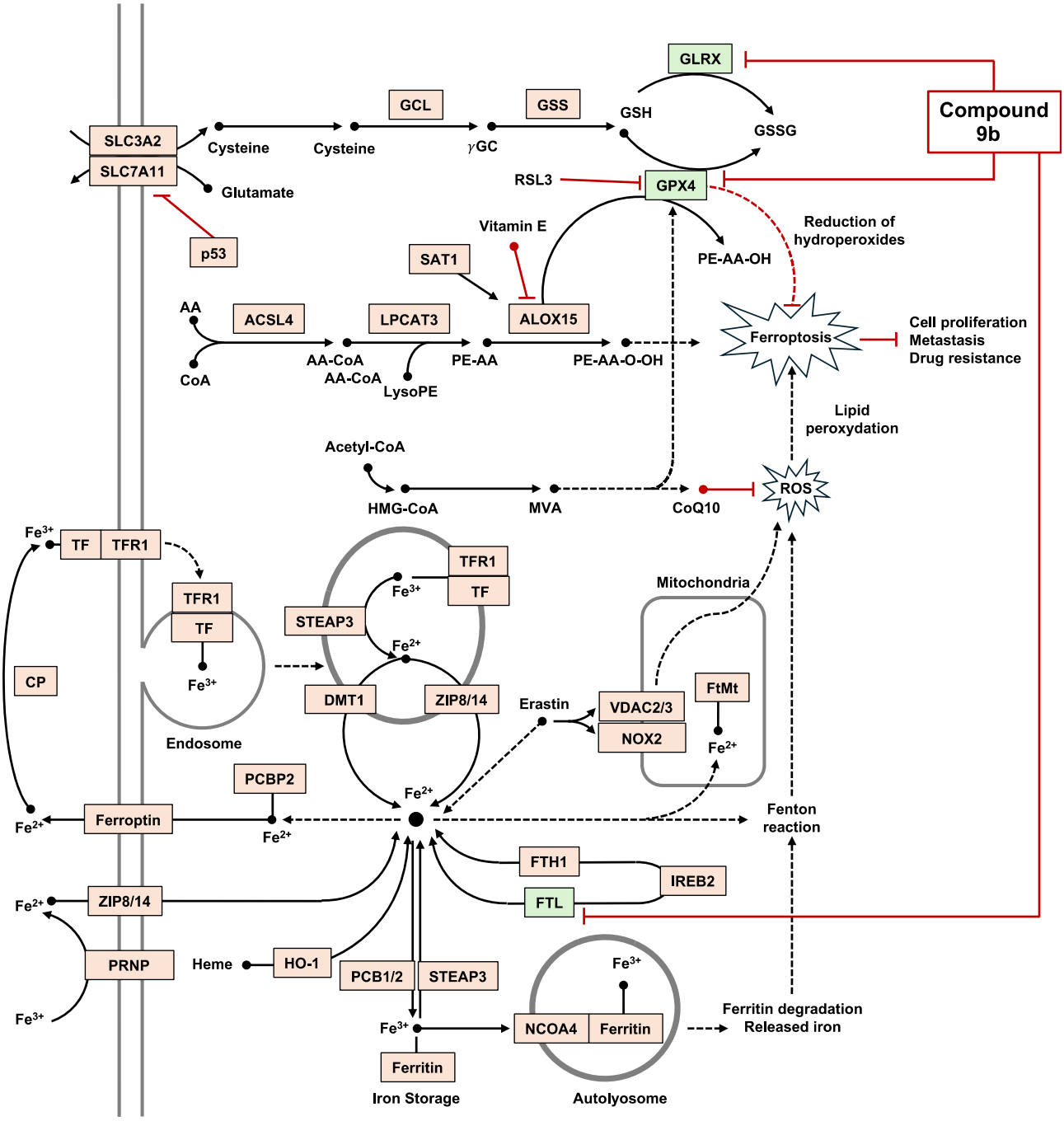

Figure S3: An illustration showing the role of GLRX, GPX4 and FTL suppression, operated by compound **9b**, in predisposing therapy-resistant cancer cells to ferroptosis. The image was generated with DAVID software (https://david.ncifcrf.gov/tools.jsp) and subsequently customized.

NMR spectra

^{1}H NMR, ^{13}C{^{1}H} NMR spectra of [Pd(1,10-phen)Cl(C_2(COOMe)$_2$$CH_3$)] (2a)

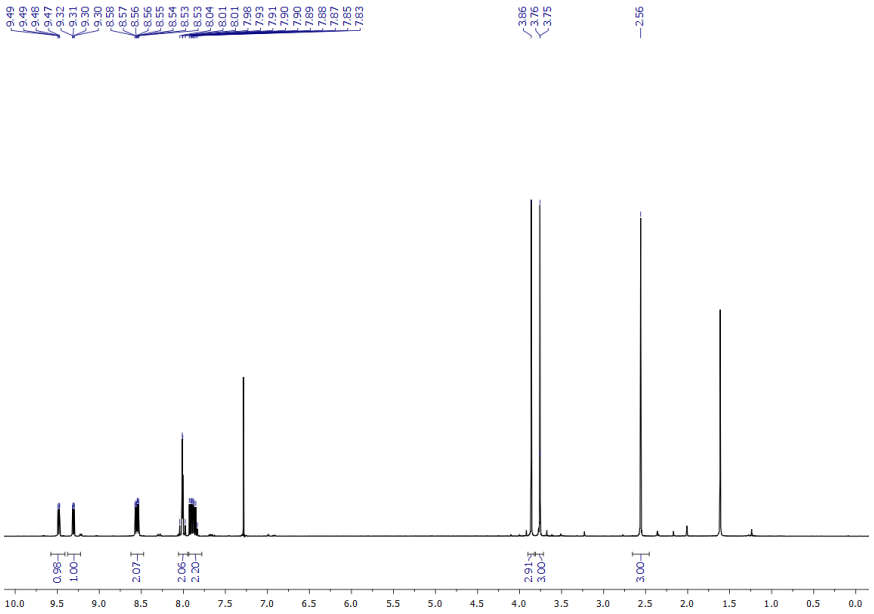

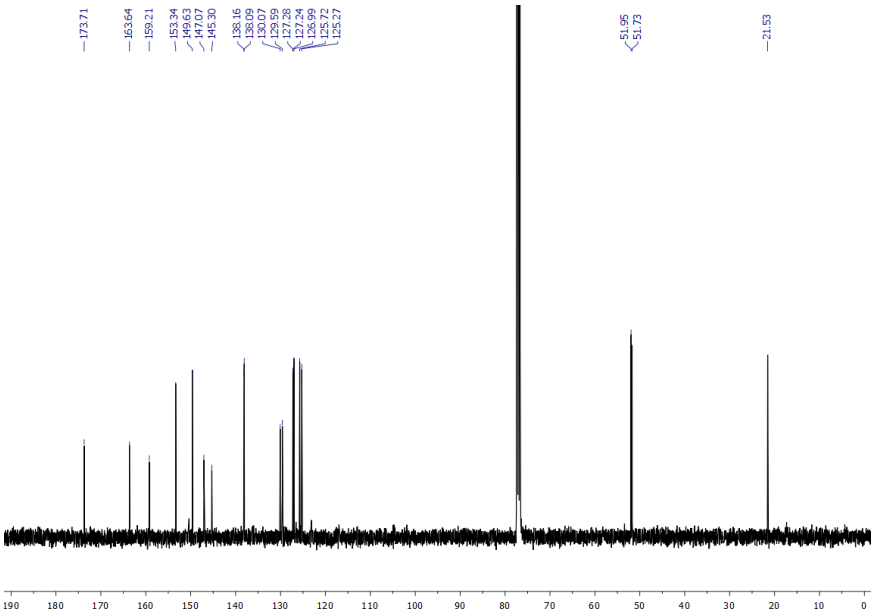

^{1}H NMR, ^{13}C{^{1}H} NMR spectra of [Pd(1,10-phen)Cl(C_4(COOMe)$_4$$CH_3$)] (2b)

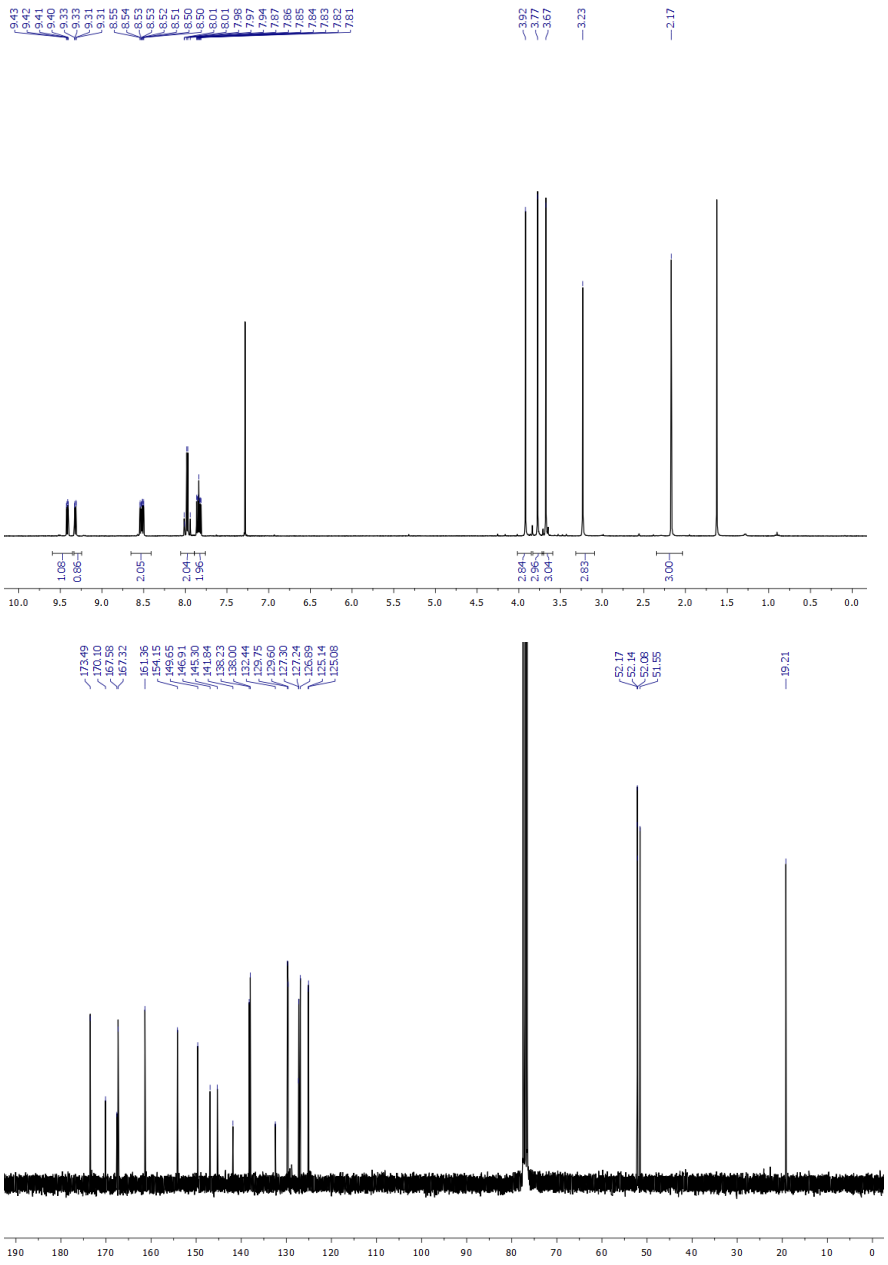

^{1}H NMR, ^{13}C{^{1}H} NMR spectra of [Pd(neocuproine)Cl(C_2(COOMe)$_2$$CH_3$)] (3a)

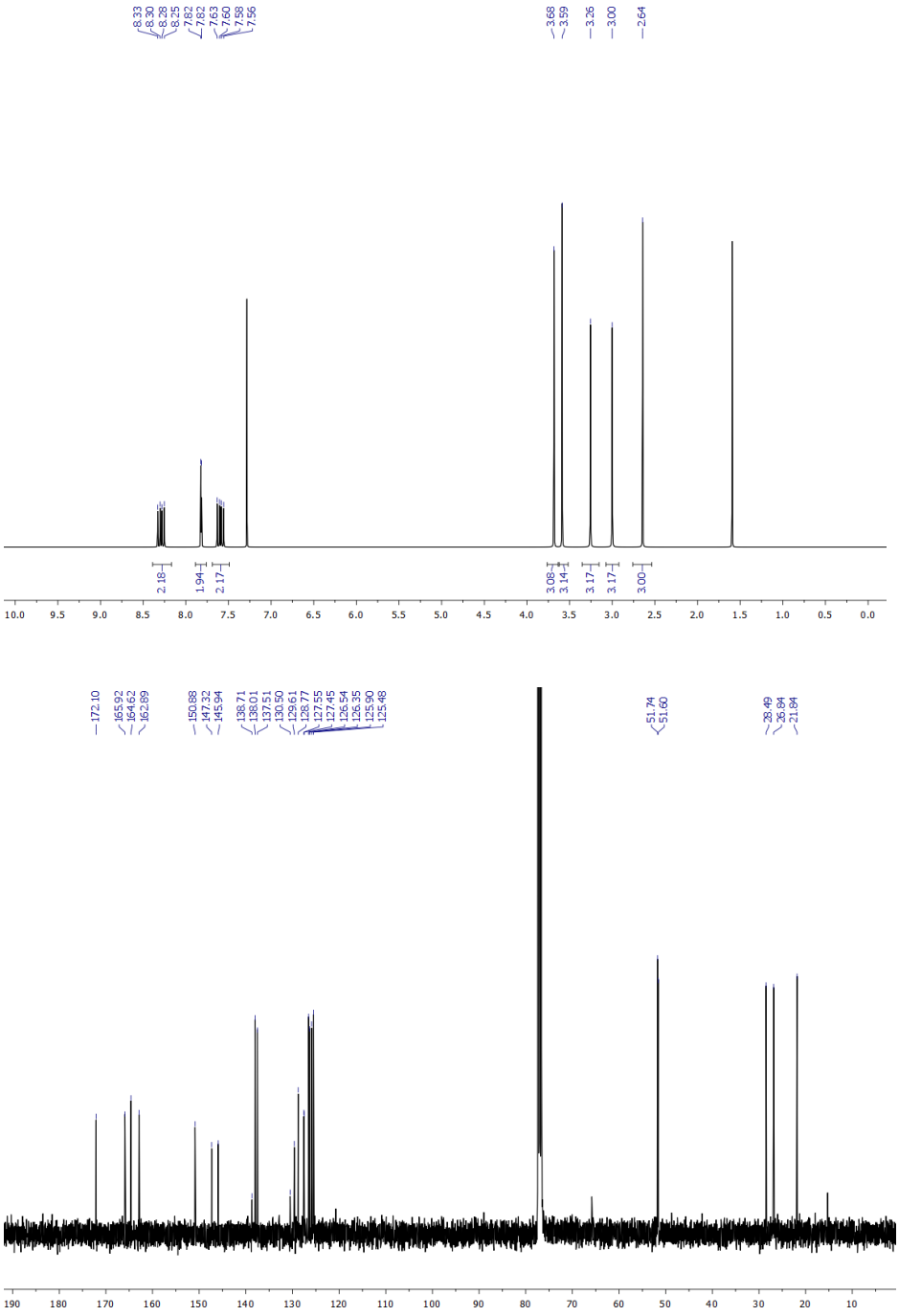

^{1}H NMR, ^{13}C{^{1}H} NMR spectra of [Pd(neocuproine)Cl(C_4(COOMe)$_4$$CH_3$)] (3b)

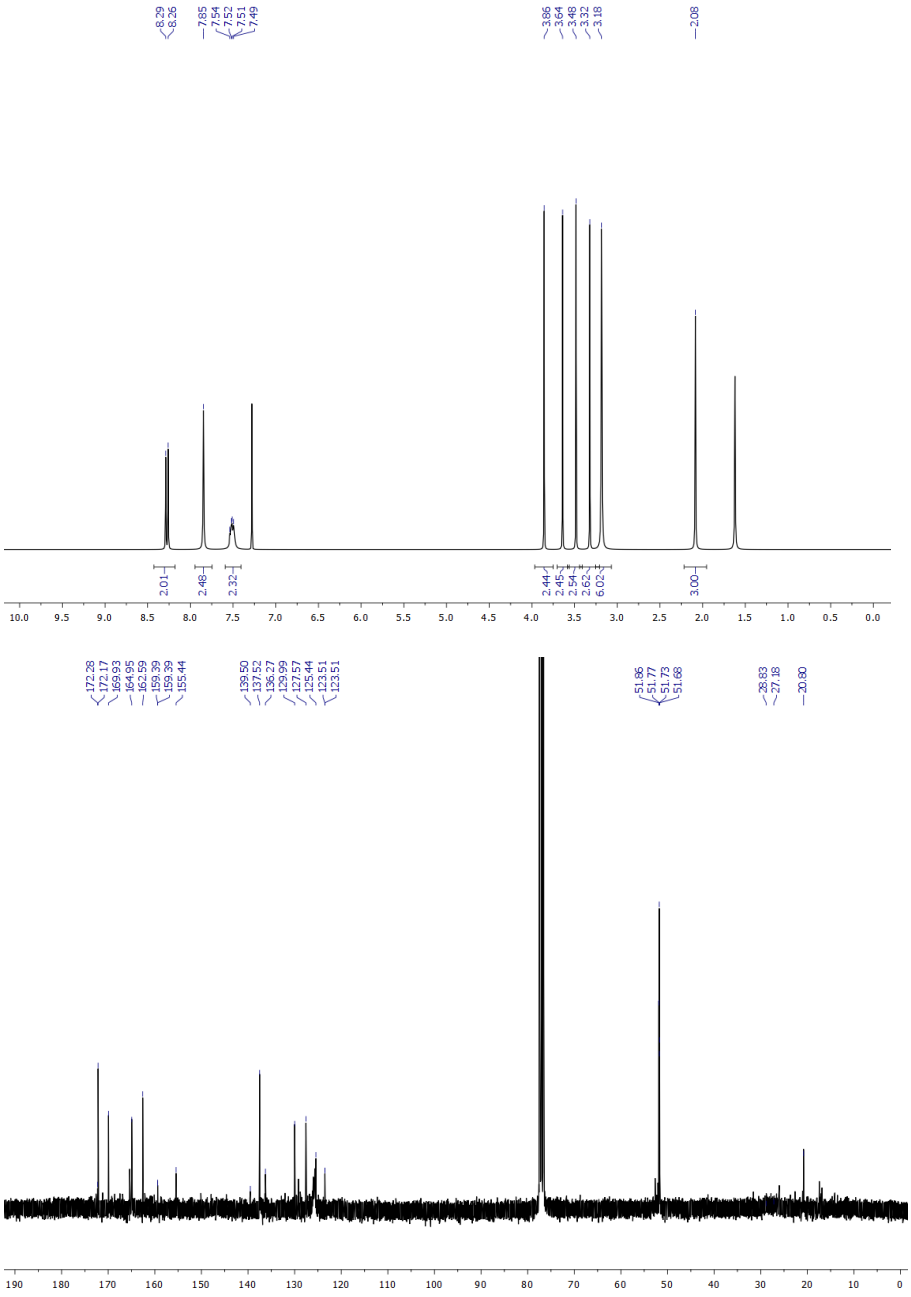

^{1}H NMR, ^{31}P{^{1}H} NMR and ^{13}C{^{1}H} NMR spectra of [Pd(dppp)Cl(C_2(COOMe)$_2$$CH_3$)] (4a)

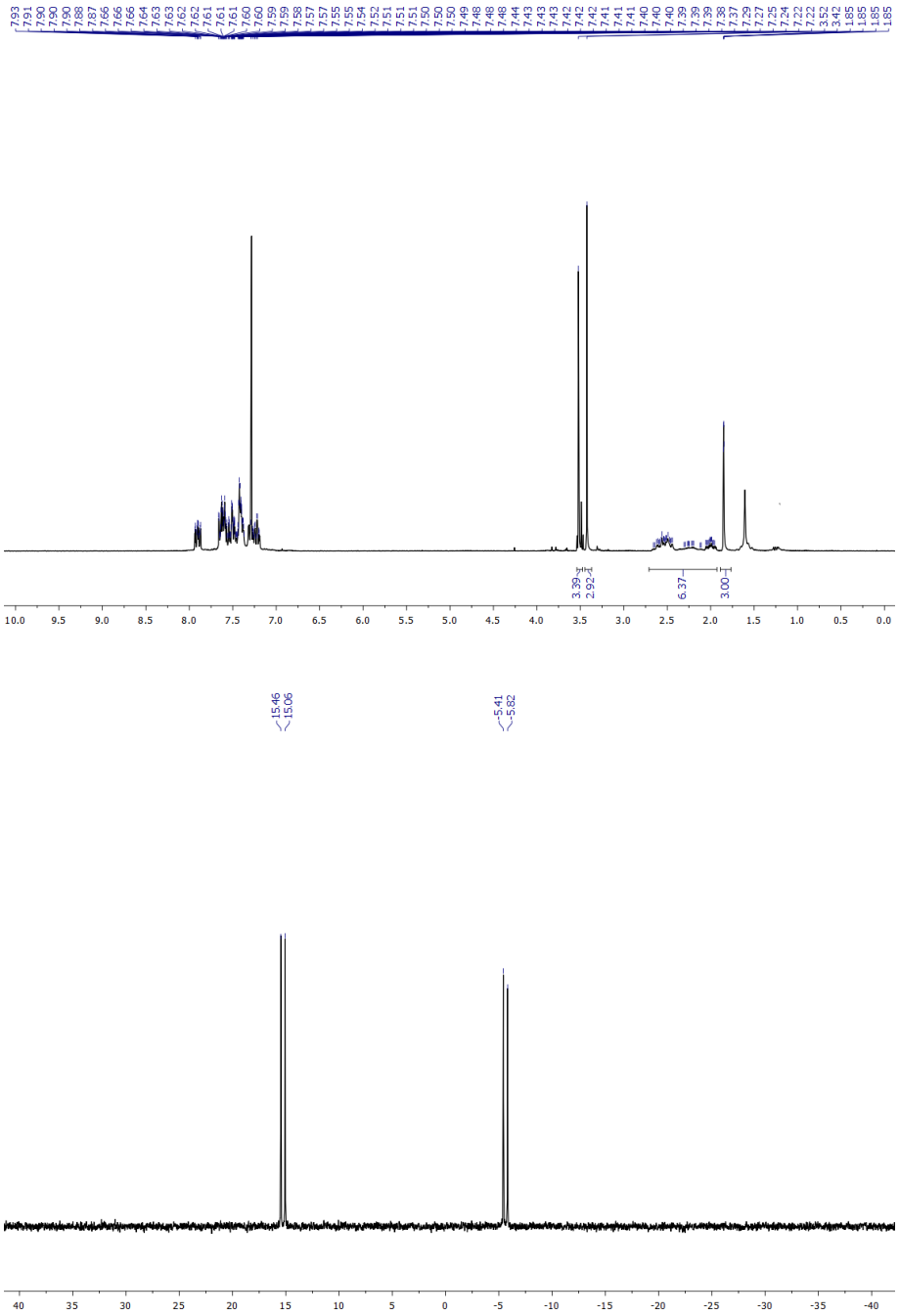

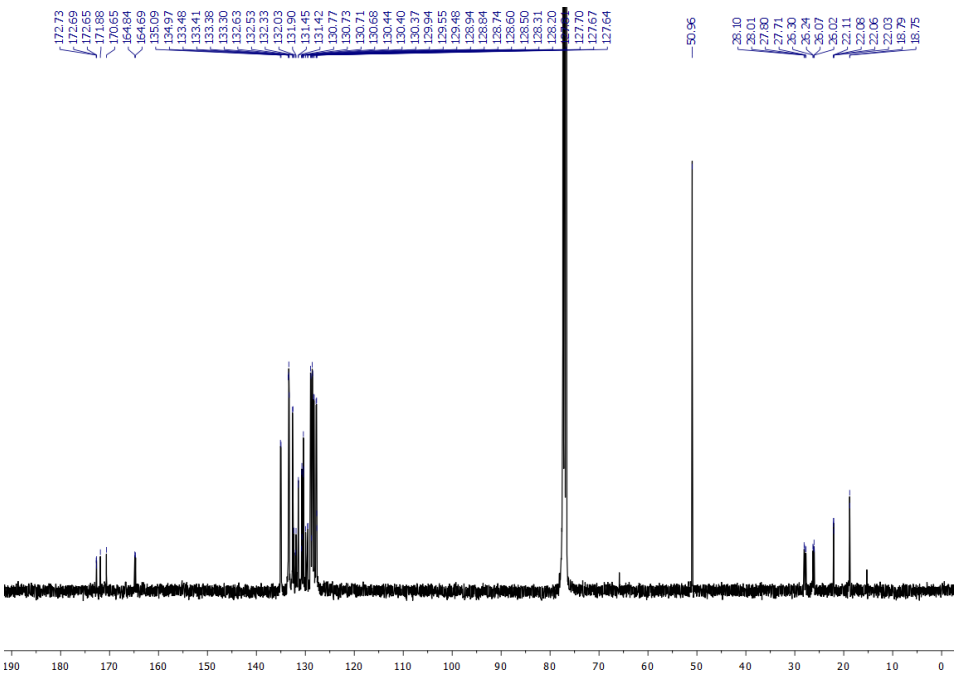

^{1}H NMR, $^{31}P\{^{1}H\}$ NMR and $^{13}C\{^{1}H\}$ NMR spectra of [Pd(dppp)Cl(C_4(COOMe)$_4$$CH_3$)] (4b)

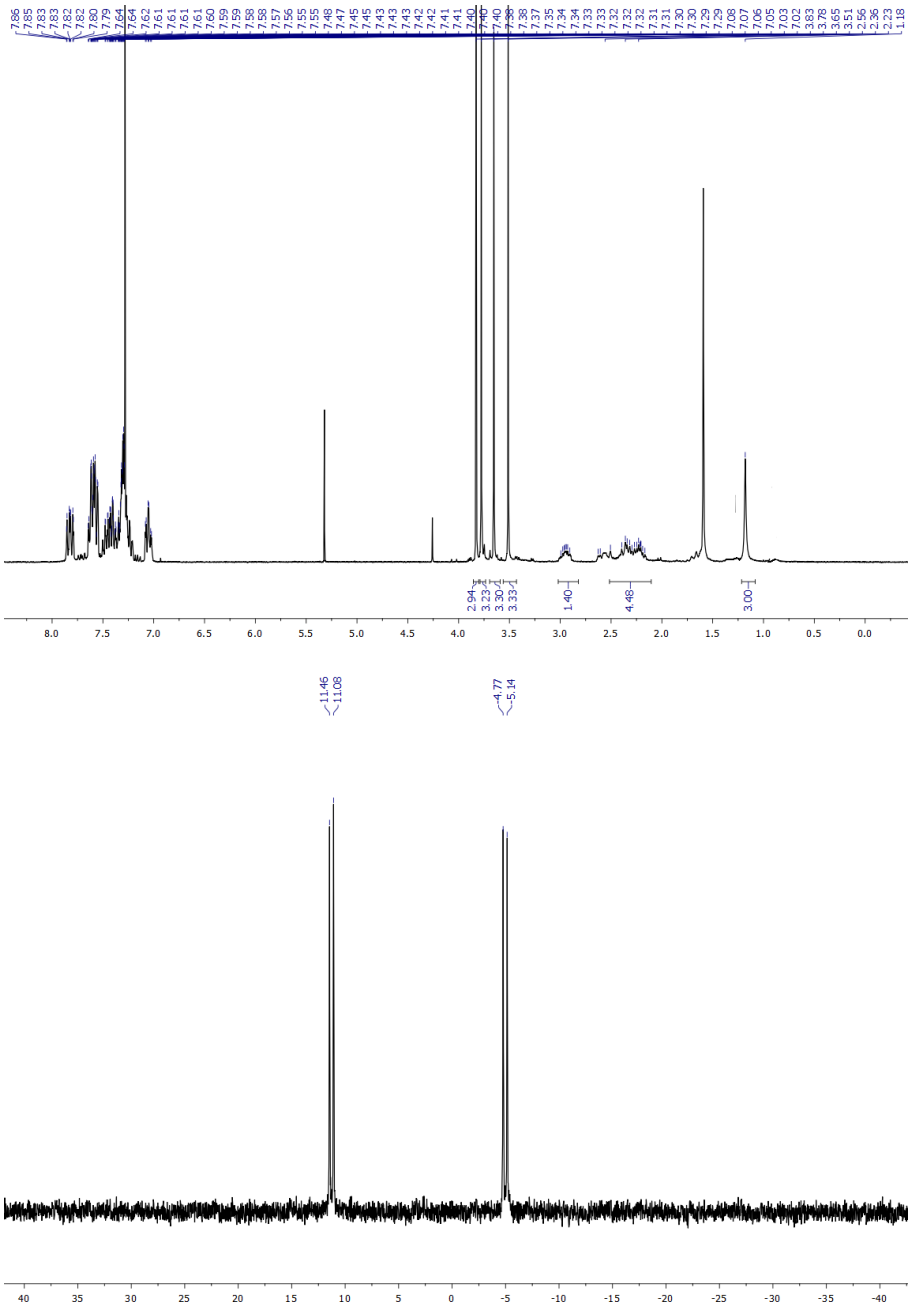

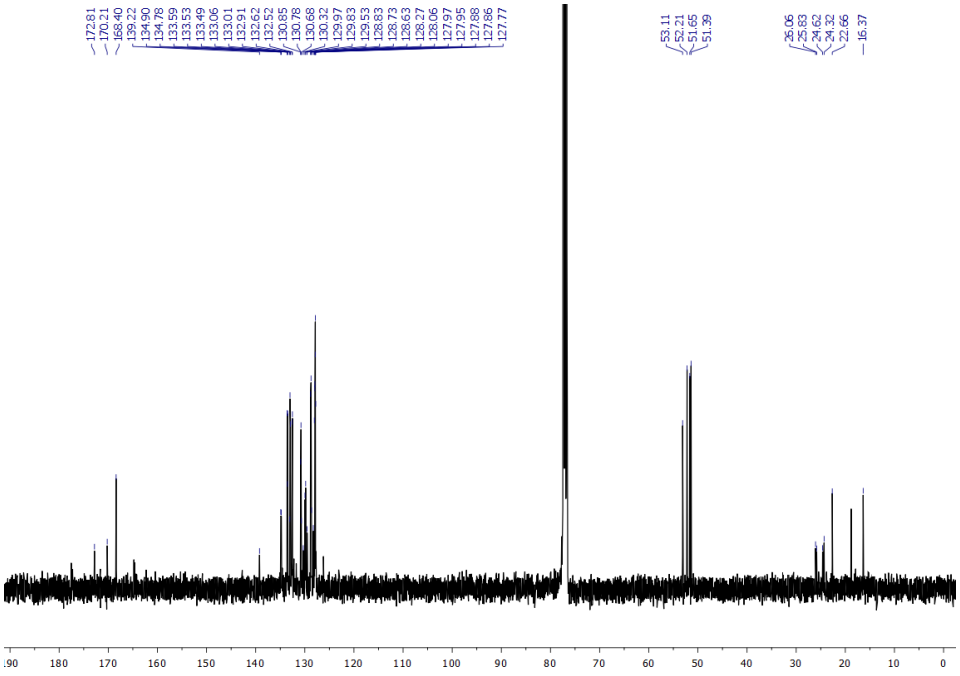

^{1}H NMR, $^{13}C\{^{1}H\}$ NMR spectra of [Pd(BnImCH$_2$ImBn)Cl(C$_4$(COOMe)$_4$CH$_3$)] (7b)

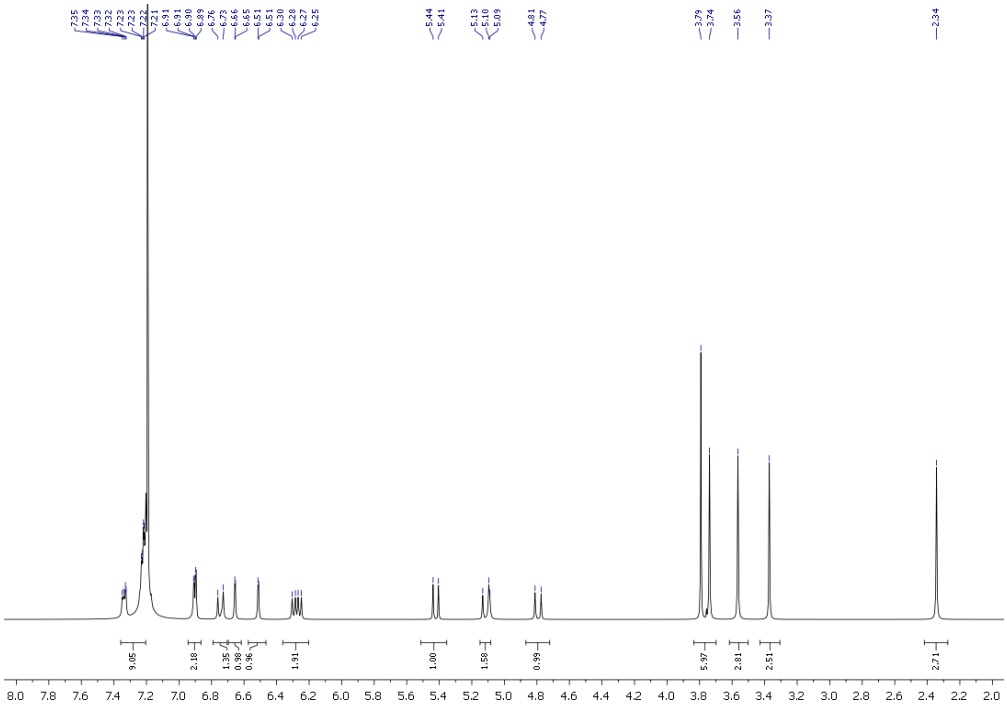

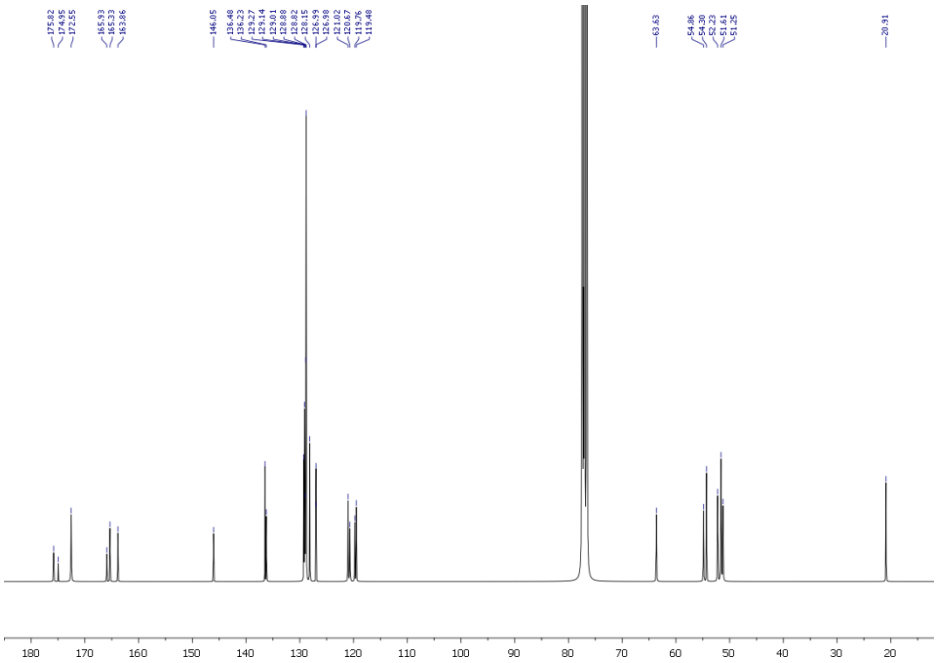

^{1}H NMR, ^{31}P{^{1}H} NMR and ^{13}C{^{1}H} NMR spectra of *trans*-[Pd(PPh$_3$)$_2$Cl(C$_2$(COOMe)$_2$CH$_3$)] (8a)

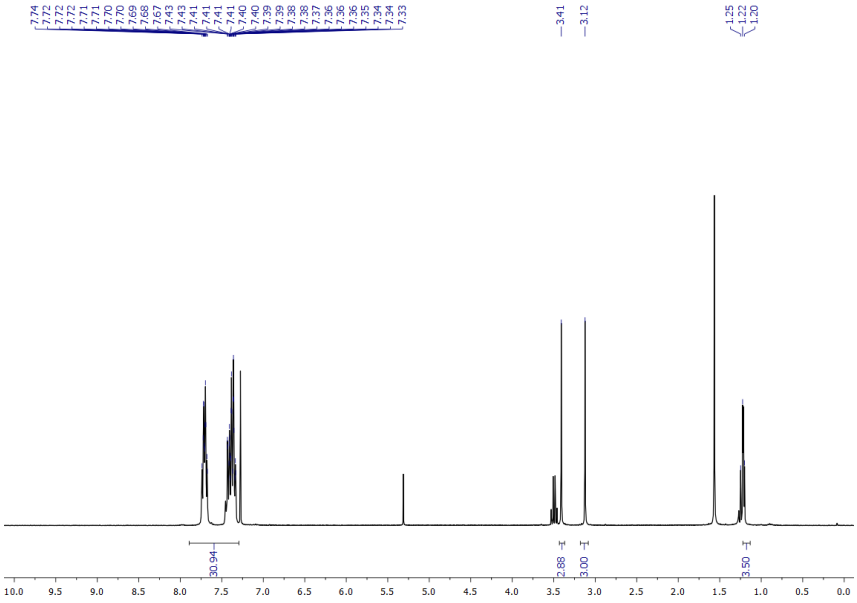

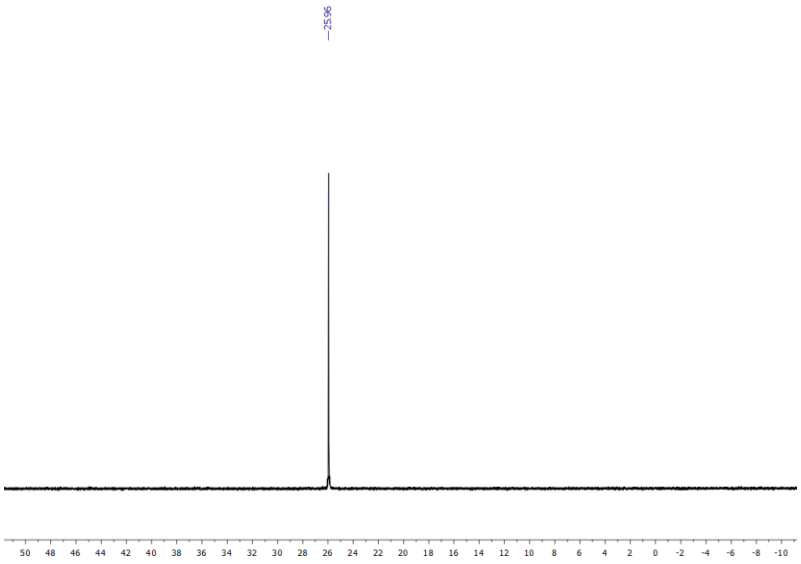

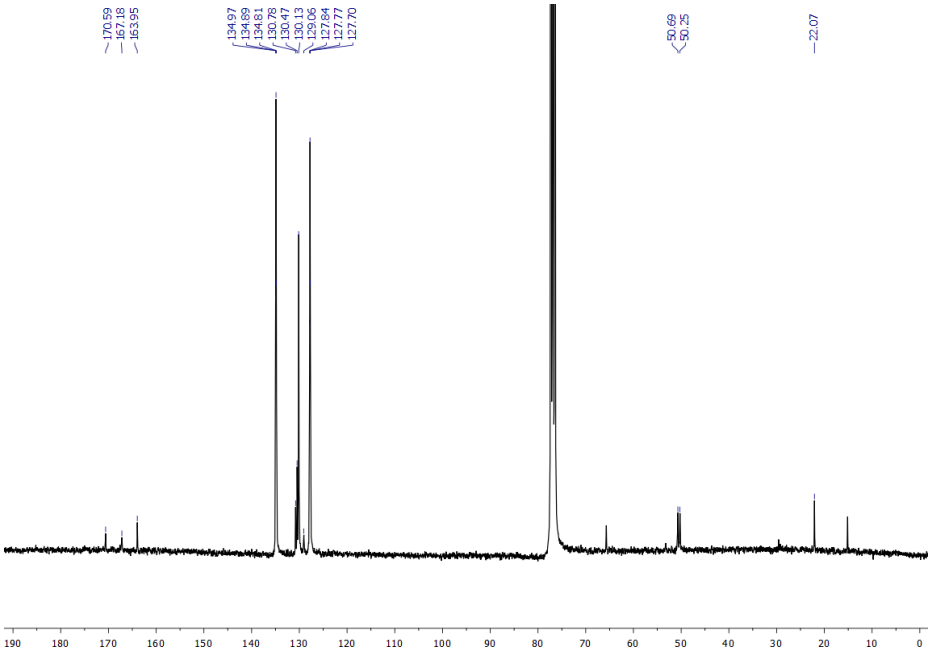

^{1}H NMR, ^{31}P{^{1}H} NMR and ^{13}C{^{1}H} NMR spectra of *trans*-[Pd(PPh$_3$)$_2$Cl(C$_4$(COOMe)$_4$CH$_3$)] (8b)

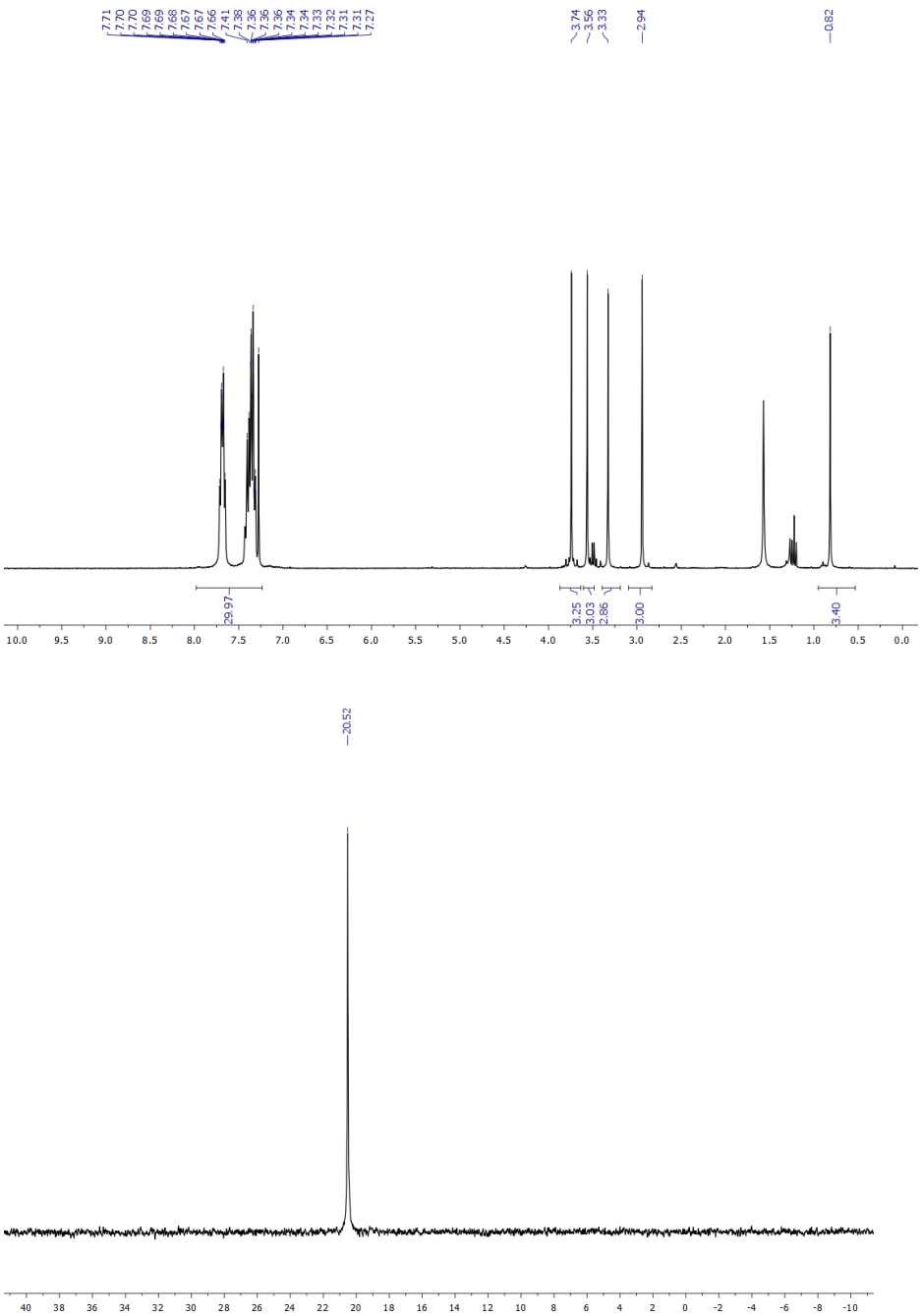

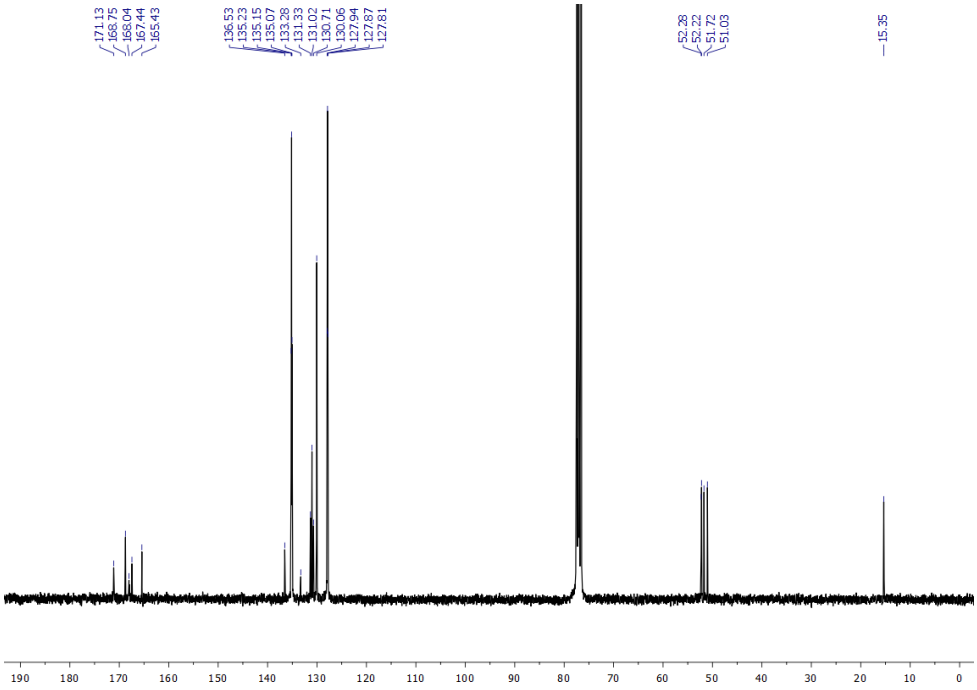

^{1}H NMR, ^{31}P{^{1}H} NMR and ^{13}C{^{1}H} NMR spectra of *trans*-[Pd(PTA)$_2$Cl(C$_2$(COOMe)$_2$CH$_3$)] (9a)

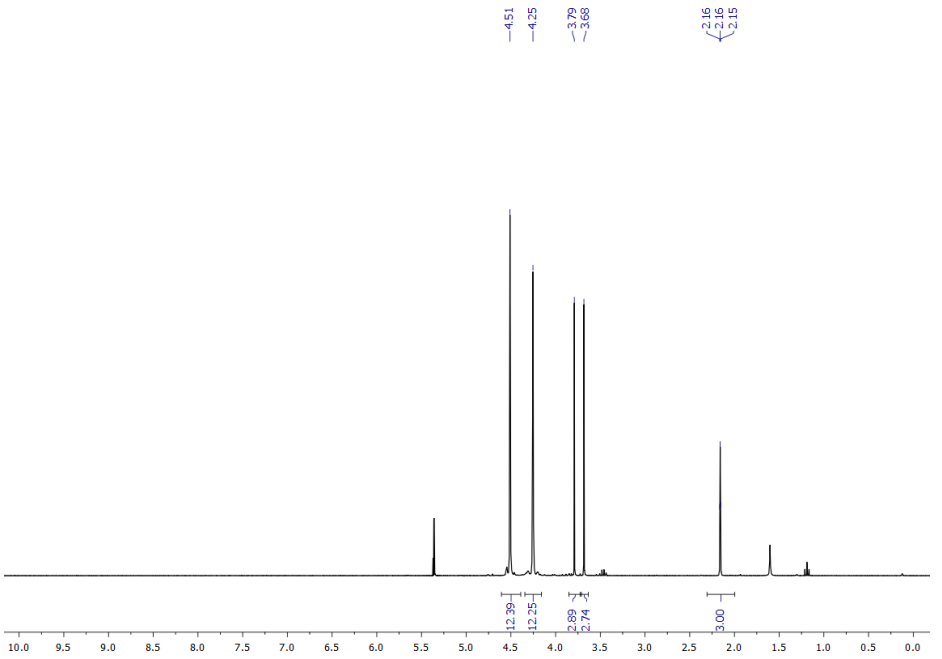

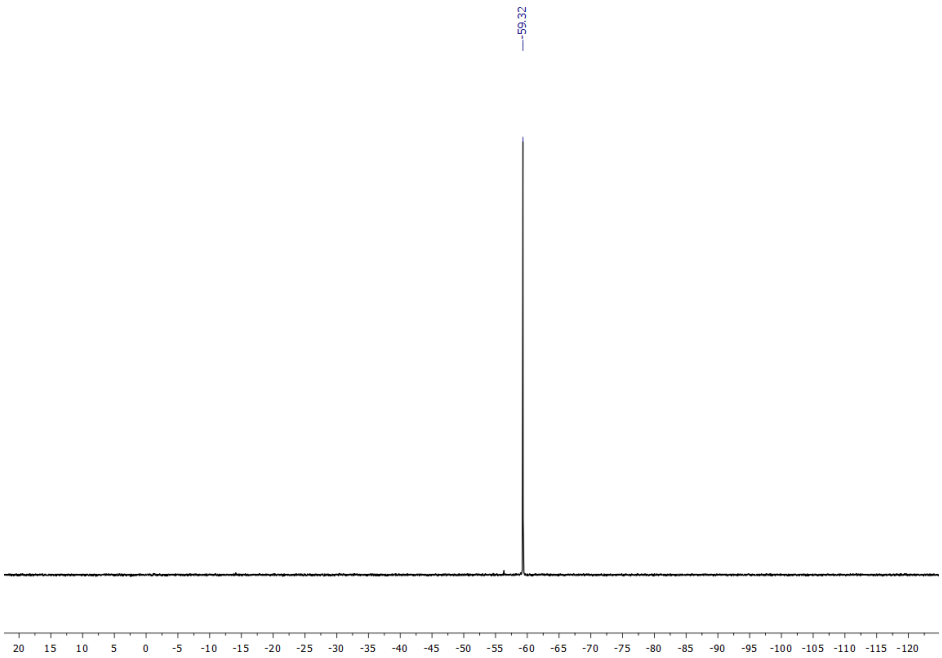

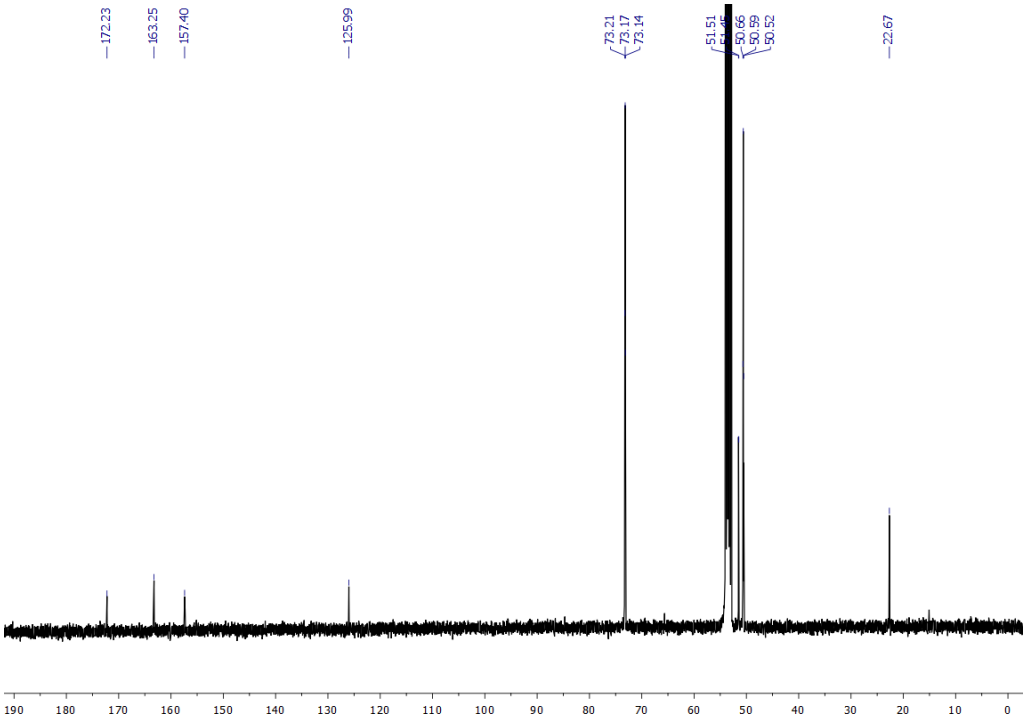

^{1}H NMR, ^{31}P{^{1}H} NMR and ^{13}C{^{1}H} NMR spectra of *trans*-[Pd(PTA)$_2$Cl(C$_4$(COOMe)$_4$CH$_3$)] (9b)

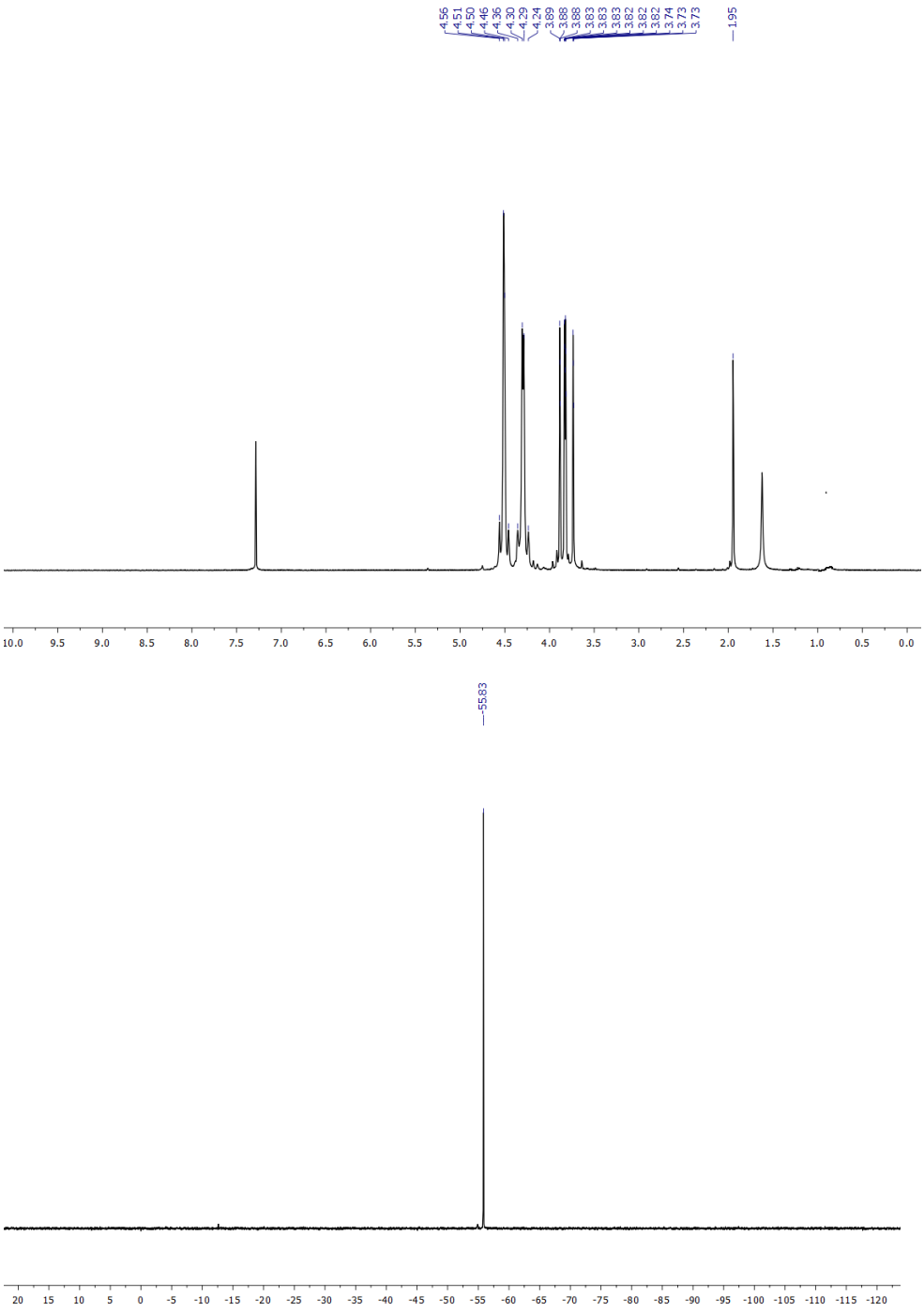

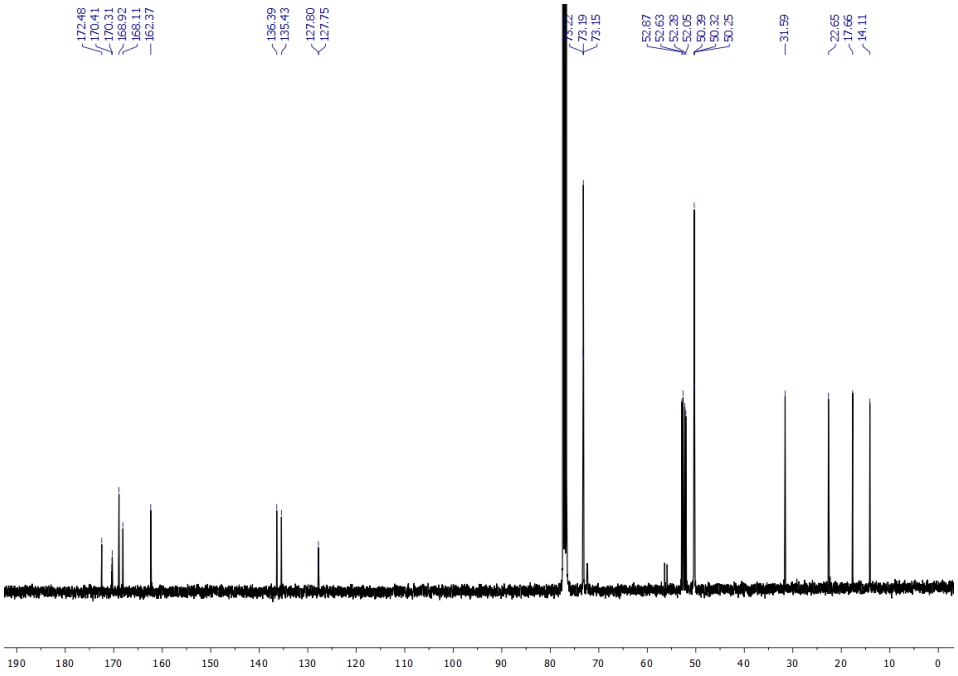

^{1}H NMR, ^{13}C{^{1}H} NMR spectra of *trans*-[Pd(AsPh$_3$)$_2$Cl(C$_2$(COOMe)$_2$CH$_3$)] (10a)

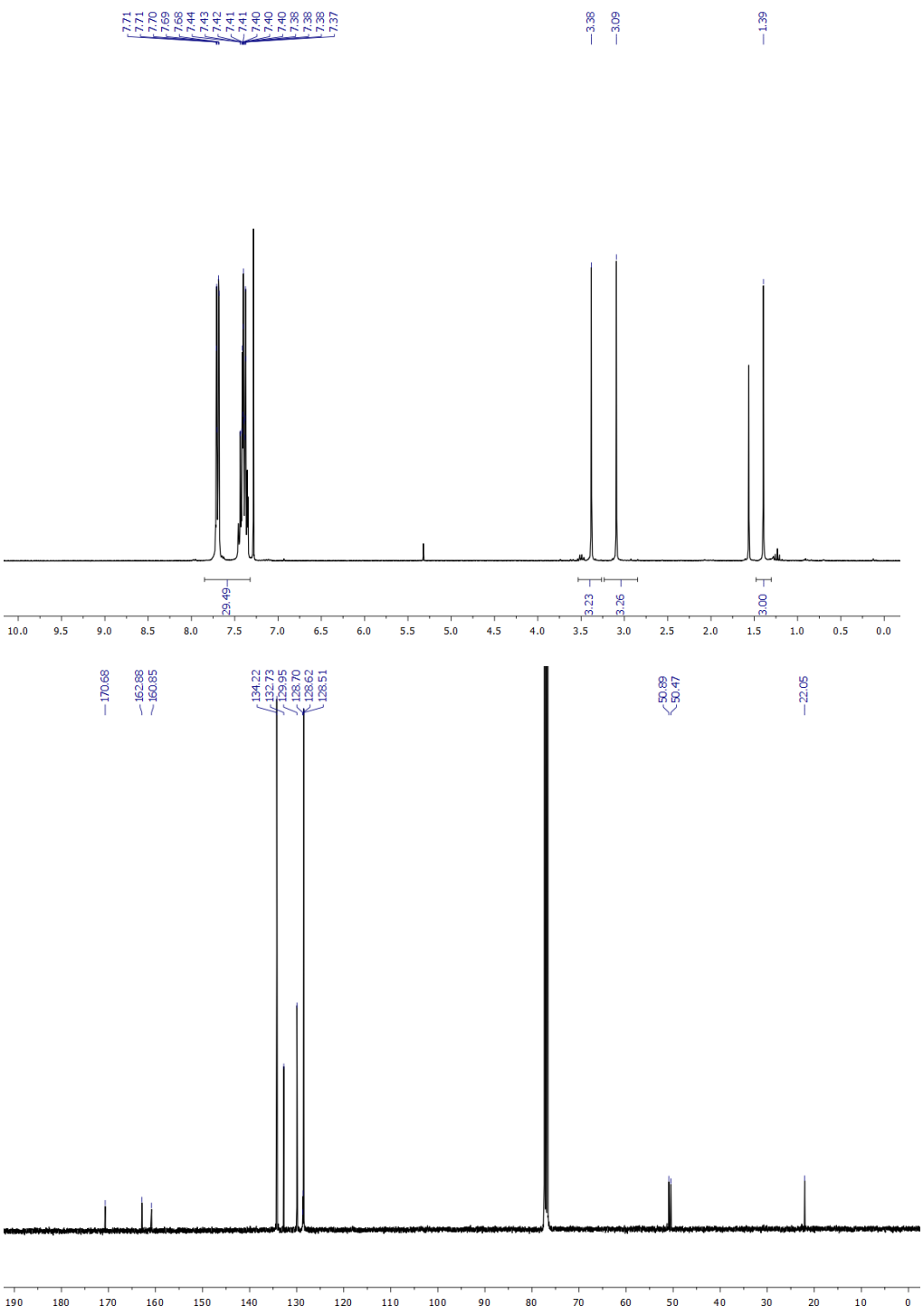

^{1}H NMR, ^{13}C{^{1}H} NMR spectra of *trans*-[Pd(AsPh$_3$)$_2$Cl(C$_4$(COOMe)$_4$CH$_3$)] (10b)

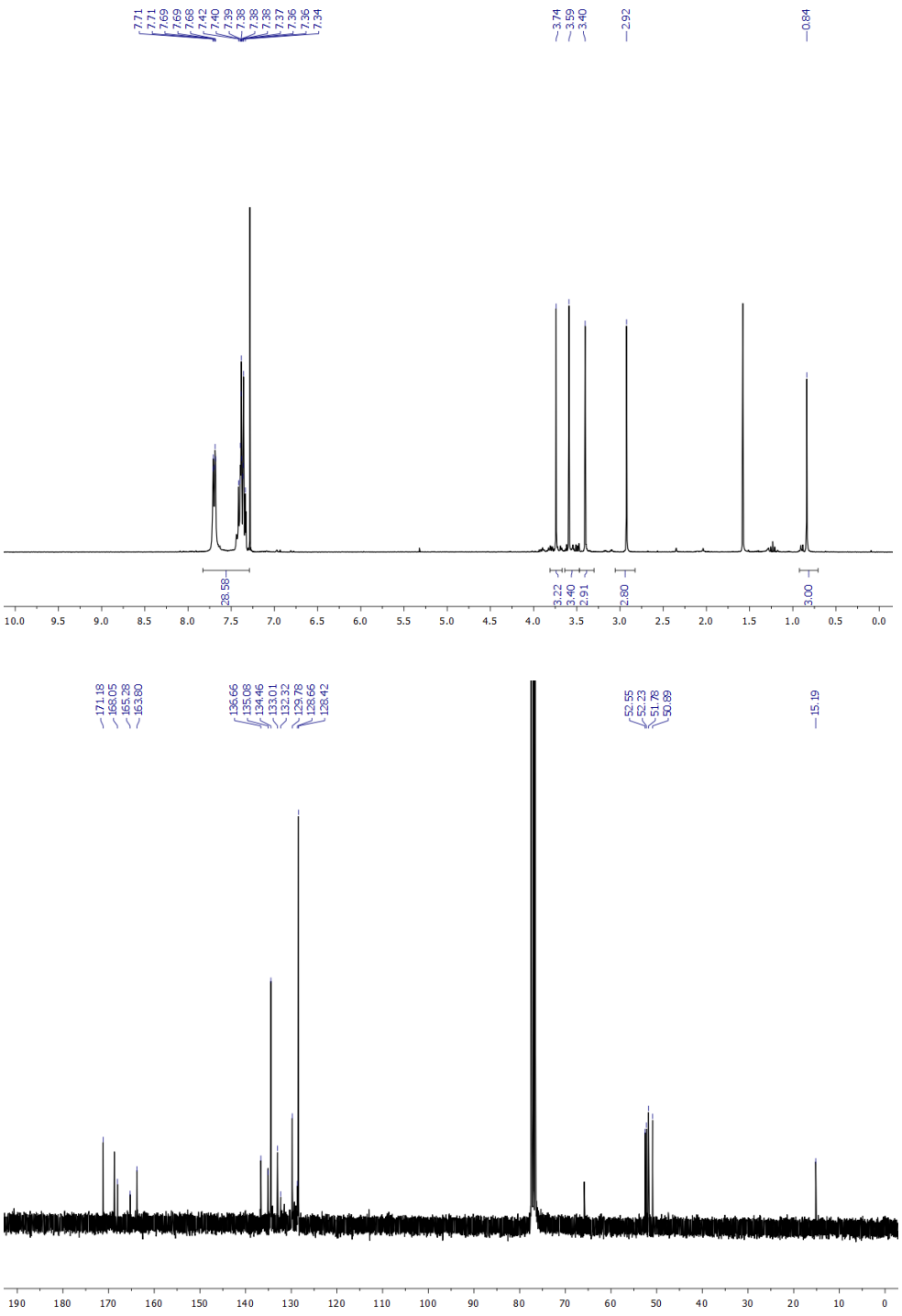

^{1}H NMR, $^{31}P\{^{1}H\}$ NMR and $^{13}C\{^{1}H\}$ NMR spectra of *trans*-[Pd(PTA)$_2$(C≡C-Ph)(C$_2$(COOMe)$_2$CH$_3$)] (13)

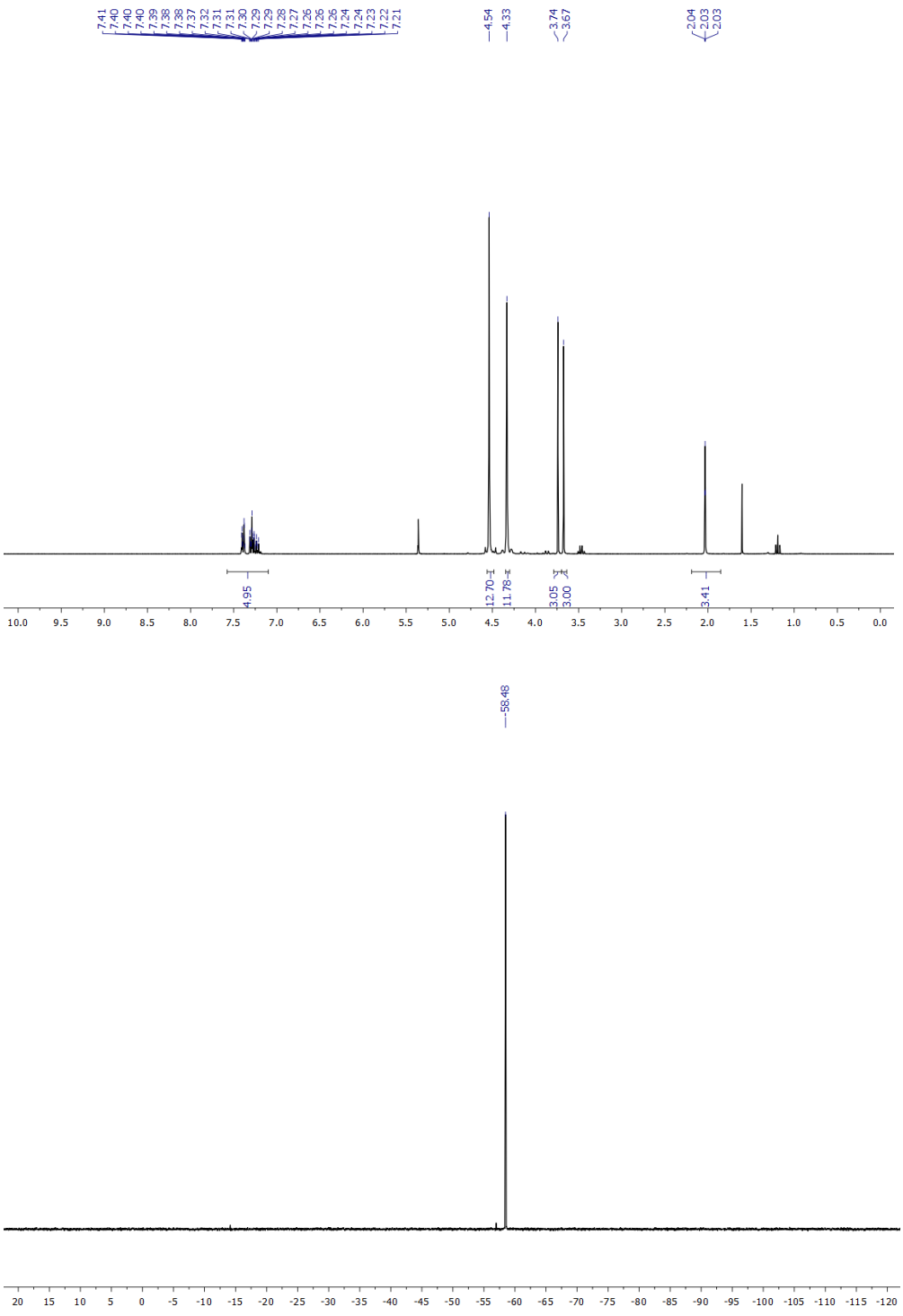

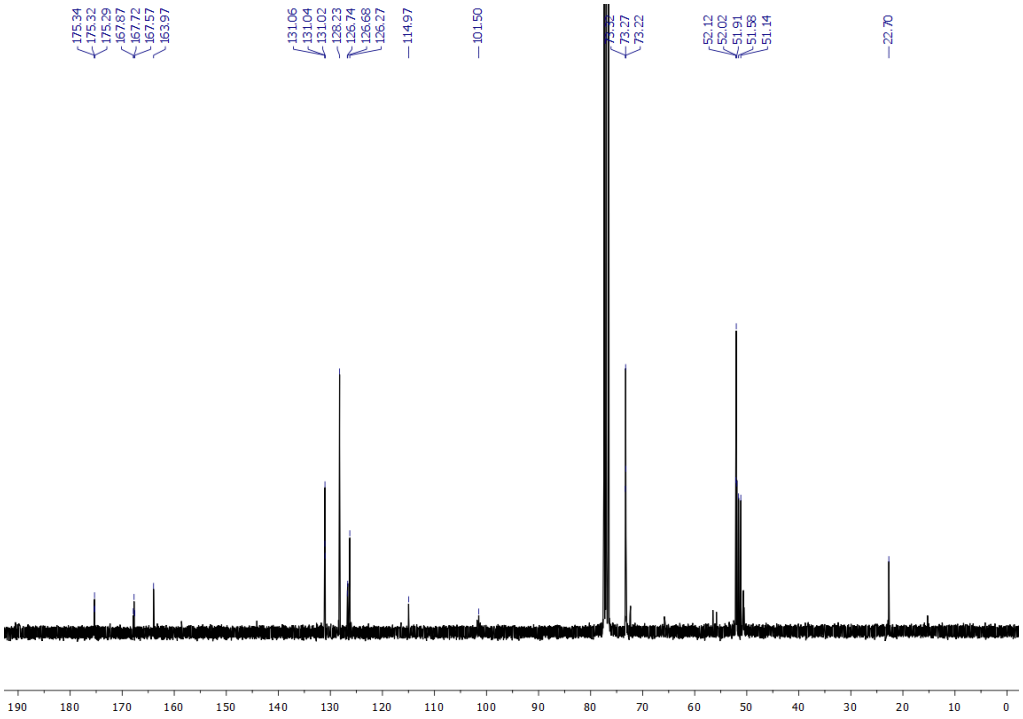

Crystallographic data

Table S2. Crystallographic data.

Compound	**2a**	**2b**	**3b**	**13**	**5a**
Formula	$[PdC_{19}H_{17}ClN_2O_4]\cdot CHCl_3$	$[PdC_{25}H_{23}ClN_2O_8]$	$[PdC_{27}H_{27}ClN_2O_8]$	$[PdC_{27}H_{38}N_6O_4P_2]\cdot CHCl_3$	$[PdC_{33}H_{34}ClO_4P_2]$ $CHCl_3$
M/g·mol^{-1}	598.56	621.30	649.35	798.34	816.75
Space group	*P* -1	*P* -1	*P* -1	*P* -1	*P* $na2_1$
Crystal system	Triclinic	Triclinic	Triclinic	Triclinic	Orthorhombic
a/Å	8.559(2)	8.605(2)	10.366(2)	10.743(2)	18.056(4)
b/Å	9.997(2)	8.866(2)	11.949(2)	12.747(3)	20.810(4)
c/Å	14.569(3)	17.383(3)	12.605(3)	13.560(3)	9.539(2)
α/°	104.46(3)	76.16(3)	82.50(3)	80.40(3)	90
β/°	90.63(3)	83.51(3)	68.40(3)	66.95(3)	90
γ/°	113.81(3)	77.13(3)	67.68(3)	86.12(3)	90
V/Å^3	1095.6(5)	1252.9(5)	1342.8(6)	1684.8(7)	3584.2(12)
Z	2	2	2	2	4
T/K	100(2)	100(2)	100(2)	100(2)	100(2)
D_c/g·cm^{-3}	1.814	1.647	1.606	1.574	1.514
F(000)	596	628	660	816	1656
μ/mm^{-1}	0.927	0.617	0.579	0.631	0.639
Measured Reflections	58846	89496	63021	79737	44667
Unique Reflections	11201	10923	11655	14689	15398
R_{int}	0.0463	0.0384	0.0380	0.0420	0.0441
Obs. Refl.ns [I≥2σ(I)]	10850	10662	11366	12953	15089
θ_{min}- θ_{max}/°	1.27 – 32.29	1.05 – 31.10	1.52 – 31.09	1.41 – 31.11	1.30 – 31.07
hkl ranges	-14,14; -16,14; -24,24	-14,14; -14,14; -28,28	-16,17; -18,18; -20,20	-17,17; -21,21; -22,22	-30,28; -32,31; -15,15
R(F^2) (Obs.Refl.ns)	0.0303	0.0321	0.0320	0.0417	0.0298
wR(F^2) (All Refl.ns)	0.0775	0.0853	0.0834	0.1156	0.0802
No. Variables	283	339	360	405	410
Goodness of fit	1.029	1.065	1.050	1.084	1.026
$\Delta\rho_{max}$; $\Delta\rho_{min}$/e·Å^{-3}	1.61; -2.21	1.04; -1.36	1.27; -1.62	1.29; -2.25	1.10; -0.74
CCDC Deposition N.	2343666	2343667	2343668	2343669	2343670

Table S3. Selected palladium coordination sphere distances and angles (Å and degrees) for **2a**.

2a (100 K) – [$PdC_{19}H_{17}ClN_2O_4$]

Distances	(Å)	Angles	(°)
Pd_1-C4_2	1.992(1)	C4_2-Pd_1-Cl_4	89.58(4)
Pd_1-N1_3	2.052(1)	C4_2-Pd_1-N1_3	95.74(5)
Pd_1- N10_3	2.098(1)	N1_3-Pd_1-N10_3	80.52(5)
Pd_1-Cl_4	2.286(1)	N10_3-Pd_1-Cl_4	94.18(4)

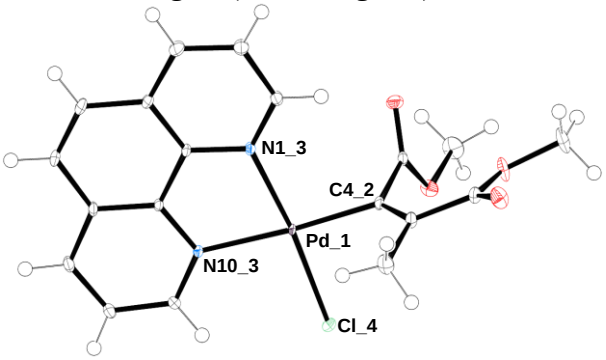

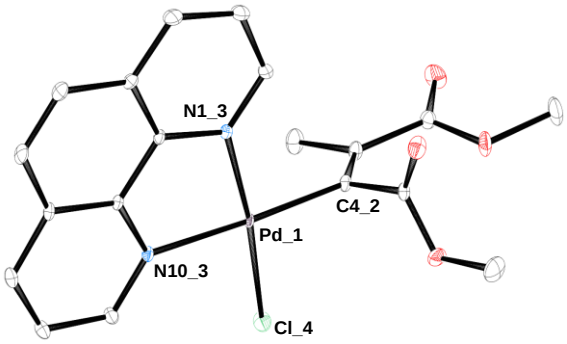

Table S4. Selected palladium coordination sphere distances and angles (Å and degrees) for **2b**.

2b (100 K) - [$PdC_{25}H_{23}ClN_2O_8$]

Distances	(Å)	Angles	(°)
Pd_1-C4_2	1.989(1)	C4_2-Pd_1-Cl_4	91.62(5)
Pd_1-N1_3	2.042(1)	C4_2-Pd_1-N1_3	93.21(5)
Pd_1- N10_3	2.106(1)	N1_3-Pd_1-N10_3	80.75(5)
Pd_1-Cl_4	2.291(1)	N10_3-Pd_1-Cl_4	94.43(4)

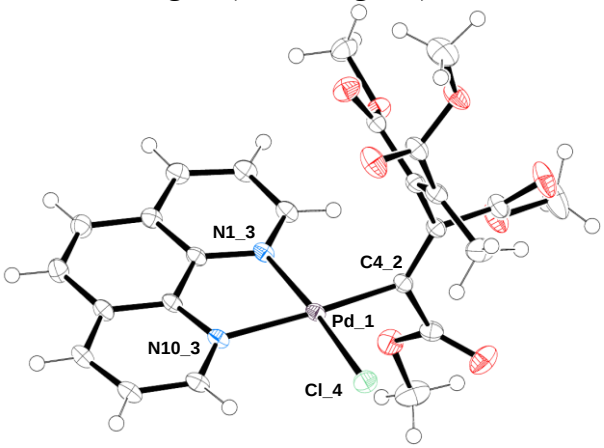

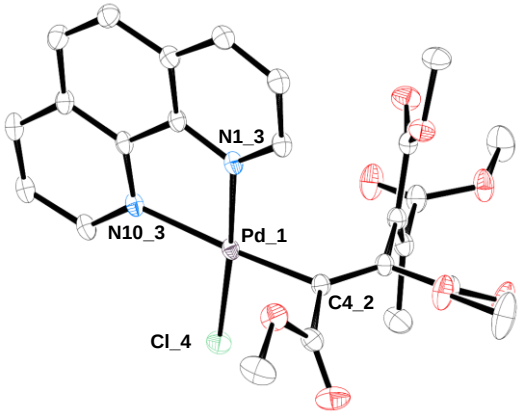

Table S5. Selected palladium coordination sphere distances and angles (Å and degrees) for **3b**.

3b (100 K) - [$PdC_{27}H_{27}ClN_2O_8$]

Distances	(Å)	**Angles**	(°)
Pd_1-C4_2	1.989(1)	C4_2-Pd_1-Cl_4	84.44(5)
Pd_1-N1_3	2.058(1)	C4_2-Pd_1-N1_3	96.32(6)
Pd_1- N10_3	2.156(1)	N1_3-Pd_1-N10_3	79.42(5)
Pd_1-Cl_4	2.310(1)	N10_3-Pd_1-Cl_4	99.35(5)

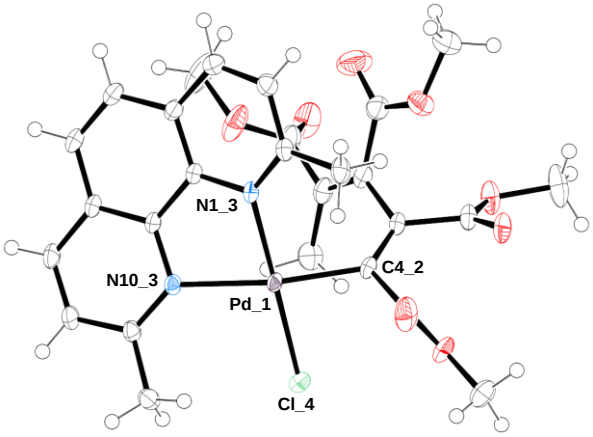

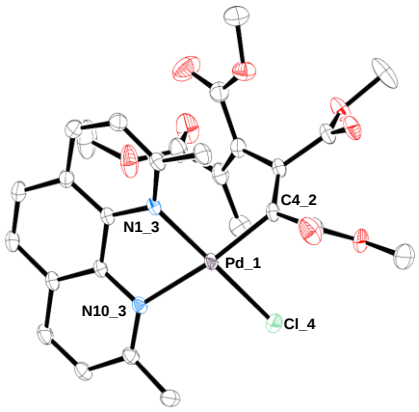

Table S6. Selected palladium coordination sphere distances and angles (Å and degrees) for **13**.

13 (100 K) - [$PdC_{27}H_{38}N_6O_4P_2$]

Distances	(Å)	**Angles**	(°)
Pd_1-C4_2	2.062(2)	C4_2-Pd_1-P1_3	92.51(5)
Pd_1-P1_3	2.289(1)	P1_3-Pd_1-C_5	90.53(5)
Pd_1- P1_4	2.276(1)	P1_4-Pd_1-C_5	87.63(5)
Pd_1-C_5	2.043(2)	P1_4-Pd_1-C4_2	89.39(5)

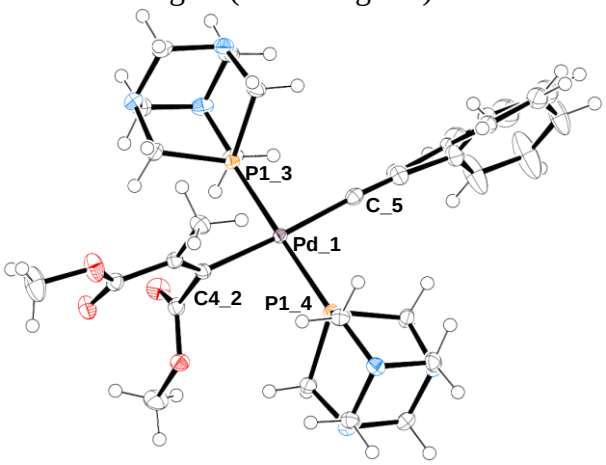

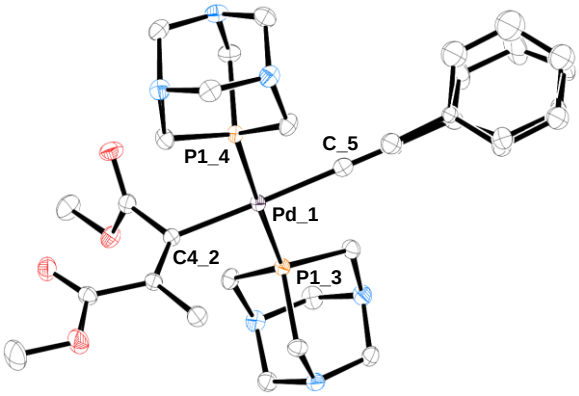

Table S7. Selected palladium coordination spheres distances and angles (Å and degrees) for **5a**.

5a (100 K) – [$PdC_{33}H_{34}ClO_4P_2$]

Distances	(Å)	**Angles**	(°)
Pd_1-C4_2	2.059(2)	C4_2-Pd_1-P1_3	92.78(6)
Pd_1-P1_3	2.233(1)	P1_3-Pd_1-P2_3	85.36(2)
Pd_1- P2_3	2.304(1)	P2_3-Pd_1-Cl_4	93.32(2)
Pd_1-Cl_4	2.366(1)	Cl_4-Pd_1-C4_2	88.55(6)

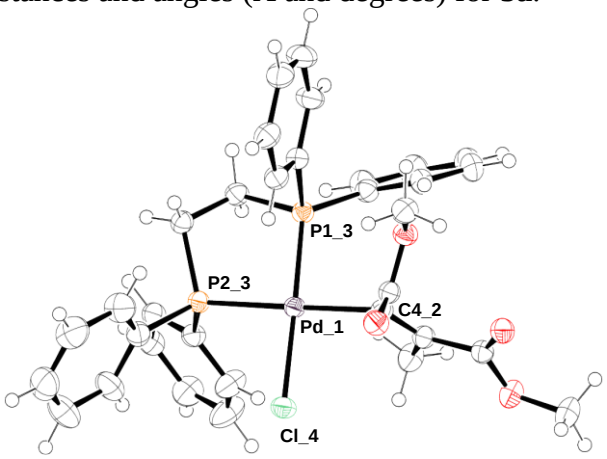

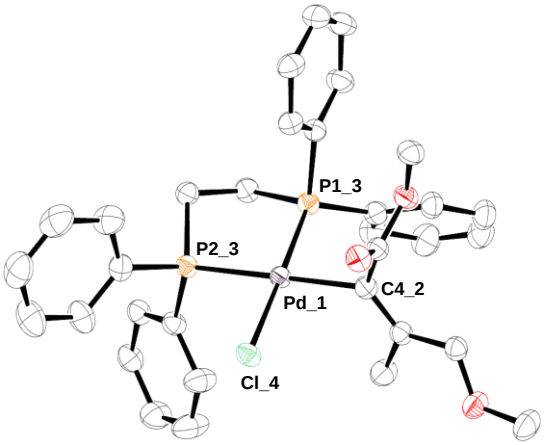

Author Contributions

Thomas Scattolin: Conceptualization, Investigation, Methodology Formal Analysis and Validation of analytical data, Visualisation, Writing-original draft; **Enrico Cavarzerani:** Conceptualization, Investigation, Methodology Formal Analysis and Validation of analytical data, Visualisation, Writing-original draft; **Dario Alessi:** Investigation, Methodology Formal Analysis and Validation of analytical data; **Matteo Mauceri:** Investigation, Methodology Formal Analysis and Validation of analytical data; **Eleonora Botter:** Investigation, Methodology Formal Analysis and Validation of analytical data; **Giovanni Tonon:** Investigation, Methodology Formal Analysis and Validation of analytical data; **Isabella Caligiuri:** Investigation, Methodology Formal Analysis and Validation of analytical data; **Ombretta Repetto:** Investigation, Methodology Formal Analysis and Validation of analytical data; **Urska Kamensek:** Investigation, Methodology Formal Analysis and Validation of analytical data; **Simona Kranjc Brezar:** Investigation, Methodology Formal Analysis and Validation of analytical data; **Maria Dalla Pozza:** Investigation; **Stefano Palazzolo:** Investigation, Methodology Formal Analysis and Validation of analytical data; **Maja Cemazar:** Investigation, Methodology Formal Analysis and Validation of analytical data; **Vincenzo Canzonieri:** Project administration, Resources; **Nicola Demitri:** Data Curation, Formal Analysis, Validation and Visualisation of X-ray Single Crystal Data; **Steven P. Nolan:** Project administration, Writing-review and editing; **Gilles Gasser:** Project administration, Writing-review and editing; **Fabiano Visentin:** Conceptualization, Investigation, Methodology Formal Analysis and Validation of analytical data, Supervision, Project administration, Writing-original draft; **Flavio Rizzolio:** Conceptualization, Investigation, Methodology Formal Analysis and Validation of analytical data, Supervision, Project administration, Writing-original draft, Resources.